REVIEWS OF GEOPHYSICS, VOL. 24, NO. 3, PAGES 493–536, AUGUST 1986

Nonlinear Interactions Among Internal Gravity Waves

PETER MÜLLER

Department of Oceanography and Hawaii Institute of Geophysics, University of Hawaii, Honolulu

GREG HOLLOWAY

Institute of Ocean Sciences, Patricia Bay, British Columbia, Canada

FRANK HENYEY AND NEIL POMPHREY[1]

Center for Studies of Nonlinear Dynamics, La Jolla Institute, La Jolla, California

This paper reviews the nonlinear interaction calculations for the internal gravity wave field in the deep ocean. The nonlinear interactions are a principal part of the dynamics of internal waves and are an important link in the overall energy cascade from large to small scales. Four approaches have been taken for their analysis: the evaluation of the transfer integral describing weakly and resonantly interacting waves, the application of closure hypotheses from turbulence theories to more strongly interacting waves, the integration of the eikonal or ray equations describing the propagation of small-scale internal waves in a background of large-scale internal waves, and the direct numerical simulation of the basic hydrodynamic equations of motion. The weak resonant interaction calculations have provided most of the conventional wisdom. Specific interaction processes and their role in shaping the internal wave spectrum have been unveiled and a comprehensive inertial range theory developed. The range of validity of the resonant interaction approximation, however, is not known and must be seriously doubted for high-wave number, high-frequency waves. The turbulence closure calculations and the direct numerical modeling are not yet in a state to be directly applicable to the oceanic internal wave field. The closure models are too complex and rest on conjectures that are not demonstrably justified. Numerical modeling can treat strongly interacting waves and buoyant turbulence, but is severely limited by finite computer resolutions. Extensive suites of experiments have only been carried out for two-dimensional flows. The eikonal calculations provide an efficient and versatile tool to study the interaction of small-scale internal waves, but it is not clear to what extent the scale-separated interactions with larger-scale internal waves compete with and might be overwhelmed by interactions among like scales. The major shortcoming of all four approaches is that they neglect the interaction with the vortical (= potential vorticity carrying) mode of motion that must be expected to exist in addition to internal waves at small scales. This interaction is intrinsically neglected in all Lagrangian-based studies and in the non-rotating two-dimensional simulations. The most promising approach for the future that can handle both arbitrarily strong interactions and the interaction with the vortical mode is numerical modeling once the resolution problem is overcome.

CONTENTS

1. INTRODUCTION

In this article we review the present knowledge of nonlinear interactions among oceanic internal gravity waves. Internal gravity waves arise in a stably stratified ocean through the restoring force of gravity on water particles displaced from their equilibrium position. In a rotating system internal waves have frequencies between the inertial frequency f and the Brunt-Väisälä or buoyancy frequency N. Internal waves are found everywhere in the

[1]Currently with Plasma Physics Laboratory, Princeton University, Princeton, New Jersey.

Paper number 6R0117.
8755-1209/86/006R-0117 $15.00

ocean. They represent a random superposition of many waves with different amplitudes, wave numbers, and frequencies. Typical velocities are about 5 cm s^{-1} and typical vertical displacements are about 7 m. The horizontal wavelengths range from a few meters to a few tens of kilometers, and the vertical wavelengths from about one meter to about one kilometer.

Internal waves are studied for a variety of reasons. First, they account for a significant fraction of the observed variability in the ocean. This alone is sufficient reason. Internal waves are also important for a variety of applied problems. They advect and disperse chemical and biological tracers [e.g., *Garrett*, 1979; *Young et al.*, 1982] and affect the transmission of sound [e.g., *Flatté et al.*, 1979]. The main reason for the study of internal waves is, however, that they are suspected to play an important role in the dynamics of the ocean, especially in affecting the large-scale general circulation and in providing a link in the presumed energy cascade from large to small scales.

Internal waves transfer momentum and hence exert a stress on larger-scale motions [e.g., *Müller*, 1976]. Internal waves also cause mixing by sporadic overturning and breaking [e.g., *Garrett and Munk*, 1972*a*]. The full understanding of these transfer and mixing processes and their proper parameterization might be essential for our understanding of the general circulation. *Gargett* [1984] gives an example of the possible sensitivity of the general circulation to subtle changes in small-scale mixing: the meridional circulation in a simple advective diffusive model of the thermohaline circulation is reversed when a constant mixing coefficient is replaced by one increasing with depth.

The scales of internal waves lie between the planetary scales where contrasts in the oceanic velocity and density field are generated by the atmosphere and the microscales where these contrasts are dissipated by molecular processes. It is a central oceanographic problem to understand how energy (the variance of the velocity and density field) and enstrophy (the variance of the potential vorticity field) are cascaded from the large generation down to the small dissipation scales. Internal waves might provide an important link in this energy cascade, since they have the unique ability to convert two-dimensional motions that are prevalent at large scales to three-dimensional motions that are prevalent at small scales.

To understand how internal waves affect the general circulation and how they cascade energy from large to small scales, one has to study their dynamics. This is a wide and complicated field. It involves the study of generation and dissipation mechanisms, of nonlinear interactions and other internal transfer processes, and of the forces that internal waves exert on their environment [*Müller and Olbers*, 1975]. The nonlinear interactions among internal waves are due to the nonlinear self-advection of momentum and buoyancy. This advection redistributes energy and momentum among different wave components, without changing the total energy and momentum. The nonlinear interactions are assumed to play a major role in the dynamics. They are thought to be responsible for the universal shape and level of the observed internal wave spectrum and for the rapid relaxation of distorted spectra toward the universal form. Deviations from the universal spectrum are only found at the equator, near seamounts, and in submarine canyons [*Wunsch*, 1976; *Wunsch and Webb*, 1979], near the surface [*Roth et al.*, 1981], and at the critical frequency over sloping bottom topography [*Eriksen*, 1982]. The deviations near seamounts become inconspicuous at very short distances and the enhancement of the spectrum at the critical frequency disappears within a few hundred meters off the bottom, suggesting a rapid, nonlinear recovery of the spectrum to an equilibrium form. For these reasons nonlinear interactions have been studied extensively and an impressive amount of knowledge about their strength, character, and role has emerged, which we will review in this paper.

Internal redistribution by nonlinear interaction is only one aspect of the dynamics of internal waves. We also need to understand the generation and dissipation processes and the other redistribution processes. Here the state of affairs is somewhat disconcerting. There exists a large variety of possible generation mechanisms: direct atmospheric forcing by fluctuations in the wind stress, buoyancy flux or pressure, generation by surface waves, by the surface tide interacting with bottom topography, by the mean current interacting with bottom topography, by instabilities of the mean current, and by wave-mean flow interaction [e.g., *Thorpe*, 1975; *Müller and Olbers*, 1975]. Some correspondence has been observed between the surface wind and surface wave field and the intensity of the upper ocean internal wave field [e.g., *Briscoe*, 1983]. Also, the wind field is clearly responsible for the large-scale, near-inertial frequency waves in the upper ocean [e.g., *D'Asaro*, 1984]. The major energy source or sources of the deep ocean internal wave field have, however, not yet been identified.

The situation is similar for dissipation. It is generally assumed that internal waves dissipate their energy in the interior of the ocean by wave breaking, either by overturning or shear instability. This is suggested by direct observations of Kelvin-Helmholtz billows [*Woods*, 1968] and by the fact that most instability parameters (Richardson number, rate of strain) are near critical [e.g., *Eriksen*, 1978]. The breaking events are envisioned as intermittent and localized in physical space. Other possible dissipation mechanisms include absorption in the bottom boundary layer [*D'Asaro*, 1982], critical reflection at sloping boundaries [e.g., *Eriksen*, 1982], and absorption at critical layers induced by the low-frequency flow [e.g., *Ruddick*, 1980; *Kunze and Sanford*, 1984]. These sinks would be concentrated at particular locations and would not be spread uniformly throughout the ocean. Again, we do not know where in the ocean and by what process internal waves dissipate their energy. We know even less where the energy sources and sinks are in wave number-frequency space. Today, the nonlinear interaction calculations constitute the major basis for the construction of the complete dynamics.

The strength and character of the nonlinear interactions depends on the kinematic structure of the internal wave field. This structure is briefly reviewed in section 2. More exhaustive discussions can be found in the review articles mentioned at the end of the introduction. We just provide some basic background and the concepts needed for the discussion of nonlinear interactions. We also point out that we do not share some of the optimistic views given in

other review articles. We feel that the kinematic structure of the fluctuations in the internal wave band might not be described adequately by the universal *Garrett and Munk* [1975] model spectrum. First, internal waves do not provide a complete description of the fluctuations. Internal waves do not carry potential vorticity. There exists another mode of motion at internal wave scales which carries potential vorticity and which we will term vortical mode [e.g., *Holloway* 1981, 1983; *Riley et al.*, 1981; *Henyey* 1983; *Müller*, 1984]. At mesoscales the vortical mode represents quasi-geostrophic flows. A proper distinction between the internal gravity and vortical mode of motion requires the measurement of potential vorticity on small scales, which has not yet been done. The implications of the existence of the vortical mode on the dynamics have not been explored, for reasons given below, but we expect the vortical mode to be intimately connected and intertwined with the internal gravity mode of motion. Second, the Garrett and Munk spectrum seems to model fairly well the energy distribution at the large, energy-containing scales [e.g., *Müller et al.*, 1978]. For most dynamical problems it is, however, the shear that is important and it is not clear how well the Garrett and Munk spectrum models the small, shear-containing scales. We know that the shear is concentrated at small vertical scales [e.g., *Gargett et al.*, 1981] but we do not know which mode of motion, which frequencies, and which horizontal scales contribute to it. Additionally, the shear is intermittent and more than a spectrum might be required to describe the shear adequately.

Nonlinear interactions among internal waves have first been studied for single internal waves, both theoretically [*Bretherton*, 1964; *Phillips*, 1966] and in the laboratory [*Davis and Acrivos*, 1967; *Martin et al.*, 1972; *McEwan et al.*, 1972]. Calculations of the nonlinear transfers in a many-wave environment started when Garrett and Munk formulated their first model spectrum in 1972 [*Garrett and Munk*, 1972*a*]. These calculations sought to determine the strength and role of the nonlinear transfers in a realistic spectrum and the sensitivity of the results to the form and level of the spectrum. Equilibrium solutions were sought, energy fluxes through the spectrum determined, and relaxation rates calculated. It is these spectral or many-wave calculations that we review in this paper. The origin and the early ideas about discrete interactions are traced in an essay by *Phillips* [1981].

For the many-wave calculations, four major approaches have been taken. The first, historically, was the analysis of weak resonant wave-wave interactions. These are discussed in section 3. To treat more strongly interacting waves, other approaches have been developed. One is the application of closure hypotheses developed in turbulence theories. This approach is discussed in section 4. One of the main results of the early studies has been that high-wave number, high-frequency waves predominantly interact with low-wave number, low-frequency waves. This scale separation has been systematically exploited in the eikonal approach, discussed in section 5. The fourth approach is the direct numerical simulation of the hydrodynamic equations of motion. This approach is described in section 6. An alternative approach, developed by Ostrovskiy and Pelinovskiy for the upper ocean, views the internal wave field as a random ensemble of solitons [see *Miropol'skiy and Sabinin*, 1977]. This approach is not discussed here.

Our review complements the recent review by *Olbers* [1983] and the reviews by *Gregg and Briscoe* [1979], *Garrett and Munk* [1979], *Munk* [1981], and *Levine* [1983]. A collection of recent research papers on internal waves and small-scale turbulence is contained in the proceedings of the 'Aha Huliko'a Hawaiian Winter Workshop [*Müller and Pujalet*, 1984]. A summary of the workshop is given by *D'Asaro and Müller*, [1984].

2. KINEMATIC STRUCTURE

The strength and character of nonlinear interactions among internal gravity waves depend on the distribution of internal wave energy in space, time, wave number, and frequency. In this section we critically review what is known about this distribution for the internal wave field in the deep, mid-latitude ocean.

Linear Eigenmodes

It is convenient to organize the observations in terms of a linear model. Over much of the spectrum linear dynamics describes the major part of the time evolution of internal waves (but, of course, the interesting part is likely to be the deviation from linear dynamics). Moreover, the theory of weakly nonlinear interactions is based on perturbations of this model. Even when nonlinear interactions are large, the linear model provides a basis for the expansion of the variables which is independent of the measurements.

There is an ambiguity in the choice of variables in which to make the linearization. Indeed, much of the art in solving nonlinear problems consists in finding the right variables in which the interaction takes a simple and uncontaminated form. In an Eulerian description the two most common choices are the two horizontal components u and v of the velocity and either the deviation $\delta\rho$ of the density from a stably stratified background state $\tilde{\rho}(z)$ or the vertical displacement ξ from that background state. The variables $\delta\rho$ and ξ are related by

$$\delta\rho(\mathbf{x},t) = \tilde{\rho}\left[z - \xi(\mathbf{x},t)\right] - \tilde{\rho}(\mathbf{x},t) \qquad (1)$$

which reduces to

$$\delta\rho = -\xi \frac{\partial\tilde{\rho}}{\partial z} \qquad (2)$$

in the linear limit. Note that ξ is an Eulerian variable and depends on $\mathbf{x}$ (and t). The density is a directly observable variable, whereas the displacement is usually inferred from density using the linear relation (2). The vertical displacement is preferred as a variable when the background density exhibits strong gradients and steps (fine structure). For weak waves on an interface the displacement is a sinusoid in space and time whereas the density jumps between the values above and below the interface. The density is preferred when diffusive effects need to be included.

Various aspects of the linear problem are independent of the choice of the expansion variables. These include

the dispersion relation and the relations between the linear parts of all variables. The nonlinear parts of variables depend very much on the choice.

In terms of (u,v,ξ) the linear equations of motion are

$$\partial_t \mathbf{u} = -\xi N^2 \hat{\mathbf{z}} - f\hat{\mathbf{z}} \times \mathbf{u} - \nabla p \quad (3a)$$

$$\partial_t \xi = \mathbf{u} \cdot \hat{\mathbf{z}} \quad (3b)$$

$$\nabla \cdot \mathbf{u} = 0 \quad (3c)$$

where $\hat{\mathbf{z}}$ is a vertical unit vector, p the excess pressure above the hydrostatic value divided by density, f the Coriolis parameter, and $N^2 = -g\tilde{\rho}^{-1}\partial\tilde{\rho}/\partial z$, the square of the Brunt–Väisälä frequency. Since we are concerned with oceanic motions we will replace the background density $\tilde{\rho}(z)$ by a constant reference density ρ_0 whenever $\tilde{\rho}(z)$ appears as a coefficient, although most of the statements in this section are also valid for systems where such a replacement is incorrect, such as the atmosphere. The equations (3) assume incompressibility, absence of dissipative effects, the Boussinesq approximation, and f–plane dynamics. Only the variables u, v, and ξ are prognostic. The vertical velocity w can be determined diagnostically from the incompressibility condition (3c). The pressure is obtained from $\partial_t(\nabla \cdot \mathbf{u}) = 0$ which implies

$$\nabla^2 p = -\partial_z(\xi N^2) + f\hat{\mathbf{z}} \cdot \nabla \times \mathbf{u} \quad (4)$$

and replaces the vertical momentum balance. To quadratic order, the energy density takes the standard form

$$E = \frac{1}{2}\rho_0[u^2 + v^2 + w^2 + N^2\xi^2] \quad (5)$$

Except for the vertical kinetic energy term $\frac{1}{2}\rho_0 w^2$, which is small over most of the spectrum, this standard form expresses the energy density in terms of the prognostic variables u, v, and ξ. The potential vorticity π is defined by

$$f + \pi = (f\hat{\mathbf{z}} + \nabla \times \mathbf{u}) \cdot \nabla(z - \xi)$$

which becomes

$$\pi = \hat{\mathbf{z}} \cdot \nabla \times \mathbf{u} - f\partial_z \xi \quad (6)$$

in the linear limit.

Assume that each variable depends on space and time through the factor $\exp[i(\mathbf{k}\cdot\mathbf{x} - \omega t)]$ where $\mathbf{k} = (k_x, k_y, k_z)$ is the wave number vector and ω the (Eulerian) frequency. The equations of motion are then converted to a set of five coupled linear algebraic equations. A solution requires the determinant to be zero. Because there are three prognostic variables this determinant is a cubic polynomial in the frequency ω. The existence of three roots corresponds to there being three independent modes of motion.

Two of the roots give the dispersion relation for internal waves:

$$\omega^2 = \frac{N^2 k_h^2 + f^2 k_z^2}{k_h^2 + k_z^2} \quad (7)$$

where k_h is the horizontal part of the wave number vector $\mathbf{k}$. The third root is $\omega = 0$ (on the f plane) and the associated mode of motion contains potential vorticity, in contrast to internal wave motions which have zero potential vorticity. These three roots are schematically sketched in Figure 1.

In the linear theory the internal wave variables of a given wave number are related by

$$\begin{pmatrix} \xi \\ u \\ v \end{pmatrix} = \begin{pmatrix} -i k_h^2 \\ (\omega k_x + i f k_y) k_z \\ (\omega k_y - i f k_x) k_z \end{pmatrix} b_{\mathbf{k}} e^{i(\mathbf{k}\cdot\mathbf{x} - \omega t)} \quad (8)$$

where $b_{\mathbf{k}}$ is a complex amplitude. The internal wave energy density is

$$E = \tfrac{1}{2} k^2 k_h^2 \omega^2 |b_{\mathbf{k}}|^2 \quad (9)$$

when averaged over a wavelength or period. This normalization assumes that the energy of the total wave field is obtained by summing over all wave numbers and positive and negative frequencies. The potential vorticity of internal waves is

$$\pi = i k_x v - i k_y u - i k_z f \xi = 0 \quad (10)$$

It is the vanishing of potential vorticity, as well as the dispersion relation, which characterizes internal waves.

The potential vorticity containing motion has variables of a given wave number related by

$$\begin{pmatrix} \xi \\ u \\ v \end{pmatrix} = \begin{pmatrix} -\frac{f}{N^2} k_z \\ -k_y \\ k_x \end{pmatrix} C_{\mathbf{k}} e^{i\mathbf{k}\cdot\mathbf{x}} \quad (11)$$

The energy density averaged over a wavelength is

$$E = \frac{1}{4}\left(k_h^2 + \frac{f^2}{N^2} k_z^2\right) |C_{\mathbf{k}}|^2 \quad (12)$$

and the potential vorticity is

$$\pi = i\left(k_h^2 + \frac{f^2}{N^2} k_z^2\right) C_{\mathbf{k}} \quad (13)$$

The normalization (12) again assumes that the energy of the total field is obtained by summing over all wave numbers. In the rotating case, $f \neq 0$ or more exactly $f >> |\nabla \times \mathbf{u}|$, this $\omega = 0$ mode is in geostrophic and hydrostatic balance, is horizontally nondivergent, $\partial_x u + \partial_y v = 0$, and satisfies the thermal wind relations $(f/N^2)\partial_z u = \partial_y \xi$ and $(f/N^2)\partial_z v = -\partial_x \xi$. It is therefore the usual geostrophic mode. This mode also exists in the nonrotating case $f = 0$, or more exactly, $f << |\nabla \times \mathbf{u}|$. In this case the fields ξ and hence ρ and p vanish in a strictly linear approximation. The flow consists of steady horizontal vortices with an arbitrary vertical structure. However, for such flows the linear expression (4) for the pressure is generally not valid, even if linear dynamics for ξ, u, and v is reasonably accurate. These flows tend to have a balance between ∇p and the nonlinear advective terms. To include this case, we will refer to this mode as the vortical mode, emphasizing its defining property of having nonzero potential vorticity.

In the actual nonlinear case, the energy is not confined to the dispersion curves but distributed about them, as indicated by the fanlike curves in Figure 1. This broaden-

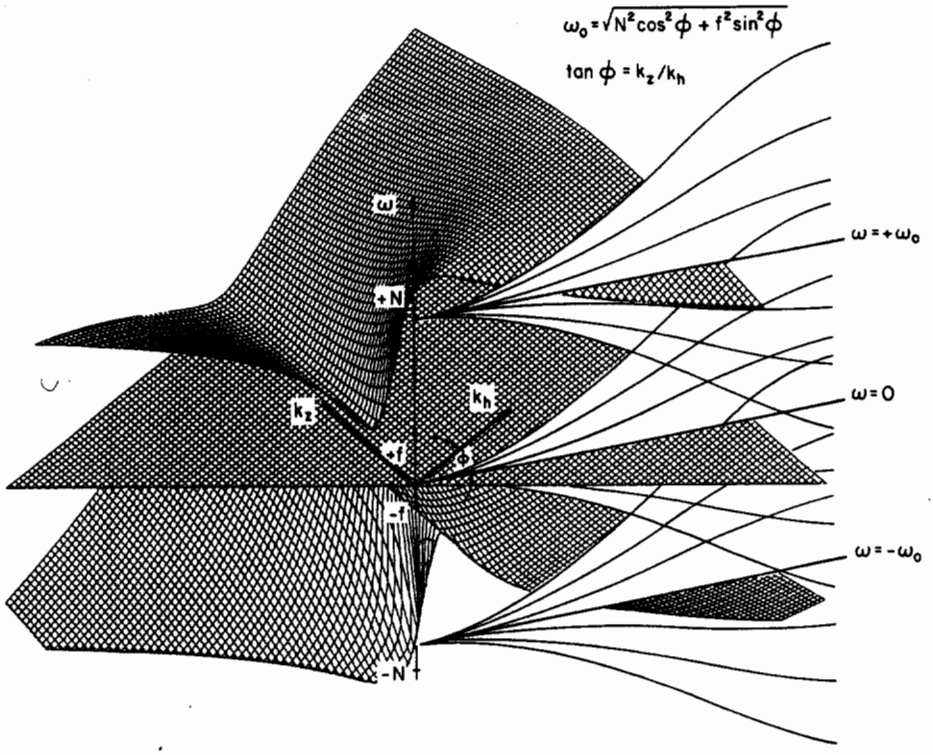

Fig. 1. Interactions among internal gravity waves and vortical motions are depicted in wave number–frequency space. Only one component of horizontal wave number (k_h) is shown. Hatched surfaces show the solution to the linear dispersion relation $\omega = 0, \pm\omega_0$; $\omega = \pm\omega_0$ corresponds to internal inertial–gravity waves, and $\omega = 0$ corresponds to vortical motion on an f plane. If all motions were of very small amplitude, the energy of these motions would lie upon the hatched surfaces. Finite amplitude, leading to nonlinear interaction, will cause energy to "diffuse" into clouds about the hatched surfaces. A cross–section through the hypothetical energy clouds is shown on the right side of the figure where one imagines a "cut" at a fixed aspect ratio k_z/k_h. At low wave numbers (large length scales) the clouds are quite dense just near the hatched surfaces; the motion is close to linearized dynamics. Toward higher wave numbers (shorter scales), nonlinear interactions become more effective at spreading the energy clouds away from the hatched surfaces. The three clouds come to completely overlap so that all semblance to linearized dynamics is lost as one approaches a condition of three–dimensional turbulence [from *Holloway*, 1983].

ing of the dispersion curves is due to the nonlinear interactions. At large wave numbers the fans become very broad, and the different modes of motion overlap. In this case the amplitude relations, such as the vanishing of the potential vorticity π for the internal waves, can conveniently be taken as the definition of the distinction between the internal gravity and the vortical mode of motion. Formally, we can use the amplitude relations (8) and (11), which represent a complete set of basis vectors in (u, v, ξ) space, to uniquely decompose any observed field into its internal gravity and its vortical mode component.

The superposition of internal gravity and vortical motions is a well–observed phenomenon in laboratory experiments [e.g., *Lin and Pao,* 1979]. Objects moving through a stratified quiescent fluid create a three–dimensional wake. The internal wave content of the wake propagates away rapidly and leaves the two–dimensional vortical motion behind.

Observations

According to the dispersion relation, free linear internal waves have frequencies between f and N. Typical vertical length scales associated with internal waves range from about one meter to about one kilometer, typical horizontal length scales from a few meters to a few tens of kilometers. These time and space scales are fairly well resolved by various oceanographic instruments and measurement techniques, and an abundance of space and time series are available. The determination of the displacement and horizontal velocity fields from these measurements requires handling a number of difficult steps. These include the following steps:

1. One step is to determine the background stratification. The background stratification is defined as the stratification obtained by leveling all density surfaces by isentropic processes. Usually, it is constructed by some temporal or spatial averaging. It is, however, not clear whether the observed fine structure is part of the irreversible structure of the background stratification or the result of the reversible straining of a smooth background stratification by the modes of motion.

2. Another step is to obtain the displacement ξ of density from measurements of the temperature T and (less adequate) measurements of the salinity S. Moored, dropped, and towed instruments do not measure displacement but density (from temperature and salinity) and infer displacement from the linear relationship (2). If the

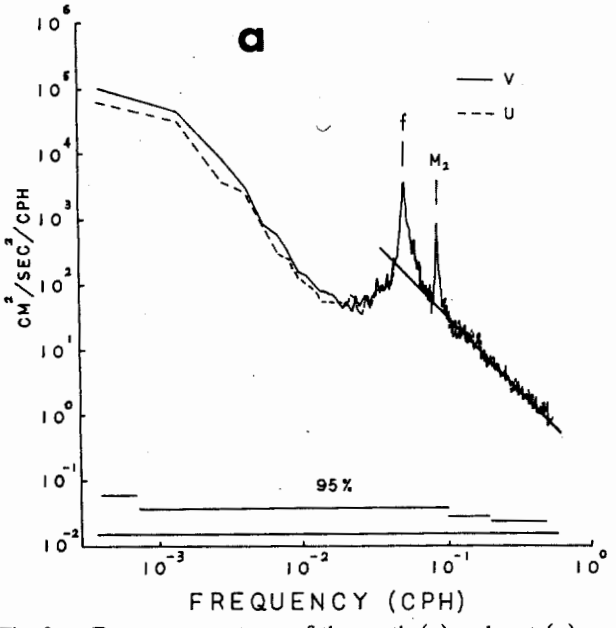

Fig. 2a. Frequency spectrum of the north (v) and east (u) component of the current velocity measured by a current meter on a subsurface mooring at a depth of 600 m in the western North Atlantic Ocean. The inertial and tidal frequencies are indicated. The local Brunt–Väisälä frequency is $N = 2.27$ cph. The straight line represents a -2.23 power law [from *Fu*, 1981].

background is not smooth but contains (irreversible) fine structure the linearization becomes inadequate and leads to a fine structure contamination of the observed signal [e.g., *Phillips*, 1971; *Garrett and Munk*, 1971]. The linearization is also incorrect when the motion field has a finite rate of strain [*Desaubies and Gregg*, 1981]. Often instruments only measure the temperature T, but not the salinity S. In this case one does not know whether changes in temperature are caused by displacement of density surfaces (the internal gravity and vortical mode of motion) or by intrusions where changes in temperature are compensated by changes in salinity.

3. Another step is to reduce measurements of velocities relative to moorings or the earth's magnetic field to absolute velocities, removing mooring motion or magnetic field variations.

The oceanic internal wave field is a random superposition of many waves with different amplitudes, frequencies and wave numbers. Observations are usually represented in the form of spectra. Frequency spectra of the horizontal current velocity and the vertical displacement show a substantial increase in energy level in the frequency band between f and N. (See Figure 2.) Within this range the spectra decay with an approximately -2 power law. In the velocity (horizontal kinetic energy) spectrum a substantial amount of energy is associated with inertial and tidal currents. In the displacement (potential energy) spectrum a substantial amount of the energy is sometimes associated with the baroclinic tides. Except for these inertial and tidal peaks, the level and form of the observed spectra are fairly universal within the mid–latitude deep ocean. Significant changes occur when the surface, the equator, seamounts and submarine canyons are approached.

Vertical wave number spectra of the vertical temperature gradient and vertical shear do not exhibit any peaks but show a smooth distribution of variance (see Figure 3). The forms of the two spectra are similar. Both are flat at low wave numbers and start to roll off as k_z^{-1} at about 0.1 cpm. Energy is concentrated at low wave numbers and shear at high wave numbers, between about 0.1 and 1 cpm. (The shear in the microstructure bumps at wave numbers larger than 1 cpm is due to intermittent three–dimensional turbulence and of no concern here.)

Internal Gravity and Vortical Mode of Motion

The decomposition of the inferred or observed u, v, and ξ fields into the internal gravity and vortical mode of motion requires the determination of the potential vorticity of the flow. One must simultaneously measure the horizontal gradients of velocity and vertical gradients of displacement (see equation (6)). This measurement cannot yet be made from a single instrument package. A combination of many instruments separated in space is needed. One of the major attempts to perform this decomposition was *Müller et al.'s* [1978] analysis of the three–legged Internal Wave Experiment (IWEX) mooring [*Briscoe*, 1975]. Using consistency tests [*Müller and Siedler*, 1976] and a least squares fit to a total of 1444 cross spectra they determined the amount of energy in the internal wave field and in various "contaminations." Their result is shown in Figure 4. The part denoted internal waves is that energy consistent with linear free internal wave motion on a smooth background stratification. The contaminations consist of a fine structure contamination of the displacement field and a fine structure and noise contamination of the current field. The current fine structure contamination is a substantial part of the observed current fluctuations. It represents about 5 percent of the energy at near inertial frequencies, about half of the energy at mid–frequencies, and most of the energy at high frequencies.

Müller et al. [1978] only determined the energy level

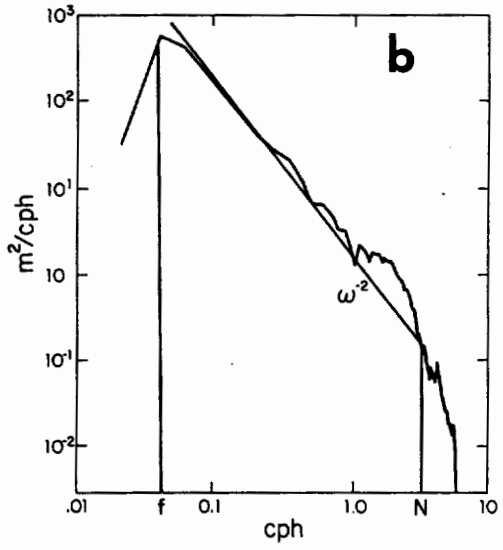

Fig. 2b. Frequency spectrum of the vertical displacement of an isotherm measured by an instrumented capsule yo–yoing at a nominal depth of 350 m in a location 800 km offshore of southern California [from *Cairns and Williams*, 1976].

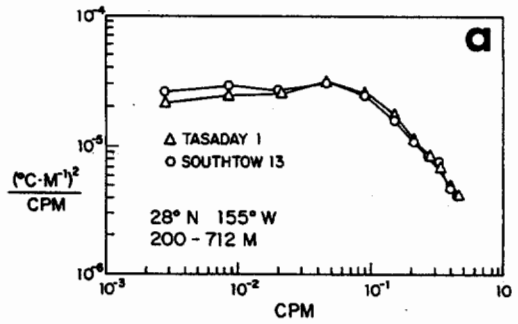

Fig. 3*a*. Vertical wave number spectra of the temperature gradient for two stations in the North Pacific [from *Gregg*, 1977].

and the approximate scales of the contaminations. Current and temperature fine structure are two–dimensional fields with vertical coherence scales smaller than about 10 m and horizontal coherence scales larger than a few hundred meters. The current noise is a three–dimensional field with vertical and horizontal coherence scales smaller than about 10 m. The further kinematical properties of the contaminations were not analyzed.

Other experiments yielded similar results. From a microstructure sensing array, *Eriksen* [1978] found that the current shear and density gradient over a 7–m vertical scale are dominated by current and density fine structure. More recently, *Pinkel* [1985] found from the analysis of conductivity, temperature, and depth and Doppler sonar data that a significant part of the current shear is concentrated at high frequencies and inconsistent with linear internal wave motion.

Note that the IWEX experiment determined lower bounds for the amount of non–internal wave motion. The analysis determined the fraction of the observed fluctuations that is consistent with linear internal wave motion. If a single time series, say of vertical displacement, is considered, all variance between f and N is consistent with linear internal wave motion. If a current time series from the same location is added linear internal wave theory requires a certain frequency–dependent ratio of potential to kinetic energy [*Fofonoff*, 1969]. The observed deviation from this ratio is a measure of how much energy is inconsistent with linear internal wave motion. As more and more instruments at other locations are added, more and more of the observed variance might turn out to be inconsistent with linear internal waves. An experiment with an accuracy and resolution larger than that of the IWEX experiment might, therefore, give even larger contaminations.

Temperature fine structure is generally viewed as either being part of the irreversible background stratification or being due to the nonlinear straining of a smooth density profile by internal waves [*Desaubies and Gregg*, 1981]. The fine structure induced by linear straining appears as an internal wave contribution in the IWEX decomposition. The analysis of *Desaubies and Gregg*, [1981] and *Johnson et al.* [1978] suggests that most of the density variance at vertical scales larger than a few meters is due to straining, linear and nonlinear. Current fine structure is often viewed as low–frequency internal wave motion that has small vertical scales or appears to have small vertical scales because of the fine structure in the density profile. P. Müller (unpublished manuscript, 1985) argues, however,

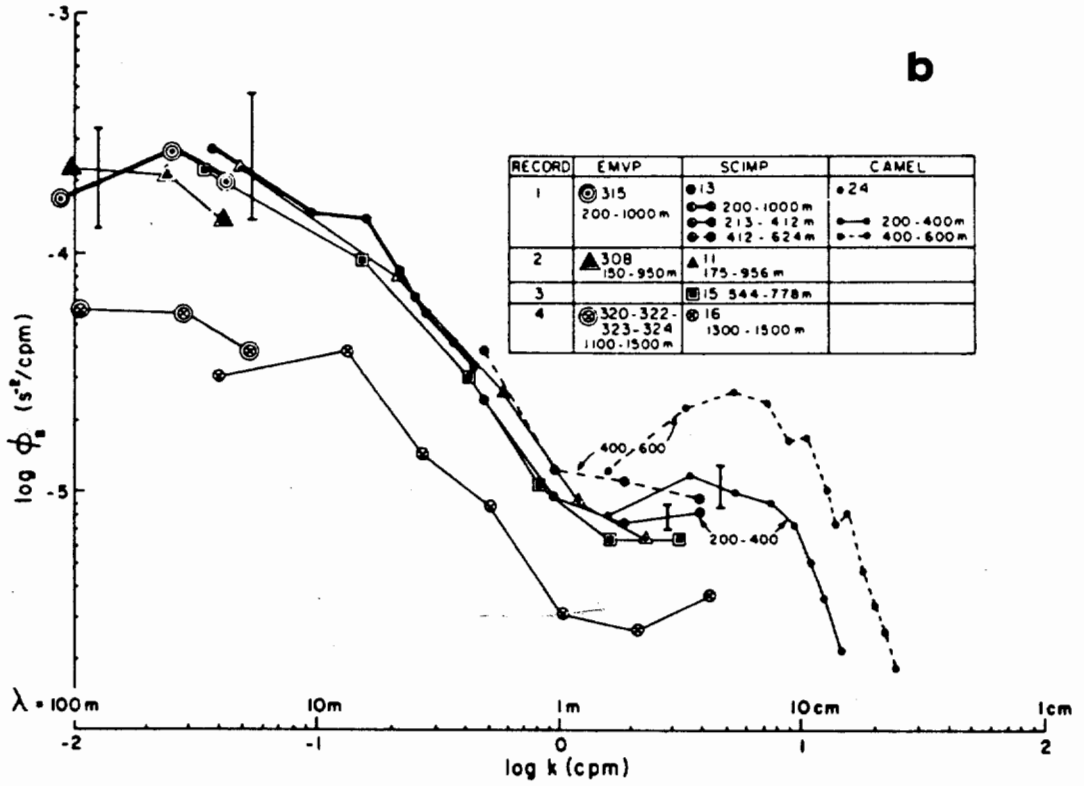

Fig. 3*b*. Composite vertical wave number spectra of the vertical shear measured by the three different profilers in four locations in the northwest Atlantic [from *Gargett et al.*, 1981].

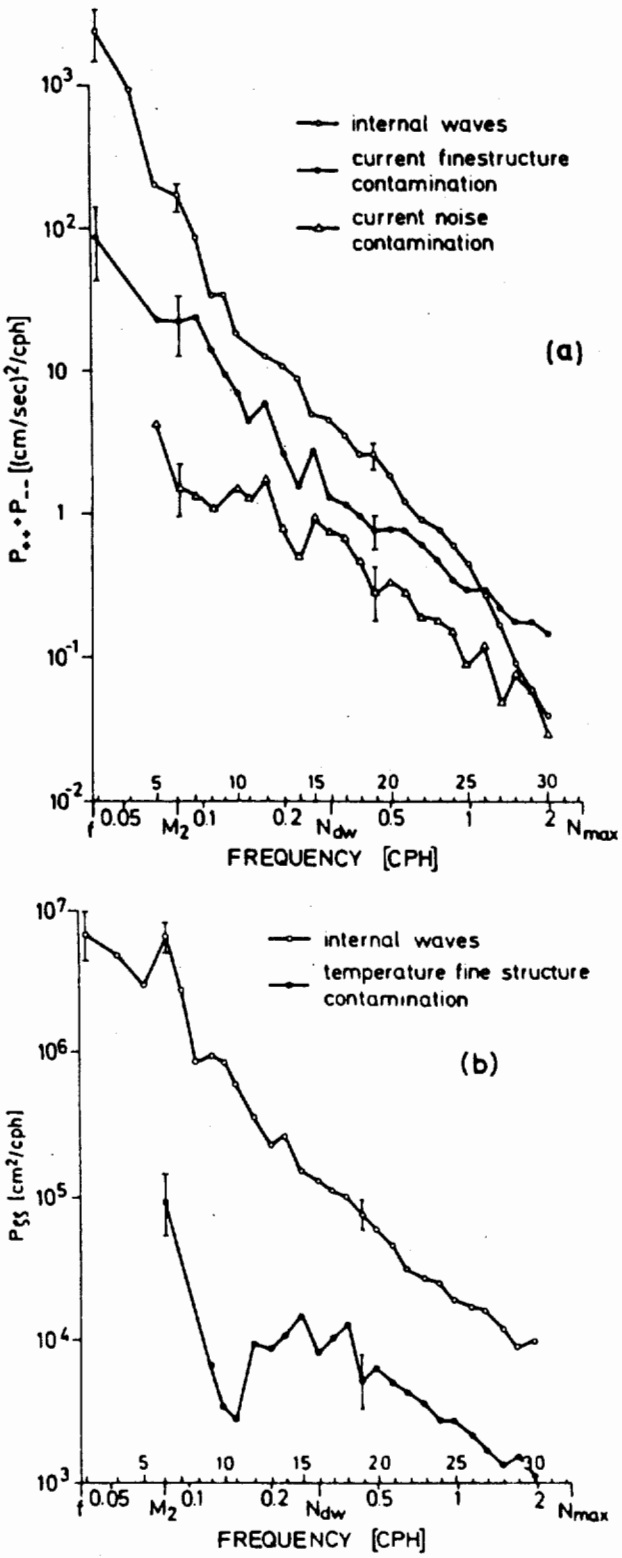

Fig. 4. Partition of the observed (*a*) horizontal current and (*b*) vertical displacement spectrum during IWEX into internal waves, current and temperature fine structure, and current noise [from *Müller et al.*, 1978].

that these two models are inconsistent with the IWEX data and suggests that current fine structure represents vortical motion.

The IWEX and other experiments indicate that the kinematic structure of the fluctuations in the internal wave band is not as well established as sometimes believed. The ambiguities are not particularly problematic for the energy which is concentrated at near–inertial frequencies and at large wave numbers. In this range the fluctuations are fairly consistent with free linear internal wave motion. This is not true for the shear, which is concentrated at small vertical scales. The *Garrett and Munk* [1975] spectrum assigns most of the shear to near–inertial internal waves. It is, however, not known which mode of motion, whether the internal gravity or vortical mode, and which frequencies and horizontal wave numbers contribute to the shear. The kinematic structure of the oceanic shear must be regarded as unknown.

The Garrett and Munk Spectrum

The diverse internal wave measurements have been combined by Garrett and Munk into a convenient model spectrum to describe the distribution of internal wave energy in wave number–frequency space. This model spectrum assumes that the fluctuations are linear internal waves, i.e., satisfy the internal wave amplitude and dispersion relation. In time this model spectrum has been improved [*Garrett and Munk*, 1972*b*; *Garrett and Munk*, 1975; *Cairns and Williams*, 1976; *Desaubies*, 1976]. The latest version [*Munk*, 1981] is formulated in discrete vertical modes for an exponentially stratified ocean

$$N(z) = N_0 e^{z/b} \tag{14}$$

with $N_0 = 5.2 \times 10^{-3}\,s^{-1}$ and $b = 1.3$ km. The model assumes horizontal isotropy. The energy spectrum per unit mass as a function of frequency ω and mode number j is given in the separable form

$$E(\omega, j) = b^2 N_0 N E_0 B(\omega) H(j) \tag{15}$$

where

$$H(j) = \frac{1}{j^2 + j_*^2} \Big/ \sum_{j=1}^{\infty} \frac{1}{j^2 + j_*^2} \qquad \sum_{j=1}^{\infty} H(j) = 1 \tag{16a}$$

$$B(\omega) = \frac{2}{\pi} \frac{f}{\omega} \frac{1}{(\omega^2 - f^2)^{1/2}} \qquad \int_f^N dw\, B(\omega) = 1 \tag{16b}$$

and $E_0 = 6 \times 10^{-5}$ and $j_* = 3$. The normalization of the frequency spectrum implies $f \ll N$. The mode number spectrum decays with a slope $t = -2$ for $j \gg j_*$; the frequency spectrum decays with a slope $r = -2$ away from $\omega = f$. To calculate other spectra and to convert to different representations the WKB approximation to the wave functions and dispersion relation is used. The spectra of the vertical displacement and of the horizontal velocity then become

$$F_\xi(\omega, j) = \frac{1}{N^2} \frac{\omega^2 - f^2}{\omega^2} E(\omega, j) \tag{17a}$$

$$F_u(\omega, j) + F_v(\omega, j) = \frac{N^2 - \omega^2}{N^2} \frac{\omega^2 + f^2}{\omega^2} E(\omega, j) \tag{17b}$$

Instead of discrete standing modes it is often convenient to introduce a continuum of upward and downward pro-

pagating modes with local vertical wave number

$$k_z = \pm k_h \left(\frac{N^2 - \omega^2}{\omega^2 - f^2} \right)^{1/2} \tag{18}$$

The discrete spectrum (15) then implies vertical symmetry (equal amount of upward and downward propagating energy) and corresponds to the continuous spectrum

$$E(\omega, k_z)\, d\omega\, dk_z = \frac{1}{2} E(\omega, j)\, d\omega\, \delta j \tag{19}$$

where the relation between the mode index j and the vertical wave number k_z is given by the WKB approximation of the dispersion relation. In the hydrostatic limit, $\omega << N$, this relation takes the simple form

$$|k_z| = \frac{\pi}{b} \frac{N}{N_0} j \tag{20}$$

The continuous model spectrum (19) is usually referred to as GM76.

The model spectra (15) or (19) can be used to calculate all second-order moments of the internal wave field. To keep the shear and the rate of strain finite, a cutoff wave or mode number must be introduced. If this cutoff wave number is taken to be the wave number where the temperature gradient and the shear spectra (Figure 3*b*) start to roll off (about 0.1 cpm), the Richardson number and the rate of strain become of order one [*Munk*, 1981].

The above model spectra provide the basis for most dynamical calculations. We must keep in mind that the model spectra assume that the observed fluctuations are linear internal waves, an untested assumption in some parts of wave number–frequency space.

3. RESONANT INTERACTIONS

Discrete Interactions

Resonant interactions were discovered in the fluid dynamical context by *Phillips* [1960, 1961] who noted that two waves with phases $\mathbf{k}_1 \cdot \mathbf{x} - \omega_1 t$ and $\mathbf{k}_2 \cdot \mathbf{x} - \omega_2 t$ force a third wave with the sum and difference phase. If this third wave is a free wave, i.e., if wave number and frequency satisfy the resonance conditions,

$$\mathbf{k}_1 \pm \mathbf{k}_2 = \mathbf{k}_3 \tag{21a}$$

$$\omega_1 \pm \omega_2 = \omega_3 \tag{21b}$$

where $\omega_i = \Omega(\mathbf{k}_i)$ is the dispersion relation, energy is systematically transferred from the two waves into the third wave. Whether or not the resonance condition (21) can be met depends on the structure of the dispersion relation. For internal waves there are many solutions to the resonance condition.

The general approach to resonant nonlinear interactions starts from the equations of motion. For a quadratically nonlinear system these may be cast into the form [*Hasselmann*, 1966, 1967]

$$\dot{a}_3 + i\omega_3 a_3 = -\epsilon i \omega_3 \sum_{k_1 + k_2 = k_3} \Gamma_{-312}\, a_1 a_2 \tag{22}$$

Here a_i denotes the wave amplitude of wave i with wave number vector $\mathbf{k}_i$ and eigenfrequency ω_i. Γ_{-312} is the coupling coefficient and ϵ a small parameter characterizing the weakness of the nonlinear interactions.

To lowest order in ϵ, the solution represents a free linear wave

$$a_i = \alpha_i e^{-i\omega_i t} \tag{23}$$

with constant amplitude α_i. If the nonlinear interactions are included the amplitude becomes a slowly varying function in time, $\alpha_i = \alpha_i(t)$.

For a discrete triad of waves that is exactly in resonance, i.e., that satisfies $\mathbf{k}_1 + \mathbf{k}_2 = \mathbf{k}_3$ and $\omega_1 + \omega_2 = \omega_3$, the evolution of the amplitude is governed by

$$\begin{aligned} \dot{\alpha}_1 &= -\epsilon i \omega_1 \Gamma^* \alpha_2{}^* \alpha_3 \\ \dot{\alpha}_2 &= -\epsilon i \omega_2 \Gamma^* \alpha_1{}^* \alpha_3 \\ \dot{\alpha}_3 &= -\epsilon i \omega_3 \Gamma\, \alpha_1 \alpha_2 \end{aligned} \tag{24}$$

where $\Gamma = \Gamma_{-312}$. From these equations it is found that the energy $E_i = \alpha_i \alpha_i{}^*$ and momentum $\mathbf{P}_i = (\alpha_i \alpha_i{}^*/\omega_i)\, \mathbf{k}_i$ of the interacting waves are conserved:

$$\begin{aligned} \sum_{i=1}^{3} E_i &= \text{const.} \\ \sum_{i=1}^{3} \mathbf{P}_i &= \text{const.} \end{aligned} \tag{25}$$

whereas action $A_i = (\alpha_i \alpha_i{}^*/\omega_i)$ changes according to

$$\partial_t A_1 = \partial_t A_2 = -\partial_t A_3 \tag{26}$$

The equations for interacting waves are analogous to the equations for interacting particles. Within this analogy action represents the number of waves [*Hasselmann*, 1966, 1967]. The number of waves is not necessarily conserved. In the above resonant triad, two waves interact and produce one third wave.

Transport Theory

Transport theory is concerned with the interaction of many triads of waves, almost all of which are off-resonant. However, the effect of such interactions can be expressed in terms of resonant interactions, and a closed evolution equation for the energy density spectrum $E_{\mathbf{k}} = <|a_{\mathbf{k}}^2|>$ can be derived, if appropriate conditions are satisfied. To understand these conditions, we outline some of the steps required to derive this evolution equation for quadratic nonlinearities. A more rigorous derivation for quadratic and higher-order nonlinearities using a systematic multiple time scale perturbation expansion can be found in *Hasselmann* [1966, 1967] and *Benney and Saffman* [1966].

First, we rewrite equation (22) in terms of the variable α_j:

$$\dot{\alpha}_3 = -\epsilon i \omega_3 \int dk_1 dk_2 \Gamma\, \alpha_1 \alpha_2 e^{-i\Delta t}\, \delta(k_1 + k_2 - k_3) \tag{27}$$

where we have written $\Delta = \omega_3 - \omega_1 - \omega_2$ and taken the continuum limit

$$\sum_k \rightarrow \int dk \ .$$

Now make the following suppositions:

1. There exists a "slow time scale" T such that α_1 and α_2 can be considered constant during the interval $0 < t < T$. Equation (27) can then be integrated to give

$$\alpha_3(t) - \alpha_3(0) = -\epsilon i\omega_3 \int dk_1\, dk_2 \Gamma\, \alpha_1(0)\alpha_2(0) \cdot e^{\frac{-i\Delta t}{2}} \frac{\sin\frac{\Delta t}{2}}{(\Delta/2)} \delta(k_1 + k_2 - k_3), \tag{28}$$

2. The "correlation time" of the wave field is short compared with T so that all modes are statistically independent at the start of any such interval. Then multiplying each mode of (28) by its complex conjugate yields

$$\langle |\alpha_3(t)|^2 \rangle - \langle |\alpha_3(0)|^2 \rangle = \left(\epsilon\omega_3\right)^2 \int dk_1\, dk_2 |\Gamma|^2 \langle |\alpha_1(0)|^2 \rangle \langle |\alpha_2(0)|^2 \rangle \frac{\sin^2\frac{\Delta t}{2}}{(\Delta/2)^2} \delta(k_1 + k_2 - k_3) \tag{29}$$

plus similar terms. As t increases, the quantity $\sin^2(\Delta t/2)/(\Delta/2)^2$ weights the integral on the right-hand side of (29) to ever smaller Δ values. If t becomes infinite, the replacement

$$\frac{\sin^2\frac{\Delta t}{2}}{(\Delta/2)^2} := t\pi\delta(\Delta) \tag{30}$$

would be exact. However, according to assumption 1, t is finite; therefore $\sin^2(\Delta t/2)/(\Delta/2)^2$ has a width $\Delta \approx 2\pi/t > 2\pi/T$ which cannot be neglected. The replacement (30) is only likely to be accurate if the third assumption holds:

3. The variation of $|\Gamma|^2 \langle |\alpha_1(0)|^2 \rangle \langle |\alpha_2(0)|^2 \rangle$ is small (the spectrum and coupling coefficients are "smooth") over that width.

If all these conditions are met, one obtains the transport equation

$$\frac{\langle |\alpha_3(t)|^2 \rangle - \langle |\alpha_3(0)|^2 \rangle}{t} \approx \frac{\partial E_3}{\partial t} = \left(\epsilon\omega_3\right)^2 \int dk_1\, dk_2 |\Gamma|^2 \langle |\alpha_1(0)|^2 \rangle \langle |\alpha_2(0)|^2 \rangle \pi\delta(\Delta)\delta(k_1 + k_2 - k_3) \cdots \tag{31}$$

which is a closed evolution equation for the spectrum. The basic statistical closure hypothesis is the assumption 2 which states that the right-hand side of (29) can be determined under the assumption that all mode amplitudes are statistically independent or Gaussian. It is shown in statistical mechanics [*Prigogine*, 1962] that this assumption is correct for infinitely weak nonlinear coupling among dispersive wave modes. A dispersive, weakly nonlinear wave field rapidly attains and never departs much from a Gaussian state.

For internal waves the transport equation takes the explicit form

$$\frac{\partial}{\partial t} A(\mathbf{k}) = \int d\mathbf{k}'d\mathbf{k}'' \Big\{ T^+ \delta(\mathbf{k} - \mathbf{k}' - \mathbf{k}'') \delta(\omega - \omega' - \omega'') \cdot [A(\mathbf{k}')A(\mathbf{k}'') - A(\mathbf{k})A(\mathbf{k}') - A(\mathbf{k})A(\mathbf{k}'')] + 2T^- \delta(\mathbf{k} - \mathbf{k}' + \mathbf{k}'') \delta(\omega - \omega' + \omega'') [A(\mathbf{k}')A(\mathbf{k}'') + A(\mathbf{k})A(\mathbf{k}') - A(\mathbf{k})A(\mathbf{k}'')] \Big\} \tag{32}$$

where $A(\mathbf{k}) = (E(\mathbf{k})/\omega(\mathbf{k}))$ is the action density spectrum and T^+ and T^- are transfer functions depending on $\mathbf{k}, \mathbf{k}'$, and $\mathbf{k}''$. Explicit expressions for T^+ and T^- can be found in the works by *Müller and Olbers*, [1975] and *Olbers* [1976]. The transfer equation can be interpreted in terms of two colliding waves or antiwaves creating or annihilating a third wave or antiwave with collision cross-sections T^+ and T^-. The δ functions assure that the collision process conserves energy and momentum.

Transfers in the Garrett and Munk Spectrum

The transfer equation (32) has explicitly been derived and evaluated for the Garrett and Munk (GM) spectrum by three different groups. These are *Olbers,* [1976], *McComas and Bretherton*, [1977], and *Pomphrey et al.*, [1980]. All these groups were motivated by similar goals but used slightly different approaches and different codes for the numerical evaluation of the transfer integral.

The common goals are at least threefold. The first one is to understand to what extent the Garrett and Munk spectrum represents an equilibrium or steady state solution for nonlinear interactions. The second goal is the determination of relaxation rates for disturbed spectra. These relaxation rates are also needed in theories which deal with other aspects of the dynamics of internal waves, for example, in the calculation of internal wave induced diffusion coefficients [*Müller*, 1976]. The third major goal is the determination of the energy flux through the spectrum, supposedly from low to high wave numbers. This energy flux provides the energy source for mixing processes in the ocean. One might hence get an estimate of mixing from the nonlinear interaction calculation, without understanding and evaluating all the complicated breaking and overturning processes that lead to mixing.

All three groups start with the equations of motion in their Lagrangian form. This is advantageous because it automatically insures the symmetry of the coupling coefficients and hence the conservation of energy and momentum. The interaction with the vortical mode of motion is excluded since the linear solutions are assumed to be proportional to $\exp\{-i\omega t\}$, whereas the displacements of the linear vortical mode ($\omega = 0$) increase linearly with time. Olbers defines the pressure fluctuations by

$$\pi'(\mathbf{r},t) = p_L(\mathbf{r},t) - \tilde{p}(r_z) \tag{33a}$$

whereas *McComas and Bretherton and Pomphrey* et al. define it by

$$\pi'(\mathbf{r},t) = p_E(\mathbf{r},t) - \tilde{p}(r_z) \tag{33b}$$

Here $p_L(\mathbf{r}, t)$ is the Lagrangian pressure, i.e., the pressure of a fluid particle at time t which was at position $\mathbf{r}$ at time

$t = 0$; $p_E(\mathbf{r}, t)$ is the Eulerian pressure, i.e., the pressure of the fluid particle which is at position r at time t; and $\bar{p}$ is a prescribed background or equilibrium pressure. This difference in definition does not affect the lowest–order quadratic interaction terms, only the higher–order terms. An Eulerian approach also yields an identical lowest–order interaction term. For all approaches the transfer functions T^+ and T^- are the same on the resonance surface. The lowest–order resonant interactions are independent of representation [*Henyey and Pomphrey*, 1983]. The structure of the transfer functions off the resonant surfaces and their possible dependence on the representation of the wave field has, however, not been systematically investigated yet. The major difference between the three groups is that Olbers and McComas and Bretherton represent the internal wave field as a continuum of vertically propagating waves whereas Pomphrey et al. represent the wave field as a discrete set of vertically standing waves. Minor differences are that Olbers uses the *Garrett and Munk* [1975] model spectrum for his calculation whereas McComas and Bretherton and Pomphrey et al. use the GM76 [*Cairns and Williams*, 1976] model spectrum and employ the hydrostatic approximation.

Despite the differences in the representation of the wave field, in the numerical codes and in the display of the results, the results from all these groups are mutually consistent. For the discussion of these results it is convenient to rewrite the transport equation in the form

$$\frac{\partial}{\partial t} A(\mathbf{k}) = -2\nu_p(\mathbf{k}) A(\mathbf{k}) + I(\mathbf{k}) \tag{34}$$

where

$$\nu_p(\mathbf{k}) = \frac{1}{2}\int d\mathbf{k}' d\mathbf{k}'' \Big\{ T^+ \delta(\mathbf{k}-\mathbf{k}'-\mathbf{k}'')\delta(\omega-\omega'-\omega'') \big[A(\mathbf{k}')+A(\mathbf{k}'')\big] + 2T^- \delta(\mathbf{k}-\mathbf{k}'+\mathbf{k}'') \delta(\omega-\omega'+\omega'')\big[A(\mathbf{k}'')-A(\mathbf{k}')\big]\Big\} \tag{35}$$

and

$$I(\mathbf{k}) = \int d\mathbf{k}' d\mathbf{k}'' \Big\{ T^+ \delta(\mathbf{k}-\mathbf{k}'-\mathbf{k}'')\delta(\omega-\omega'-\omega'') + 2T^- \delta(\mathbf{k}-\mathbf{k}'+\mathbf{k}'')\delta(\omega-\omega'+\omega'')\Big\} A(\mathbf{k}')A(\mathbf{k}'') \tag{36}$$

Here $2\nu_p(\mathbf{k})$ is the rate at which wave–wave interactions scatter energy out of wave number $\mathbf{k}$ whereas $I(\mathbf{k})/A(\mathbf{k})$ is the rate at which resonant interactions between other waves force energy into wave number $\mathbf{k}$. The rate ν_p is the Langevin rate when (34) is viewed as the transport equation for a Langevin type equation of motion. It is also the decay rate of *McComas'* [1977] spike experiments and the fast decay rate of *McComas and Müller* [1981*a*] since $\partial_t A(\mathbf{k}) \rightarrow -2\nu_p(\mathbf{k}) A(\mathbf{k})$ for a narrow spike at wave number $\mathbf{k}$.

The overall rate at which the spectrum changes is given by the Boltzmann rate

$$2\nu_B(\mathbf{k}) = \frac{\partial_t A(\mathbf{k})}{A(\mathbf{k})} \tag{37}$$

and the rate of energy input into wave number $\mathbf{k}$ by

$$2\nu_F = \frac{I(\mathbf{k})}{A(\mathbf{k})} = 2\nu_B + 2\nu_p \tag{38}$$

The result of a typical calculation of the Botzmann rate ν_B is shown in Figure 5 from *McComas*, [1977]. Figure 5*a* shows the spectral density of the GM76 spectral model as a function of vertical wave number and frequency. Figure 5*b* shows the interaction time $\tau = (2\nu_B)^{-1}$ for that spectrum. The interaction time changes from a few days at low wave numbers to tens of minutes at high–wave numbers. The Langevin rate ν_p for the GM76 spectrum as a function of frequency and mode number is shown in Figure 6, from Pomphrey (1981). Beyond the straight long–dashed line the Langevin rate is larger than the frequency. Figures 5 and 6 give a first view of the characteristic time scales of resonant wave–wave interactions in the GM model spectrum. The Boltzmann rate describes the evolution of the smooth spectrum, and the Langevin rate the decay of spikes in the spectrum or the relaxation of a distorted spectrum to a smooth spectrum. Small Boltzmann rates indicate that the spectrum is approximately in equilibrium with respect to nonlinear interaction. The normalized Boltzmann rate

$$R = \frac{\nu_B}{\nu_F} = \frac{\nu_B}{\nu_B + \nu_p} \tag{39}$$

is shown in Figure 7 as a function of mode number and frequency for the GM76 spectrum. In the "steady" region, R is smaller than 0.1. In the "nonsteady" region the transfer is from the low mode number region to the high mode number–low–frequency region.

Basic Interaction Mechanisms

The above results represent the basic findings of the resonant wave–wave calculations. They were obtained by the complicated yet straightforward numerical evaluation of the transfer integral. Some understanding into this mathematical exercise was brought by *McComas and Bretherton* [1977] who discovered that much of the complicated transfers can be understood in terms of three simple limiting interaction mechanisms. This simplification is made possible because the transfer functions $T^{\pm}(\mathbf{k},\mathbf{k}',\mathbf{k}'')$ in the source function (32) vary much less than the action density spectra $A(\mathbf{k})$. To demonstrate this, contours of $|T^-|$ are plotted in Figure 8 as a function of k''_h/k_h and k'_h/k_h. For a given horizontal wave number $\mathbf{k}_h$ wave triads that satisfy $\mathbf{k}_h - \mathbf{k}_h' \pm \mathbf{k}_h'' = 0$ must lie within the open rectangle, the "kinematic box." In most parts of the box, $|T^-|$ is seen to vary much less than the GM spectrum. Thus, the signature and strengths of the nonlinear transfers are mostly determined by the structure of the GM spectrum, with the transfer strongest where there exists an action imbalance between triad members.

The three interaction mechanisms identified by McComas and Bretherton are termed elastic scattering, induced diffusion and parametric subharmonic instability. Typical wave triads for these interaction mechanisms are shown in Figure 9. Elastic scattering denotes the backscatter of a downward propagating high–frequency wave $(\mathbf{k}', \omega')$ into an upward propagating wave $(\mathbf{k}, \omega)$ by a low–frequency near–inertial wave $(\mathbf{k}'', \omega'')$. See Figure 9*a*. The incident and the reflected wave have nearly the same frequency

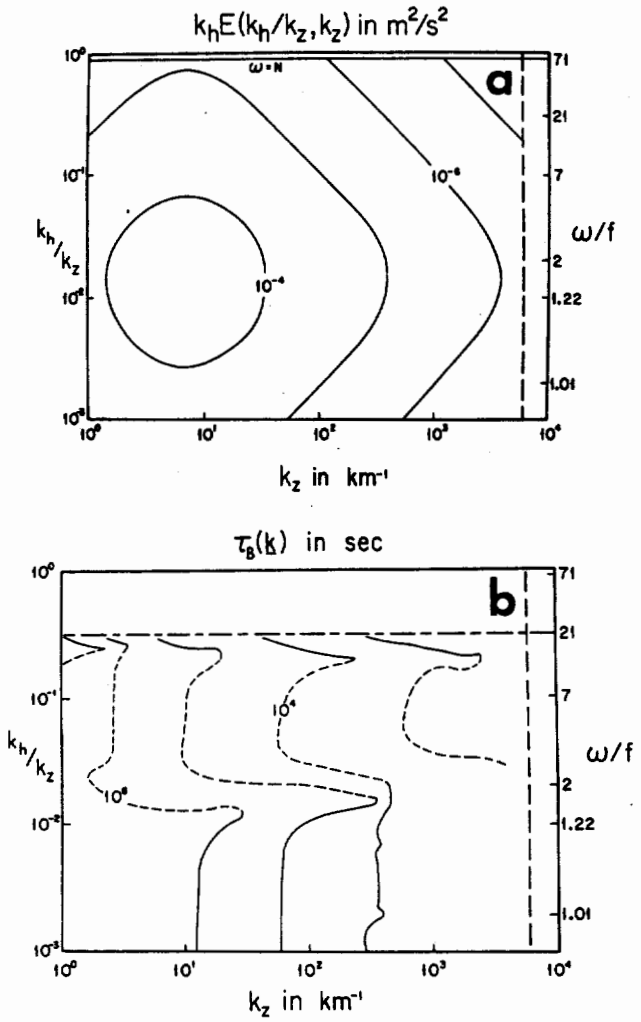

Fig. 5. (*a*) Spectral density and (*b*) interaction time $\tau_B = (2\nu_B)^{-1}$ for the unperturbed GM76 spectrum as a function of vertical wave number k_z and aspect ratio k_h/k_z or frequency. Dashed contours in Figure 5*b* represent negative values. No interactions are allowed for waves of frequency greater than $\omega = 0.3$. $N = 21\,f$ in order to simplify numerical procedure [from *McComas*, 1977].

and horizontal wave number, but their vertical wave numbers are almost the opposite of each other. The third component, the low–frequency component, has almost twice the vertical wave number, i.e., $|k_z''| \approx 2|k_z''| \approx 2|k_z|$. Elastic scattering is similar to Bragg scattering at a low–frequency field. There is little energy exchange with the low–frequency component. Elastic scattering transfers energy out of the more energetic of the high–frequency waves to the other until their energies are equal. This process acts only in vertically asymmetric spectra and efficiently damps out any asymmetries in the high–frequency part of the spectrum. The symmetric GM model spectrum is in equilibrium with respect to elastic scattering.

The elastic scattering mechanism describes the backscatter of high–frequency internal waves by low–frequency inertial currents. High–frequency waves are also backscattered by low–frequency density fluctuations, i.e., by the irreversible fine structure of the density stratification. This scattering process has the same effect on asymmetries and is of similar efficiency [*Mysak and Howe*, 1976; *McComas and Müller*, 1981*a*].

Induced diffusion (ID) denotes the interaction of small–scale waves with large–scale waves. More precisely, it is the scattering of a high–frequency, high–wave number wave $(\mathbf{k}, \omega)$ by a low–frequency, low–wave number wave (k'', ω'') into another nearby high–frequency, high–wave number wave $(\mathbf{k}', \omega')$. See Figure 9*b*. This process can also be viewed as a small–scale wave packet propagating through random waves with scales much larger than the ones of the packet (see section 5). The wave packet experiences random perturbations of its wave number as it propagates through the large–scale wave field. It prescribes a random walk. The packet forgets its initial wave number and the root–mean–square deviation grows linearly in time. Since action is conserved [*Bretherton and Garrett*, 1968] the random walk leads to diffusion of wave action in wave number space. The shear of the large–scale waves is responsible for this diffusion. For the Garrett and Munk spectrum the vertical shear of the horizontal current is the largest. Hence diffusion in vertical wave number space is dominant. The ID mechanism governs the nonlinear interactions in the high–frequency, high–wave number range of the spectrum (denoted by "steady region" in Figure 7).

Parametric subharmonic instability (PSI) is the decay of a large–scale wave $(\mathbf{k}, \omega)$ into two small–scale waves $(\mathbf{k}', \omega')$ and $(\mathbf{k}'', \omega'')$ of approximately half the frequency. See Figure 9*c*. This interaction is the parametric subharmonic instability of a system where the parameters defining the natural frequencies vary with time. The most prominent example is a simple pendulum whose length is changed at twice the natural frequency of the pendulum. In the internal wave problem the primary effect is that the large–scale wave changes the buoyancy frequency of the

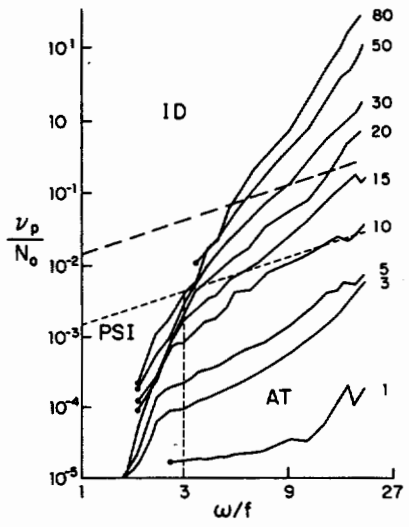

Fig. 6. Normalized Langevin rate ν_P for the GM76 spectrum as a function of frequency for various vertical mode numbers. Above the long–dashed line the Langevin rate is larger than the frequency. The short–dashed lines separate regions where the nonlinear interactions are dominated by induced diffusion (ID), parametric subharmonic instability (PSI) and an "assortment of triads" (AT) [from *Pomphrey*, 1981].

small–scale waves. This effect has been clearly seen in the laboratory [*McEwan and Robinson*, 1975]. The PSI mechanism is responsible for the transfer from low–to high–wave number near–inertial oscillations (from the positive to the negative region in Figure 7).

Induced Diffusion

To assess quantitatively the role of the basic interaction mechanisms in shaping the spectrum one needs to evaluate their transfer rates. This can be done by taking the appropriate limits in the transfer integral. For the ID mechanism one finds

$$\frac{\partial}{\partial t}\tilde{A}(\mathbf{k}) = \frac{\partial}{\partial k_z} D_\zeta \frac{\partial}{\partial k_z}\tilde{A}(\mathbf{k}) \tag{40}$$

with a diffusion coefficient [*McComas and Müller*, 1981*a*]

$$D_\zeta = \pi k_h^2 f^{-1} S\left(\frac{f}{\omega} k_z\right) \tag{41}$$

where

$$S(k_z) = f\,|\,k_z\,|^3 A(k_z) \tag{42}$$

is the shear content spectrum. The diffusion equation (40) describes the evolution of the high–frequency, high–wave number part of the spectrum, indicated by a tilde in (40). Wave action diffuses in vertical wave number space only. The diffusion coefficient depends on the shear content of the low–frequency near–inertial oscillations at which the high–frequency waves scatter. Also, the diffusion coefficient depends on the vertical wave number in general.

The action of the high–frequency, high–wave number region is conserved:

$$\frac{\partial}{\partial t}\tilde{A}(\mathbf{k}) + \frac{\partial}{\partial k_z}\tilde{Q}_A(\mathbf{k}) = 0 \tag{43}$$

where

$$\tilde{Q}_A(\mathbf{k}) = -D_\zeta \frac{\partial}{\partial k_z}\tilde{A}(\mathbf{k}) \tag{44}$$

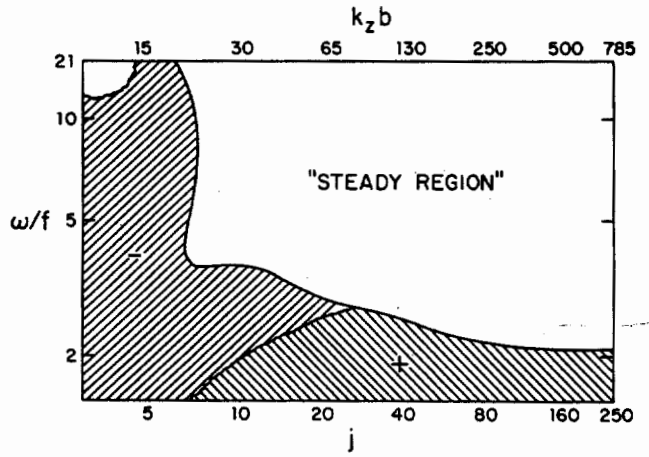

Fig. 7. Frequency–vertical mode number plane showing the energy growth (plus sign) and energy decay (minus sign) regions for the GM76 spectrum. The "steady region" is where $R = \nu_B/\nu_F \leq 0.1$ [from *Pomphrey*, 1981].

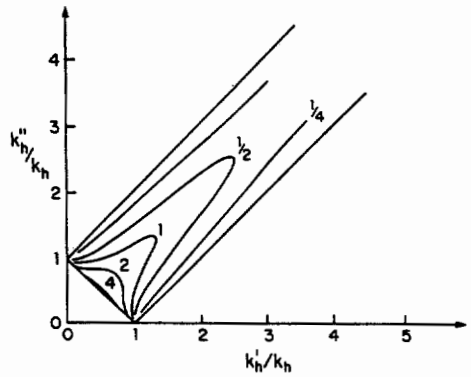

Fig. 8. Contours of the transfer function $|\,T^{-}\,|$ as a function of k_h''/k_h and k_h'/k_h. For a given horizontal wave number vector $\mathbf{k}_h$ the wave triads that satisfy $\mathbf{k}_h - \mathbf{k}'_h \pm k_h'' = 0$ must lie within the open rectangle [from *Pomphrey*, 1981].

is the action flux. The energy of the high–frequency, high–wave number region is, however, not conserved. The energy equation takes the form

$$\frac{\partial}{\partial t}\tilde{E}(\mathbf{k}) + \frac{\partial}{\partial k_z}\tilde{Q}_E(\mathbf{k}) - \frac{1}{\omega}\frac{\partial \omega}{\partial k_z}\tilde{Q}_E(\mathbf{k}) = 0 \tag{45}$$

where

$$\tilde{E}(\mathbf{k}) = \omega \tilde{A}(\mathbf{k})$$

is the energy density and

$$\tilde{Q}_E(\mathbf{k}) = \omega \tilde{Q}_A(\mathbf{k})$$

the energy flux. The last term in (45) describes the energy exchange of the high–frequency, high–wave number region with the low–frequency waves which cause the diffusion.

When calculating the characteristic rate of change

$$2\nu(\mathbf{k}) = \frac{1}{\tilde{A}(\mathbf{k})}\frac{\partial}{\partial k_z} D_\zeta \frac{\partial}{\partial k_z}\tilde{A}(\mathbf{k}) \sim \frac{D_\zeta \Delta \tilde{A}}{(\Delta k_z)^2 \tilde{A}} \tag{46}$$

we must distinguish two cases. One rate corresponds to the fastest possible time scale, which one obtains by choosing the maximum gradients, i.e., $\Delta\tilde{A}/\tilde{A} \sim 1$ and $\Delta k_z \sim k''_z \sim (f/\omega)\, k_z$. This yields the relaxation or Langevin rate

$$2\nu_p(\mathbf{k}) = \pi\omega \frac{1}{N^2}\left(\frac{\omega}{f}\right)^3 S\left(\frac{f}{\omega} k_z\right) \tag{47}$$

For smooth spectra, $(\Delta\tilde{A}/\Delta k_z) \sim (\tilde{A}/k_z)$ is a more realistic approximation and yields the Boltzmann rate

$$2\nu_B(\mathbf{k}) = \pi\omega \frac{1}{N^2}\frac{\omega}{f} S\left(\frac{f}{\omega} k_z\right) \tag{48}$$

These analytical approximations reproduce remarkably well the complete transfer integrals. This can be inferred from Figure 10 which compares the relaxation rate (47) with the full evaluation of the transfer integral.

Contour plots of the two diffusion time scales are shown in Figure 11 for the GM76 spectrum. The slow time scale $(2\nu_B)^{-1}$ describes changes in a smooth spectrum. The fast time scale $(2\nu_p)^{-1}$ describes the relaxation of spikes in the spectrum. It can be seen that smooth spectra vary slowly,

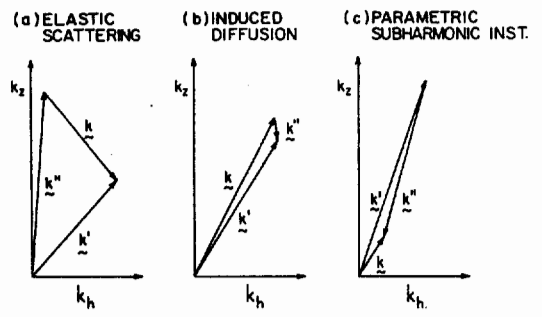

Fig. 9. Schematic representation of (*a*) elastic scattering, (*b*) induced diffusion and (*c*) parametric subharmonic instability triads in a vertical–horizontal wave number plane [from *McComas and Müller*, 1981*a*].

whereas superimposed spikes decay rapidly, indicating some sort of equilibrium for the high–wave number, high–frequency part of the GM spectrum. What kind of equilibrium is this? The diffusion equation (40) has two stationary solutions for the high–frequency, high–wave number spectrum $\tilde{A}(\mathbf{k})$: a no–action–flux solution where the spectrum $\tilde{A}(\mathbf{k})$ is independent of k_z (equipartition of action) and a constant–action–flux solution where the action flux $\tilde{Q}_A(\mathbf{k}) = -D_\zeta\,(\partial/\partial k_z)\,\tilde{A}(\mathbf{k})$ is independent of k_z. The GM76 spectral model has a high–wave number slope of $t = -2$ at all frequencies. Such a slope makes the action density spectrum $\tilde{A}(\mathbf{k})$ independent of k_z. The present analysis hence implies that the GM76 spectrum represents a no–action–flux solution and does not support any diffusive action flux to high–wave numbers.

In a search for a more appealing constant–action–flux solution *McComas and Müller* [1981*a*] made a distinction between the wave number slopes at high and low–frequencies. If the low–frequency slope is $t = -2$ then $D_\zeta \sim k_z^2$ and a high–frequency slope of $t = -3$ represents a constant–action–flux solution. If the low–frequency slope is $t = -2.5$ then $D_\zeta \sim |k_z|$ and a high–frequency slope very close to $t = -2$ represents a constant–flux solution. They argue that this latter case might be realized in the ocean since vertical wave number spectra of currents, which are sensitive to the energy at low–frequencies, often show slopes close to $t = -2.5$ whereas spectra of the vertical displacement, which are sensitive to the energy at high–frequencies, show slopes around $t = -2$.

A constant–action–flux solution, however, is also not easy to interpret. Consider such a solution, as shown in Figure 12. At vertical wave number $k_z = \beta_1$ a constant–action–flux $\tilde{Q}_A$ enters the hatched region. At vertical wave number $k_z = \beta_2$ the same flux leaves the region. Action is conserved; $\partial_t \tilde{A} = 0$. The energy flux into the region is $\omega_1 \tilde{Q}_A$. The energy flux out of the region is $\omega_2 \tilde{Q}_A$. Since action is diffused in vertical wave number space at a constant horizontal wave number it follows that $\omega_1 > \omega_2$. Hence the energy flux out of the region is smaller than that entering. A constant–action–flux solution leads to a convergent energy flux. This can also be inferred from the energy equation (45). For a stationary spectrum the divergence of the energy flux and the energy exchange with the low–frequency waves must balance.

The energy equation (45) also shows that a constant energy flux solution, $\tilde{Q}_E(\mathbf{k})$ independent of k_z, is not a stationary solution for the high–frequency, high–wave number spectrum $\tilde{E}(\mathbf{k})$. *McComas and Müller* (1981*b*), however, proved that a constant energy flux solution at high–wave numbers leads to a stationary vertical wave number spectrum $E(k_z) = \int d\mathbf{k}_h\, E(\mathbf{k})$ where the integration is over all horizontal wave numbers or, equivalently, over all frequencies, high and low.

Finally, we mention that the no–action–flux solution or the equipartition of action can be derived using statistical mechanics, and that this result is connected with the more familiar state of equipartition of energy. For this derivation we regard the high–frequency, high–wave number waves as the test waves and the low–frequency, low–wave number waves as the background. The energy of the total system is conserved, and so is the action of the test waves, in a linearized treatment. Let E_j and A_j denote the energy and action in wave mode j. Then the probability density for wave action (in a grand canonical ensemble) is $g \exp(-\beta E_j + \mu A_j)$. Here, β is the "inverse temperature" of the system, μ is the "chemical potential" for wave action, and g is a normalization factor. Thus, the expectation value (denoted by angle brackets) of the wave action is

$$\langle A_j \rangle_{TW} = g \int_0^\infty dA_j\, A_j \exp(-\beta E_j + \mu A_j) = \frac{1}{\beta\omega_j + \mu} \tag{49}$$

while the background waves, whose action is not conserved, have

$$\langle A_j \rangle_{BG} = \frac{1}{\beta\Omega_j} \tag{50}$$

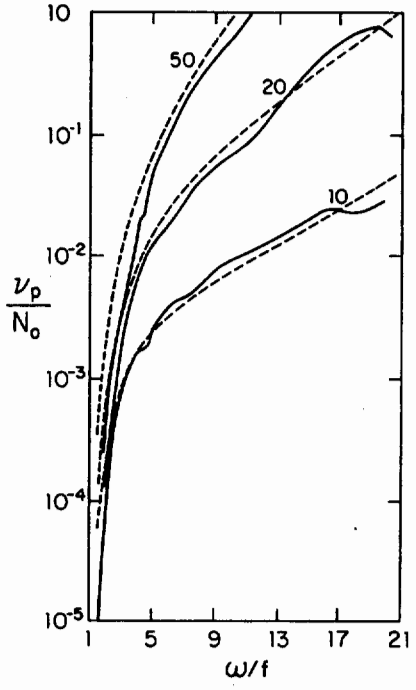

Fig. 10. Comparison between the Langevin rate calculated from the dominant induced diffusion transfer mechanism (equation (47)) (dashed) and the numerical evaluation of the complete transfer integral for three different vertical mode numbers [from *Pomphrey et al.*, 1980].

Here, ω_j denotes the frequencies of the test waves and Ω_j the frequencies of the background waves.

The development of the induced diffusion equation has ignored the effect of the small scale test waves on the background, since the background is much more intense than the test wave field. Thus, built into the theory is the assumption that

$$< A_j >_{TW} \ll < A_j >_{BG} \tag{51}$$

In fact, the test wave action should be infinitesimal compared with the background action. Thus $\beta\omega_{TW} \ll \mu$ and $< A_j >_{TW} = 1/\mu$, independent of j; i.e., action is equipartitioned. The dominance of $\beta\omega_{TW}$ over μ would have given the contrary (but more familiar) result, that energy is equipartitioned.

Parametric Subharmonic Instability

The parametric subharmonic instability mechanism (PSI) is an instability wherein a low–wave number wave decays into two high–wave number waves of half the frequency. Because of the specific structure of the internal wave dispersion relation this mechanism is most efficient at low frequencies. Assuming $A(\mathbf{k}')$, $A(\mathbf{k}'') \ll A(\mathbf{k})$ and

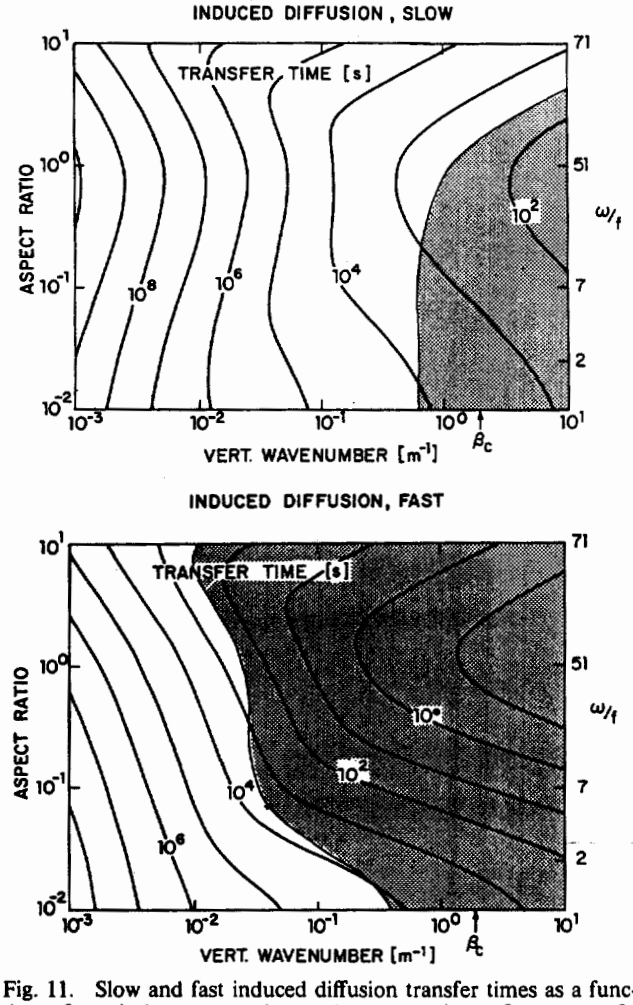

Fig. 11. Slow and fast induced diffusion transfer times as a function of vertical wave number and aspect ratio or frequency. In the shaded areas the transfer times are 2π times smaller than the wave periods [from *McComas and Müller*, 1981*a*].

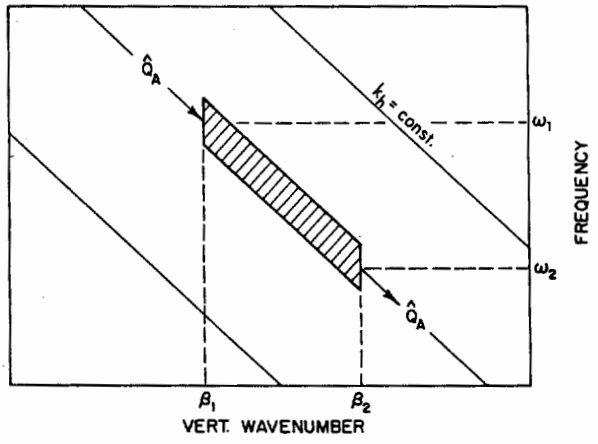

Fig. 12. Schematic representation of the constant–action–flux solution. If there is a constant action flux through the hatched region, energy will be transferred out of that region and accumulate in the low–frequency, low–wave number waves which cause the diffusion [from *McComas and Müller*, 1981*b*].

$\omega \sim 2\omega' \sim 2\omega'' \sim 2f$ and $|k_z| \ll |k'_z|, |k''_z|$ one finds that high–wave number near–inertial oscillations are generated at a rate

$$\frac{\partial}{\partial t} A(\mathbf{k}') = 4A(\mathbf{k}') \int d^3k\, T^{-} \delta [\omega - \omega' - \Omega(\mathbf{k} - \mathbf{k}')] A(\mathbf{k}) \tag{52}$$

where $T^{-} = 9/16\pi k_h^2 f$. The PSI mechanism hence supports a downscale energy flux into near–inertial oscillations. Explicitly, the growth rate is given by

$$2\nu_B(\mathbf{k}') = \frac{27}{4}\pi \frac{f^2}{N^2} S\left(\frac{k'_z}{x'}, 2f\right) \tag{53}$$

where

$$x' = \left(\frac{3}{2}\,\frac{f}{\omega' - f}\right)^{1/2} \tag{54}$$

The growth rate of the high–wave number near–inertial waves depends on the shear content of the double–frequency wave with a wave number x' times smaller. The factor x' arises because near–inertial waves $(\mathbf{k}', \omega')$ can only be generated by double frequency waves $(\mathbf{k}, \omega)$ with vertical wave numbers $|k_z| \leqslant (|k'_z|/x')$, because of the resonance constraints. The GM average value of x' is about $\sqrt{10}$.

The PSI mechanism dominates the nonlinear transfers for the high–wave number near–inertial oscillations and (53) is a good representation of the transfer rates for these waves. The PSI mechanism, however, does not dominate the transfers for the low–wave number double–frequency wave.

Since the frequency resonance requires $\omega' + \omega'' = \omega$ and since $\omega', \omega'' \geqslant f$, the unstable wave, ω, must have a frequency larger than $2f$. The PSI mechanism hence transfers energy out of the $4f - 2f$ frequency band into the $f - 2f$ band. All transfers are contained in this region from $f - 4f$. We can hence define a one–dimensional energy flux by

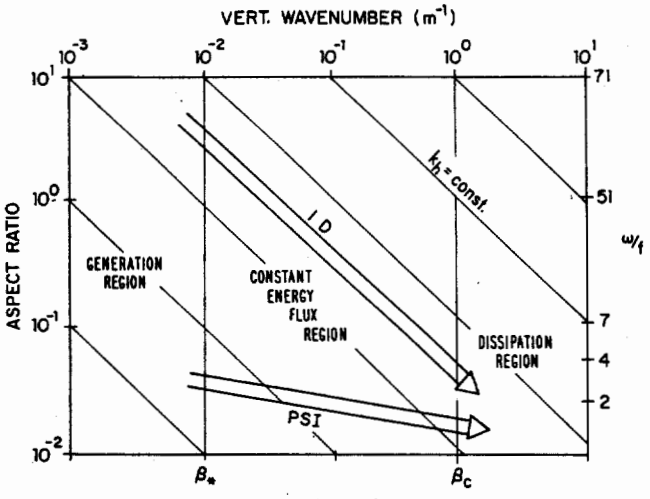

Fig. 13. Schematic representation of the dynamical balance of *McComas and Müller* [1981*b*]. Energy is generated at low vertical wave number $|k_z| < \beta_*$. Between β_* and β_c there is an inertial range where the ID mechanism at high frequencies and the PSI mechanism at low frequencies provide a constant energy flux to high wave numbers $|k_z| > \beta_c$, where energy is dissipated. The wave number β_c is determined as the wave number where the spectrum must roll off because the nonlinear transfer can no longer keep up with dissipation.

$$\frac{\partial}{\partial t} E(k_z) + \frac{\partial}{\partial k_z} Q_E(k_z) = 0 \tag{55}$$

The flux $Q_E(k_z)$ can be calculated by integrating over the growth (or decay) region of the spectrum (see Figure 7). For the GM76 spectrum *Pomphrey et al.* [1980] obtain a value of

$$\int_{-h}^{0} dz\, Q_E(k_z) \approx 6.4 \times 10^{-4}\ W\,m^{-2} \tag{56}$$

Equilibrium with respect to the PSI mechanism requires $A(\mathbf{k}') \sim A(\mathbf{k}'') \sim 2A(\mathbf{k})$ or $E(\mathbf{k}') \sim E(\mathbf{k}'') \sim E(\mathbf{k})$. Partial equilibrium may be obtained by increasing the energy of inertial waves, i.e., by an inertial peak. The primary effect of the PSI mechanism is hence the creation of an inertial peak. The GM spectrum is not in equilibrium. Its inertial peak is not sufficiently pronounced. Energy is still transferred from high to low-frequencies, as calculated above. The observed inertial peak is also partly due to a latitudinal turning-point effect [*Munk*, 1980; *Fu*, 1981].

In the GM spectrum the PSI and ID mechanism represent the low- and high-frequency limits of the transfers at high vertical wave numbers. High vertical wave number waves with frequencies close to f interact mainly with low-wave number waves of twice the frequency. This is the PSI mechanism. High vertical wave number waves with frequencies much larger than f interact mainly with low-wave number, low-frequency waves. This is the ID mechanism. In the intermediate frequency range the transfers are not dominated by any particular scale selective interaction triad.

Dynamic Balance

An attempt to fit the resonant interaction calculations into a complete and consistent model of the dynamics of the internal wave field was put forward by *McComas and Müller*, [1981*b*]. Their model assumes that internal wave energy is generated at low vertical wave numbers $|k_z| < \beta_*$ and dissipated at high vertical wave numbers $|k_z| > \beta_c$. See Figure 13. McComas and Müller then prove analytically that there exists an inertial range between β_* and β_c in which resonant interactions provide a constant (independent of vertical wave number) downscale energy flux from the generation to the dissipation region. At high-frequencies the flux is provided by the induced diffusion mechanism, and at low frequencies by the parametric subharmonic instability mechanism (see Figure 13). The inertial range has a stationary vertical wave number spectrum

$$E(k_z) \propto k_z^{-2} \tag{57}$$

as observed. This vertical wave number dependence cannot be obtained from simple dimensional arguments because the dominant transfer mechanisms (the ID and the PSI mechanisms) are nonlocal in wave number space. Dimensional arguments lead to $E(k_z) \propto |k_z|^{-3}$. The downscale energy flux under the PSI mechanism is given by

$$Q_E^{PSI} = \frac{27}{32\sqrt{10}} \frac{\pi f}{N^2} E^2 \beta_*^2 \tag{58}$$

The flux depends on the total energy E and the wave number bandwidth β_*. Both dependencies are quadratic so that a ten-fold change in either of them results in a hundred-fold change of the energy flux. The downscale flux under the ID mechanism is determined by matching with the low-frequency region. It has the same functional dependence on f, N, E, and β_* and constitutes 40% of the total flux. The total energy flux $Q_E = Q_E^{\psi} + Q_E^{ID}$ determines the overall dissipation time scale

$$\tau_{diss} = \frac{E}{Q_E} \tag{59}$$

The wave number β_c at which the spectrum must roll off because the nonlinear interactions cannot keep up with dissipation can be determined from the fact that the flux at β_* must be equal to the flux at β_c. This yields

$$\beta_c = \frac{S}{\beta_* E} \tag{60}$$

where S is the total shear of the internal wave field. Note that β_c decreases as the energy level of the spectrum and the energy flux through the spectrum increase. These are the principal results of McComas and Müller's theory. They hold for any spectrum as long as the energy is concentrated at low, and shear at high, vertical wave numbers. They are based on the dominance of the ID and PSI mechanisms. For the GM76 spectrum their formulas yield an energy flux at the surface of

$$Q_E(z = 0) = 1.5 \times 10^{-6}\ W\,m^{-3} \tag{61}$$

and a depth dependence

$$Q_E(z) \sim N^2(z) \tag{62}$$

since $E \sim N$ and $\beta_* \sim N$ for the GM spectrum. The vertically integrated energy flux is

$$\int dz Q_E(z) = 10^{-3}\ W\,m^{-2} \tag{63}$$

The flux due to the PSI mechanism is 0.6×10^{-3} W m^{-2}, in excellent agreement with *Pomphrey et al.*'s [1980] values (equation (56)). The overall dissipation time scale has a surface value

$$\tau_{\text{diss}}(z = 0) = 20d \tag{64}$$

and increases with depth as

$$\tau_{\text{diss}}(z) \sim N^{-1}(z) \tag{65}$$

If a fraction δ of the energy flux is used for mixing, the equivalent mixing coefficient K_v is determined by

$$\rho_o K_v N^2 = \delta Q_E \tag{66}$$

For $\delta = 0.2$ [*Thorpe*, 1973] we find

$$K_v = 10^{-5} \text{ m}^2 \text{ s}^{-1} \tag{67}$$

independent of depth. This value is roughly consistent with kinematic estimates (which are based on the statistics of the frequency and thickness of mixing events) and with estimates from microstructure measurements [*Garrett*, 1984]. However, there are also observational and theoretical results which conflict with some of the above results. Direct observations of kinetic energy dissipation rate ϵ, which we would expect to scale as Q_E, (cf. (62)), have been made in the upper kilometers of the ocean. They tend to show ϵ increasing with increasing N but not so rapidly as N^2. *Gargett and Osborn* [1981] and *Lueck et al.*, [1983] show results closer to $\epsilon \propto N^{+1}$ but with significant uncertainty in the exponent. If indeed $Q_E \propto N^{+1}$, then (66) implies $K_v \propto N^{-1}$. Inferred K_v from many environments characterized by a wide range of N also appear to support $K_v \propto N^{-1}$ and hence, by (66), $Q_E \propto N$ [*Gargett*, 1984]. However, the depth dependence of K_v is far from being established and much more data are needed to draw definite conclusions. A theoretical discussion by *Gargett and Holloway* [1984] also suggests $\epsilon \propto N$ with $K_v \propto N^{-1}$, an item to which we return in section 4.

The roll-off wave number β_c is independent of depth if one assumes a constant Richardson number, since Ri = constant implies $S \sim N^2$. For GM76 parameters and $Ri = 1$ one finds

$$\beta_c = 1.3 \text{ m}^{-1} \sim 0.2 \text{ cpm} \tag{68}$$

Both the constancy with depth and the value are consistent with the observed roll-off of the shear spectrum (see Figure 3 and *Gargett et al.*, [1981].

McComas and Müller's [1981*b*] balance predicts the slope and roll-off wave number β_c of the observed vertical wave number spectrum. It is, however, not a complete balance. It does not explain the energy E, the wave number bandwidth β_*, and the shear S. These are expected to depend on the specifics of the generation and dissipation processes. The balance only predicts the energy flux Q_E and the roll-off wave number β_c, given E, S, and β_*.

Besides these principal limitations McComas and Müller's balance also has difficulties in predicting a stationary frequency spectrum. Under the ID mechanism the high-frequency region loses energy, which is gained by the near-inertial waves which cause the diffusion. Only in combination is the vertical wave number spectrum stationary. Further, the PSI mechanism removes energy from the $4f-2f$ band and transfers it into the $2f-f$ band at smaller scales. As long as there is a downscale flux this mechanism will deplete the upper frequency band and fill the lower one. To analyze the mechanisms which compensate for these frequency transfers McComas and Müller analyzed results of a time-stepping model that includes all interacting triads, not just the ID and PSI mechanism. From this model and their analytic balance the roles of resonant wave-wave interactions in shaping the internal wave spectrum can be summarized as follows:

1. The primary effect of nonlinear interaction is to make the spectrum symmetric at high-wave numbers (by the elastic scattering mechanism), smooth at high-wave numbers and high-frequencies (by rapid diffusion with the fast time scale), and to create an inertial peak (by the parametric subharmonic instability mechanism). The observed spectra are symmetric and smooth and are in equilibrium with respect to the first primary processes. The observed inertial peak is, however, not sufficiently pronounced to be in equilibrium with respect to the PSI mechanism.

2. The secondary effect of the nonlinear interactions is to adjust the spectrum to deliver a constant downscale flux under the PSI and ID mechanisms. This creates a transfer in frequency space which is a tertiary effect and is balanced by nonidentifiable interactions.

Relaxation

The relaxation of distorted spectra is characterized by the Langevin rate (35) which describes the decay of spikes in an otherwise smooth (equilibrium) spectrum. This decay rate has been calculated for the GM spectrum by *McComas*, [1977], *Pomphrey et al.* [1980], and *McComas and Müller* [1981*a*]. *McComas* [1977] also calculated the relaxation rates for a vertically asymmetric GM spectrum with 10 percent more energy in the upward than in the downward propagating waves. However, observed and theoretically predicted deviations from the GM spectrum are more complicated. See, for example, *Frankignoul*, [1974], *Wunsch* [1976], *Wunsch and Webb* [1979], *Eriksen* [1982], *Pinkel* [1983], and *Briscoe and Weller* [1984] for observed deviations from the smooth, vertically symmetric, horizontally isotropic, stationary GM spectrum. No attempts have yet been made to calculate relaxation rates for such more complicated and realistic distortions.

Relaxation rates of distorted spectra also occur in various theories. A background shear flow causes the internal wave field to become increasingly more asymmetric and anisotropic. *Müller* [1976] argues that this increase is balanced by resonant wave-wave interactions which tend to reestablish a symmetric and isotropic state. Such a balance gives rise to an internal wave momentum flux which is proportional to the shear of the background flow. The effect of the internal wave on the background flow can hence be described by wave-induced viscosity coefficients. To calculate these viscosity coefficients accurately one needs the relaxation rate for a certain asymmetric and anisotropic spectrum. This rate has never been calculated. Using instead the Boltzmann rate from early calculations of *Olbers* [1976], Müller estimated a vertical internal wave-induced viscosity coefficient A_V of about 0.4 m^2 s^{-1}.

Ruddick and Joyce [1979] showed from data that A_V cannot be larger than 0.02 $m^2 s^{-1}$ in magnitude, and is uncertain in sign. Müller's overestimate is, however, not so much due to his inaccurate relaxation rate but to his failure to realize that much of the GM76 spectrum shows equipartition of wave action in vertical wave number space and hence does not interact with vertical background shear. His estimate of the horizontal viscosity coefficient is $A_H = 10\ m^2 s^{-1}$, smaller than the recently observed value of $100\ m^2\ s^{-1}$ [*Brown and Owens,* 1981] which is, however, hard to reconcile with the observed long lifetime of some mesoscale features.

C. S. Cox and C. L. Johnson (unpublished manuscript, 1979) suggested that internal wave energy does not radiate but diffuses in physical space, in much the same way that heat diffuses in crystals. The reason for this diffusion lies in the nonlinear wave–wave interactions, or phonon–phonon interactions in crystals. The specifics of Cox and Johnson's theory require the relaxation rate for an anisotropic spectrum. More recently, *Eriksen,* [1985] calculated the spectrum which results when an incident GM spectrum is reflected off of a sloping bottom and showed that it grossly differs from the incidental spectrum. The reflected spectrum exhibits strong enhancement and horizontal anisotropy over a frequency band centered at the critical frequency. Within a few hundred meters off the bottom the spectrum is observed [*Eriksen,* 1982] to relax back to its GM form, supposedly by nonlinear interactions. Relaxation calculations for the reflected spectrum have not been carried out yet. Since the observed adjustment is so rapid, a comparison of the calculated and observed relaxation might provide a critical test for theories of nonlinear interactions.

Validity

The *McComas and Müller* [1981*b*] balance and all the other work described in this section are based upon the resonant interaction approximation (RIA). As discussed, almost all of the possible interactions are off–resonant, and thus not described by RIA. However, for sufficiently small amplitudes, resonant interactions become very much more efficient than off–resonant interactions. For infinitely small amplitudes the transport equation (32) becomes exact. The outstanding question then is whether or not RIA is applicable for actual oceanic wave amplitudes. To answer this question one has to check whether or not the various suppositions leading to the RIA transport equation are met for actual oceanic amplitudes. A rigorous test is the comparison of the theoretical bispectrum arising from RIA interactions with the actually observed bispectrum [*Hasselmann et al.,* 1963]. Unfortunately, numerical computations by *McComas and Briscoe* [1980] indicate that the level of the bispectrum is too low and too contaminated to be detected by any reasonable observational programs. The validity of RIA has thus been assessed (and criticized) using simplified criteria.

One such simplified criterion for the validity of RIA is

$$\nu/\omega < 1 \tag{69}$$

The nonlinear transfer rate ν of a given wave should be smaller than the frequency of the wave. How well a criterion such as (69) needs to be satisfied is not known. Simple heuristics might suggest that nonlinear transfer ought not modify a wave by $O(1)$ on a time scale shorter than the wave period $2\pi/\omega$, suggesting that the right side of (69) be more of the order of $(2\pi)^{-1}$. However, even the applicability of these criteria is open to question, as we will discuss below. *Holloway* [1980] applied a criterion such as (69) to the early calculations by *McComas* [1977]. Given a GM background spectrum, McComas made RIA calculations for the relaxation of a narrow–band perturbation ("spike") to the spectrum. At high–frequencies and high wave numbers it was found that the spike relaxation time was very much less than a wave period. See Figures 6 and 11 where the ranges are indicated in which ν exceeds ω. *Holloway* [1980] then pointed to the McComas spike experiments to argue that RIA is not applicable at GM amplitudes.

A couple of points of ambiguity need be noted. *McComas and Müller* [1981*a, b*] have argued that RIA could remain valid for a smoothly varying spectrum such as GM although invalid for spike type features such as those of *McComas* [1977]. On the contrary, as mentioned by *Holloway* [1980] and developed more carefully by *Holloway* [1982], the fast process of spike relaxation does remain appropriate for smooth spectra, although the relaxation process may be masked by other fast processes of wave–wave excitation.

Another point of ambiguity arises because the GM spectrum is quite "red," i.e., most energy is concentrated at low wave numbers. It is this energy at low wave numbers which contributes substantially to the fast interaction rates at high–wave numbers. Yet, is it the case that these high–wave number waves are being created and destroyed so rapidly? A similar question occurred during the early development of modern turbulence theory [*Kraichnan,* 1965; *Kadomtsev,* 1965] and is discussed in relation to finite amplitude wave–wave interactions by *Holloway* [1979]. The concern is that the interaction rate reflects, in part, advection of short waves by large–scale velocity fields due to energetic long waves. If treated deterministically and in the limit of infinite scale separation, the result is to Doppler–shift the frequency by $\delta\omega = \mathbf{u}\cdot\mathbf{k}$. However, statistical treatments recognize only large–scale energy, hence rms speed u, leading to a frequency broadening by "random Doppler shifting" $u\cdot k$ which appears in ν. To the extent that high interaction rates may describe a random but coherent quasi–translation, it would seem possible that RIA is not so severely violated.

The third point of ambiguity is that the criterion (69) might not be adequate. The ratio ν/ω describes how well waves are fit by the linear dispersion relation, i.e., how closely the energy is distributed around the dispersion curves (see Figure 1). For a randomly forced oscillator the criterion for the validity of RIA is [*Van Kampen,* 1981]

$$\nu_I \tau_c << 1 \tag{70}$$

Here, ν_I is the interaction rate roughly identifiable with ν above, and τ_c is the correlation time of the random force. The parameter $\nu_I\tau_c$ is called the "Kubo number" [*Kubo,* 1962]. The equations describing nonlinear wave–wave interaction are certainly more complicated than the stochastic oscillator equation, yet it is reasonable to expect

that a simplified criterion for the validity of RIA will involve a product of a nonlinear interaction rate with a correlation time of the "background," instead of (69). In most situations it is, however, hard at best and perhaps not even meaningful to define the "background" and a single correlation time scale.

Ideally, we would hope that a theory for finite amplitude, or "strong," interactions could be developed. If such a theory contained RIA as a limit, then the domain of validity of RIA as well as the nature of breakdown of RIA could be examined. One such analysis described by *Holloway* [1979] shows that the criterion of validity of RIA will involve a "group period" defined by a characteristic group length divided by group speed. Then it is seen that the product of transfer rate by group period must be less than unity to support RIA. This restriction may be more severe than (69).

There is a further worrisome possibility that RIA may be a "singular" limit of finite amplitude theory (though not in a mathematical sense), and thus could lead to qualitatively as well as quantitatively incorrect results. *Carnevale and Frederiksen* [1983] make the interesting observation that, if the frequency resonance condition is strictly imposed, then resonant wave–wave interactions preserve (linear) vertical wave momentum $\int d\mathbf{k}\, E(\mathbf{k})\, (k_z/\omega)$. However, if slight off–resonant interactions are permitted then, after sufficiently long time, vertical wave momentum may be quite altered. In this sense Carnevale and Frederiksen suggest that resonant interactions are a "singular" limit of weak interactions.

Both the high interaction rates at high–wave numbers and the conservation of linear vertical wave momentum have cast considerable doubt on the RIA calculations and spurred efforts to explore the alternate approaches discussed in the next three sections.

4. STRONG INTERACTIONS

Major impediments stand in the way of accomplishing a successful, strong interaction theory. First, the deductive basis for such a theory is not at all well established. Second, the technical complexity and, especially, computational requirements will be difficult to overcome. Here, we sketch some considerations and some of the efforts made to date to extend the resonant interaction approximation (RIA).

Given the uncertain state of development, this section is necessarily eclectic. Systematic derivations following the direct interaction approximation (DIA) have only been carried out to a point, the most thorough evaluation being performed under a two–dimensional (vertical plane) idealization. To provide a broader view, we recall certain classical constructions from stably stratified turbulence, i.e., a limit of very strong interaction. Further, it is seen that some results from DIA will suggest an alternative to the more classical stratified turbulence theories. Finally, these developments may be related to the previous discussion in section 3 concerning dissipation and diffusion.

Holloway [1980, 1981] speculates that two steps will be needed. First, all RIA efforts thus far have been based upon a Lagrangian derivation of the equations of motion which consists of an expansion in powers of the small fluid particle displacements about hypothetical equilibrium positions. Hence, there is already a small amplitude restriction built into the derived equations of motion. Moreover the Lagrangian derivation omits modes of motion associated with zero eigenfrequency, i.e., the vortical motion field. Interactions among internal waves and vortical modes loom as one of the important questions to be addressed by a strong interaction theory. To meet these challenges may require returning to a formulation based upon the Boussinesq equations for the evolution of the velocity and density fields. The second item raised by Holloway is the need to carry out a renormalization of the spectral evolution equations in the spirit of the DIA of *Kraichnan* [1959]. The random Doppler shift problem, mentioned in the previous section, is a known defect of DIA and may pose special difficulty for the renormalization of internal wave interaction theory. Whereas *Holloway* [1980, 1981] offers only speculative suggestions, actual calculations using the DIA equations have been made by *DeWitt and Wright* [1982, 1984] and by *Carnevale and Frederiksen* [1983].

Direct Interaction Approximation

DeWitt and Wright [1982, 1984, hereafter DWW] do not attempt to deal with arbitrarily strong interactions but rather seek to obtain a small–amplitude correction to RIA and, in so doing, to provide a broader interpretation of RIA methods and results. DWW adopt the Lagrangian–derived equations after *Olbers* [1976], and proceed to obtain evolution equations for the ensemble–averaged second–order correlation and response functions. Methods followed by DWW are in the spirit of quantum field theory [*Kadanoff and Baym*, 1962], following particularly the Feynman path integral formalism after *Phythian* [1977]. In the language of diagrammatic expansions, by retaining the lowest–order propagator renormalization and omitting vertex renormalization, DWW write out the DIA equations for the problem as posed by Olbers. (Note our previous caution that a truncated Lagrangian derivation already has a small–amplitude limitation and an incompleteness problem.)

However, even at this level of approximation, the equations require inordinate computer effort to evaluate, so DWW consider a more limited problem. In the DIA equations there occurs an expression for "self–energy," denoted $\Sigma_1(\mathbf{k},\omega)$ by DWW. In the RIA limit, Σ_1 reduces to the damping rate ν_p (see equation (35)), which is independent of ω. The defining equation for Σ_1 contains Σ_1 itself. When $\Sigma_1 = \nu_p$ is substituted DWW find a Σ_1 with a strong dependence on ω in the induced diffusion region. When they solve self–consistently for a frequency–independent Σ_1, as in their second paper, they find a value for Σ_1 which differs from ν_p. Both these results suggest that corrections to the RIA are important. On a more general level, DWW both establish the connection between internal wave interaction theory and more general methods of physics and also reveal the substantial difficulties that will be anticipated in efforts to devise an adequate strong interaction theory.

A different and rather a bold effort has been undertaken by *Carnevale and Frederiksen* [1983, henceforth CF] following the formalism from *Martin, et al.* [1973]. In order

to pose a more tractable problem, CF consider a two–dimensional idealization in which all motion is restricted to lie in a vertical plane. Although this restriction is certainly unrealistic with regard to oceanic internal waves, the remaining problem is non–trivial and allows exploration of strong internal gravity wave–wave interactions. Moreover, as will be seen in section 6, the vertical plane problem has received substantial attention as an object for numerical simulation. Explicit testing of theoretical hypotheses becomes a possibility, as seen in the works by *Frederiksen and Bell* [1983, 1984].

CF make their derivation from the Eulerian field equations for density and vorticity, thereby avoiding amplitude and completeness questions associated with Lagrangian–based derivations. Linear recombination of density and vorticity allows the problem to be recast in complex wave amplitude coefficients $A_{\mathbf{k}}^{s}(t)$ where $s = \pm 1$ denotes nominal left/right–going waves. Mean rotation is omitted, so wave eigenfrequencies are not bounded away from zero. CF then develop the DIA equations for the evolution of second–order correlation and response functions. In addition, CF include slow spatial variation of average properties and hence obtain terms related to quasi–homogeneity.

The derivation of CF is rather formalistic. To provide some interpretation, further simplifying assumptions are made. The problem is limited to single time correlations while reference to response functions is omitted by assuming a "fluctuation–dissipation relation" [*Leith*, 1971] between the response function and two–time correlation function. Further, CF assume no cross–correlation between left– and right–going waves of equal $\mathbf{k}$. It should be emphasized that the latter assumption, termed "diagonal dominance," is not necessary and was only made by CF for convenience and clarity of results. The assumption of diagonal dominance places a small–amplitude restriction in a theory which, otherwise, might describe very strong interactions. In particular, cross–correlation of left– and right–going waves is the mechanism which supports vertical mass flux. However, should one consider nondissipative absolute statistical equilibrium, then the vertical mass flux will vanish and diagonal dominance will be satisfied for large–amplitude motions also.

A main point in CF is to obtain a quantity termed "triad relaxation time," denoted $\Phi_{s_1 s_2 s_3}(\mathbf{k},\mathbf{p},\mathbf{q},\mathbf{X},T)$ by CF. Effectively, Φ is a multiplier in the interaction among waves $(\mathbf{k},s_1)$, $(\mathbf{p},s_2)$ and $(\mathbf{q},s_3)$ at slowly varying coordinates $(\mathbf{X},T)$. The expression for Φ has a form

$$\Phi_{s_1 s_2 s_3}(\mathbf{k},\mathbf{p},\mathbf{q},\mathbf{X},T) = \left(\mu_{\mathbf{k}}^{s_1} + \mu_{\mathbf{p}}^{s_2} + \mu_{\mathbf{q}}^{s_3}\right) \Big/ \left[\left(\hat{\Omega}_{\mathbf{k}}^{s_1} + \hat{\Omega}_{\mathbf{p}}^{s_2} + \hat{\Omega}_{\mathbf{q}}^{s_3}\right)^2 + \left(\mu_{\mathbf{k}}^{s_1} + \mu_{\mathbf{p}}^{s_2} + \mu_{\mathbf{q}}^{s_3}\right)^2\right] \tag{71}$$

where $\mu_{\mathbf{k}}^{s}$ is a relaxation rate or "frequency broadening" and $\hat{\Omega}_{\mathbf{k}}^{s}$ is a shifted mean frequency of mode $(\mathbf{k},s)$. Expressions for $\mu_{\mathbf{k}}^{s}$ and for the shift $\hat{\Omega}_{\mathbf{k}}^{s} - \Omega_{\mathbf{k}}^{s}$, where $\Omega_{\mathbf{k}}^{s}$ is the natural frequency at $(\mathbf{k},s)$, are given in terms of integrals over the energy spectrum. For vanishingly small energy, $\mu_{\mathbf{k}}^{s} / \Omega_{\mathbf{k}}^{s} \to 0$ and

$$\Phi_{s_1 s_2 s_3}(\mathbf{k},\mathbf{p},\mathbf{q},\mathbf{X},T) \to \pi\delta\left(\Omega_{\mathbf{k}}^{s_1} + \Omega_{\mathbf{p}}^{s_2} + \Omega_{\mathbf{q}}^{s_3}\right) \tag{72}$$

so that one recovers the resonant interaction condition, as noted previously by *Holloway and Hendershott* [1977], *Holloway* [1979] or *Carnevale and Martin* [1982]. As previously mentioned, CF remark that if frequency resonance is strictly imposed, then wave–wave interactions preserve the linear vertical wave momentum which is not preserved by the finite amplitude theory.

Buoyant Turbulence

While the purpose of this paper is to review nonlinear interactions among internal gravity waves, the limit of very strong interaction is more commonly termed stably stratified or buoyant turbulence which, from the wave interactionist viewpoint, must also involve interaction with the vortical mode. It would take us far afield to review even a small part of the literature concerning buoyant turbulence. However, one might very well imagine a goal of strong wave (and vortex) interaction theory to recover a condition of buoyant turbulence in the limit of large amplitudes, especially as the DIA approach and variants thereon are known to exhibit some skill for the limiting case of neutrally stratified turbulence.

Briefly we recall classical concepts from *Monin* [1962] or *Lumley* [1964]. A central tenet since *Richardson* [1920] is that stable stratification suppresses turbulence by expending turbulent kinetic energy to perform work against gravity via a vertical mass flux. This work (per unit mass) is $g\rho^{-1}\overline{\rho' w'} = N^2\overline{\xi w'}$, with ξ the vertical displacement. *Lumley* [1964] assumed that $\overline{\xi w'}$ was not modified by the stratification, so that its spectrum is proportional to $\epsilon^{1/3} k^{-7/3}$ by dimensional analysis. Following arguments of *Kolmogorov* [1941], and taking account of the energy lost to mass flux, he predicted a kinetic energy spectrum

$$E(k) = A\epsilon_0^{2/3}\left(1 + (k_b/k)^{4/3}\right) k^{-5/3} \tag{73}$$

where A is the empirical Kolmogorov constant, ϵ_0 is the kinetic energy dissipation rate by viscosity and $k_b \equiv (N^3/\epsilon_0)^{1/2}$, the buoyancy wave number, up to a constant factor of order unity. Oceanic vertical wave number spectra reported by *Gargett et al.* [1981] are indeed quantitatively consistent with (73) in the wave number range around $k \sim 1$ cpm.

A possible difficulty for the classical theory was suggested by *Phillips* [1965] who argued that the development by Lumley ought to predict a temperature–varianced spectrum $Q(k)$ varying as k^{-1} over $k < k_b$ whereas oceanic observations such those of *Gregg* [1977] indicate vertical wave number spectra $Q \propto k^{-3}$ on $k_0 < k < k_b$ where k_0 is an outer scale. Recently, *Weinstock* [1985] pointed out that Phillips chose an inappropriate limit for an integration. Weinstock shows that on reconsideration one obtains $Q(k)$ taking the same form as $E(k)$ in (73), thus consistent with the observations of Gregg. A further consequence of Weinstock's analysis is to predict a reversal of sign of temperature variance transfer such that variance is transferred toward lower wave numbers for $k < k_b$.

Of concern here are possible implications of these classical turbulence theories relative to wave–wave interaction theories. The crucial difference is the role of the mass flux $\overline{\rho' w'}$ whose cospectrum, denoted $B(k)$, is given by

Lumley:

$$B(k) \propto N^2 \epsilon_0 \left[1 + (k_b/k)^{4/3}\right]^{1/2} k^{-7/3} \qquad (74)$$

To support such a cospectrum by wave–wave interaction requires a cross–correlation between waves whose frequencies must be shifted off the natural (linear) frequencies. $B(k) \neq 0$ requires strong wave interaction. A difficulty is that $B(k)$ increases with decreasing k as k^{-3} from (74) whereas one expects weaker wave–wave interaction, hence smaller $B(k)$, at larger scales.

A second difficulty concerns the transfers of kinetic and potential energies implied by buoyant turbulence theory. Lumley's theory implies a large transfer of kinetic energy toward high k while Weinstock's theory implies that the kinetic energy transfer is accompanied by a transfer of available potential energy (as temperature variance) toward low k, i.e., of opposite sign from the kinetic energy transfer. Wave–wave interactions discussed in section 3 were seen to predict like–signed transfers both of kinetic and potential energies toward high k. Obstacles to a possible synthesis of wave–wave interaction and turbulence theories are thus apparent.

The buoyant turbulence theory of Lumley together with the discussion by Weinstock were seen to predict velocity and temperature spectra in some agreement with oceanic observations. However, vertical mass flux increasing with decreasing k as well as oppositely signed transfers of kinetic and potential energies are also implied.

A different account of buoyant turbulence has been suggested by *Holloway* [1983]. His suggestion is that net work against gravity plays no significant role in the energetics of buoyant turbulence. Then $B(k)$, while nonzero, is too small to affect the transfer rates of kinetic and potential energies, which are both presumed to be directed toward high k. Holloway starts with the wave–wave interaction theory, and estimates, albeit speculatively, the triad relaxation time (71). For sufficiently strong interaction, proximity to resonance is not important and one may scale

$$(\hat{\Omega}_{\mathbf{k}} + \hat{\Omega}_{\mathbf{p}} + \hat{\Omega}_{\mathbf{q}})^2 \approx N^2 \qquad (75)$$

in (71). Assuming dominance by wave number local interactions, he further followed Lumley in taking relaxation rates to obey Kolmogorov scaling. In (71)

$$\mu_{\mathbf{k}} + \mu_{\mathbf{p}} + \mu_{\mathbf{q}} \approx \epsilon^{1/3} k^{2/3} \qquad (76)$$

where ϵ is the transfer of kinetic energy from scales $< k$ to scales $> k$ but unlike Lumley's assumption, this may be approximated by the dissipation rate ϵ_0 since ϵ is nearly independent of k given negligible $B(k)$.

Expressions (75) and (76) are only suggested to be approximate within some order unity coefficients. Nonetheless, assuming that efficiency of turbulent transfers of kinetic and potential energies should be multiplied by some

$$\Phi = \frac{\epsilon_0^{1/3} k^{2/3}}{N^2 + \epsilon_0^{2/3} k^{4/3}} \qquad (77)$$

and assuming small $B(k)$, *Holloway* [1983] shows that both velocity and temperature spectra should take just the form (73). As previously noted, this is quantitatively consistent with oceanic observations. A discriminating test will have to be based upon observation of $B(k)$.

Dissipation and Diffusion

We return here to the discussion from section 3 concerning dynamical balances. It was seen that weak wave or resonant interaction studies implied an energy throughput rate Q_E, hence dissipation rate, proportional to N^2. A corresponding implication was that vertical diffusivity K_ρ be nearly independent of N. In the context of a wave–wave/buoyant turbulence theory described in the preceding section, *Holloway* [1983] sought to address these relationships by requiring that spectra (73) be matched to GM levels at a wave number $(10E_0b)^{-1}$ following *Munk* [1981]. Such a match may be obtained with no imposed relationship between ϵ_0 or K_ρ and N, since $E(k) \approx A N^2 k^{-3}$ independent of ϵ_0 for $k << k_b$.

A different approach to this question was pursued by *Gargett and Holloway* [1984, hereafter GH]. Consistently with the preceding discussion which sought a synthesis of waves and turbulence methodologies, GH also avoid the classical Reynolds decomposition into "turbulent" and "mean" fields, the latter sometimes presumed to include internal wave motion. GH work with the kinetic energy density equation. They neglect horizontal divergences and the pressure–velocity correlation and assume that a flux Richardson number defined as

$$R_f = \frac{-\frac{g}{\rho_0}\overline{\rho' w'}}{u_i w \frac{\partial u_i}{\partial t}} \qquad i = 1,2 \qquad (78)$$

is small compared with unity. The dissipation rate is then balanced by the vertical divergence of the energy flux and may hence be approximated

$$\epsilon \approx \overline{-u_i w \frac{\partial u_i}{\partial z}} \equiv C_1 \left[\overline{u^{i2}}\ \overline{w^2} \overline{\left(\frac{\partial u_i}{\partial z}\right)^2}\right]^{1/2} \qquad (79)$$

with C_1 a triple correlation coefficient. Assuming WKB scaling for $\overline{u_i^2}$ and $\overline{w^2}$ and assuming that shear variance $\overline{(\partial u_i/\partial z)^2}$ is limited by N^2, GH assert that no other intrinsic time scale is available by which to form a nondimensioned quantity and that hence C_1 is independent of N. The result is $\epsilon \propto N$ with $K_\rho \propto N^{-1}$. A similar development is applicable to temperature variance dissipation.

Although observations cited by *Gargett* [1984] are consistent with results obtained in this section, the disparity from results in section 3 remains to be reconciled. Certain consequences of these differences may have wider implications. A familiar practice consists of estimating vertical diffusivity from measured temperature variance dissipation rates, following *Osborn and Cox* [1972] who equate dissipation with production due to vertical heat transport. However, the account suggested by *Holloway* [1983] or seen in GH shows that observed turbulence and dissipation may be consistent with a hypothesis of no significant (i.e., very small) heat transport. Rather, dissipation would be balanced by vertical divergence of wave–supported energy flux. On the other side, the result of *Weinstock* [1985] would imply heat transport significantly greater than that inferred from dissipation.

5. SCALE-SEPARATED INTERACTIONS

Induced Diffusion

McComas and Bretherton [1977, henceforth MB] were the first to identify the importance of scale-separated interactions within the internal wave field. They identified the induced diffusion mechanism that governs the interaction of small-scale internal waves with large-scale internal waves. The fundamental equation in MB's study was the Hasselmann transport equation (32). MB therefore emphasized the weak interaction assumption. If scale separation is also assumed, the full transport equation reduces to a much simpler diffusion equation for small-scale wave action in wave number space. The diffusion is induced by the large-scale components of the wave field. According to weak interaction theory, the diffusivity tensor is given by a weighted average over the large-scale wave spectrum:

$$D_{ij} = \int d\mathbf{K} < K_i \mathbf{U}_\mathbf{k} \cdot \mathbf{k}\, K_j \mathbf{U}_\mathbf{K} \cdot \mathbf{k} > \delta\,(\Omega - \mathbf{v} \cdot \mathbf{K}) \tag{80}$$

Here we have introduced the notation that capital letters Ω, $\mathbf{K}$, and $\mathbf{U}$ refer to the large-scale "background," and lower-case letters ω, $\mathbf{k}$, and $\mathbf{u}$ refer to the small-scale "test wave." $\mathbf{U}$ is the background velocity; $\mathbf{v}$ is the group velocity of the test wave. The tensor element corresponding to both i and j being vertical coordinate indices dominates all other elements. In an isotropic background, the important diffusivity is therefore

$$D_\zeta = \frac{k^2}{2} \int d\mathbf{K}\, K_z^2 < \mathbf{U}_k^2 > \delta\,(\Omega - \mathbf{v} \cdot \mathbf{K}) \tag{81}$$

The shear spectrum of the background is weighted with the resonant delta function. If the shear is assumed to be concentrated at inertial frequencies (as is the case for the Garrett and Munk spectrum) we obtain the *McComas and Müller* [1981*b*] form (41) of the diffusion coefficient.

The Eikonal Approach

Since the weak interaction assumption has been called into question by *Holloway* [1980, 1982] and others, *Henyey and Pomphrey* [1983, henceforth HP] have initiated a study of induced diffusion which emphasizes the scale separation assumption, but makes no weak interaction assumption. The technique used by HP is a Monte Carlo integration of the eikonal or ray equations. The eikonal or ray tracing technique has been used for internal waves propagating in a low-frequency or steady geostrophic current (e.g., *Müller*, 1976, 1977; *Olbers*, 1981], but has not previously been applied to the interactions within the internal wave field.

The eikonal or ray tracing technique consists of imagining a decomposition of the small-scale part of the wave field into wave packets, each with a small spread of wave numbers, centered on a value $\mathbf{k}$ and occupying a region near some point $\mathbf{x}$. Wave packets (generally with different $\mathbf{k}$) can overlap, and fill space, and in the approximation that the test wave field is of low intensity, can be regarded as independent of each other. The evolution of the small-scale wave field is constructed from the motion of individual wave packets as they move through the large-scale background.

The ray equations are defined by a (Eulerian) frequency function

$$\omega = \sigma + \mathbf{U} \cdot \mathbf{k} \tag{82}$$

and the set of equations

$$\dot{\mathbf{x}} = \frac{\partial \omega}{\partial \mathbf{k}} = \frac{\partial \sigma}{\partial \mathbf{k}} + \mathbf{U} \tag{83a}$$

$$\dot{\mathbf{k}} = -\frac{\partial \omega}{\partial \mathbf{x}} = -\frac{\partial \sigma}{\partial \mathbf{x}} - \frac{\partial}{\partial \mathbf{x}} \mathbf{U} \cdot \mathbf{k} \tag{83b}$$

The function ω includes the "intrinsic" frequency σ and the Doppler shift $\mathbf{U} \cdot \mathbf{k}$. The intrinsic frequency is given by the internal wave dispersion relation

$$\sigma = \left(\frac{N^2 k_h^2 + f^2 k_z^2}{k_h^2 + k_z^2} \right)^{1/2} \tag{84}$$

If the wave packet is described in proper variables the interaction with the buoyancy field of the background waves can be removed [*Henyey*, 1983]. The N^2 in (84) is then the Brunt-Väisälä frequency of the basic state and the interaction of the wave packet with the background is entirely due to the Doppler shift term.

The ray equations (82) and (83) are of Hamiltonian form, where the Hamiltonian can be chosen as $H = A\omega$, and the momentum as $\mathbf{P} = A\mathbf{k}$. A is the wave action of each packet, and is conserved along packet trajectories. The relationship of H to the wave energy and of P to the Stokes drift is discussed in detail by HP.

Each term in the ray equations has a simple interpretation. The velocity $\dot{\mathbf{x}}$ is the sum of the wave group velocity and the advection by the background flow. The evolution of the wave number, $\dot{\mathbf{k}}$, is the sum of the WKB scaling term and the shearing of the waves by the background. The most important part of the transport comes from the vertical shear of horizontal current

$$\dot{\mathbf{k}}_z = -\partial_z \mathbf{U}_h \cdot \mathbf{k}_h \tag{85}$$

The ray equations do not constitute a transport theory; the average over the ensemble of background flows has yet to be done. However, if one assumes that interactions are sufficiently weak, a transport theory can be derived for the ray equation which, to lowest order, recovers induced diffusion. By any of a number of formalisms, it can be shown that a Hamiltonian system weakly interacting with a random background undergoes diffusion in phase space. Each packet in the ensemble of background flows separately undergoes diffusion, and since the action of each packet is conserved, it is the ensemble-averaged action density which diffuses. The diffusivity is given by the integral along straight-line trajectories of the autocorrelation function of the perturbation of phase space velocity. Specializing to wave number diffusion (and ignoring the small, deterministic, WKB scaling term) we obtain

$$D_{ij} = \int_0^\infty d\tau < \partial_i \mathbf{U}(\mathbf{x},t) \cdot \mathbf{k}\ \partial_j \mathbf{U}\left[\mathbf{x} - \frac{\partial \sigma}{\partial \mathbf{k}}\tau, t - \tau\right] \cdot \mathbf{k} > \tag{86}$$

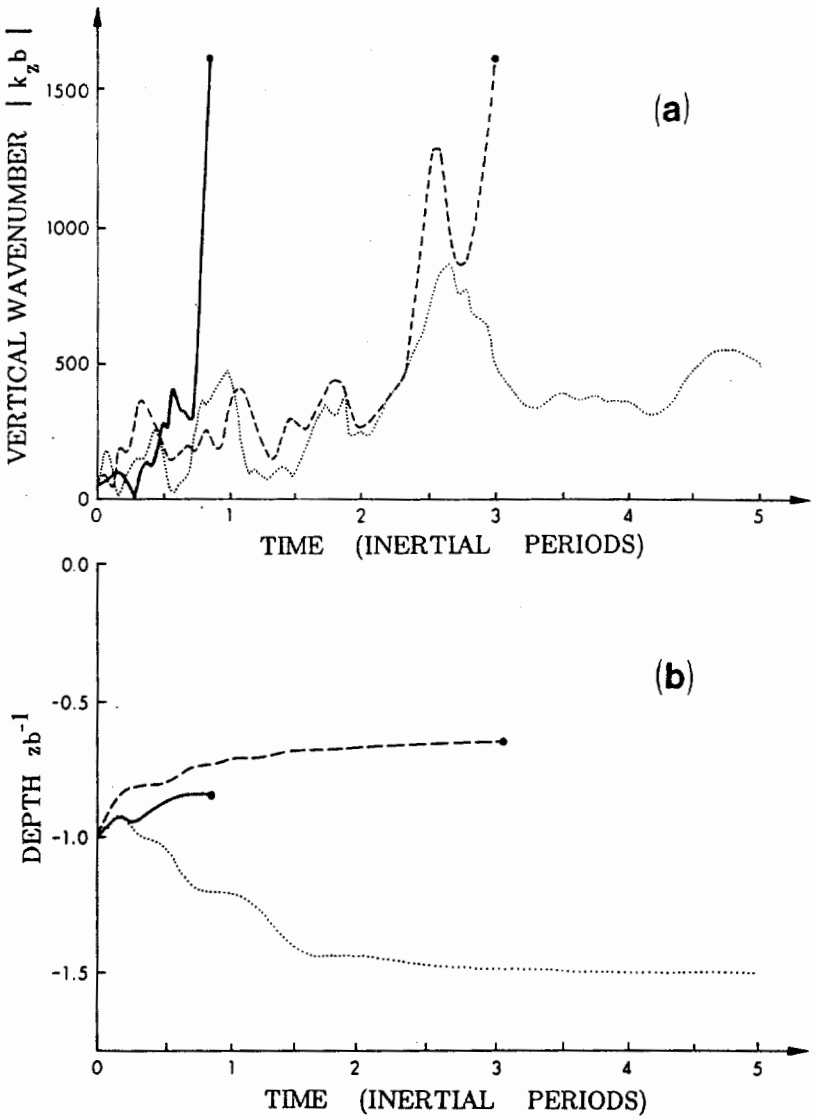

Fig. 14. (*a*) Vertical wave numbers and (*b*) depth of small–scale waves as a function of time for three realizations of the background flow. Two of the three trajectories show large excursions in k_z, which are interpreted as approaches toward a critical layer. The integration is terminated when the vertical wavelength falls below the cutoff value $\lambda = 2\pi/|k_z| = 5$ m [from *Henyey and Pomphrey*, 1983].

Upon expressing each **U** in terms of its Fourier transform, we recover the MB result, equation (80).

Instead of deriving an approximate transport theory, HP perform a Monte Carlo simulation of internal wave transport by integrating the "exact" ray equations (83), and obtain average (transport) properties by averaging over trajectories. The initial wave number and frequency of the wave packet were chosen to lie in the induced diffusion kinematic regime, and the background was chosen to model the Garrett–Munk spectrum. Specifically, HP chose

$$k_z(0) = 58b^{-1} \qquad k_h(0) = 40b^{-1}$$
$$z(0) = -b \qquad \sigma(0) = 15f$$

where $b = 1.3$ km is the e–folding scale of the Väisälä frequency $N(z)$, and f is the inertial frequency. The background was formed out of a superposition of 50 linear waves whose frequencies and wave numbers were selected by random uniform sampling from the GM spectrum, with a cutoff in vertical mode number corresponding to $j = 250$. The integration was terminated when the vertical wavelength fell below the cutoff value of $\lambda = 2\pi/|k_z| = 5$m. Results consisted of both explicit phase space trajectory plots in single realizations of the background (Figure 14), and averages taken over 50 background realizations (Figure 15).

The results for this model indicate that changes in vertical wave number magnitude are very significant. There is a mean motion of k_z to large values, with the same sign as at $t = 0$, and fluctuations about that mean. The individual excursions in k_z (see Figure 14) are of large magnitude and are a striking feature of the results.

Results such as these led HP to suggest a picture of transport of small–scale oceanic internal waves which is very different from the traditional weak interaction view of

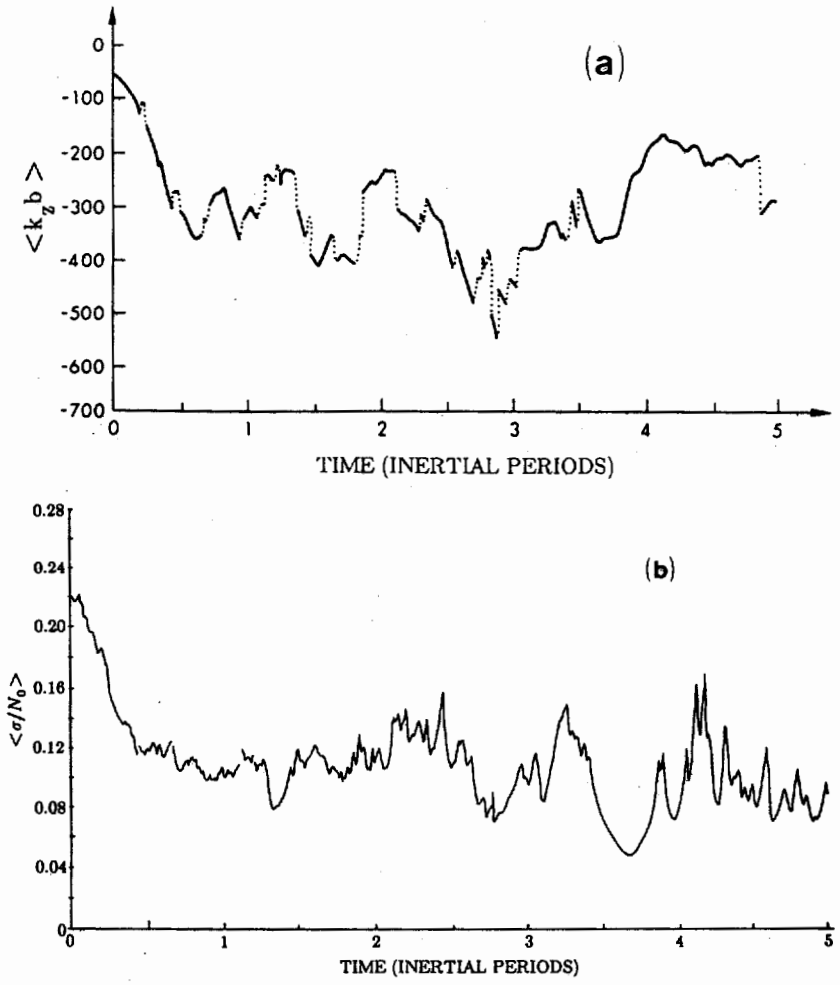

Fig. 15. (*a*) Average vertical wave number and (*b*) average intrinsic frequency as a function of time. The average (denoted by angle brackets) is taken over 50 realizations of the background. Breaks in the curves correspond to "critical layer events" when the vertical wavelength falls below the cutoff value $\lambda = 5$ m [from *Henyey and Pomphrey*, 1983].

diffusion in wave number space. This picture is best understood in a grossly simplified model which does not change the results in any important way. If $k_h \ll k_z \ll k_h\ (N/f)$, which is true over most of the spectrum, the dispersion relation for internal waves can be simplified to

$$\sigma \approx N \left| \frac{k_h}{k_z} \right| \tag{87}$$

so that the vertical group velocity is

$$\dot{z} = -N \left| \frac{k_h}{k_z^2} \right| \operatorname{sgn}(k_z) \tag{88}$$

Let us, for the moment, ignore the horizontal and time dependence of the background flow, and concentrate on its vertical dependence. The vertical wave number of the test wave evolves according to

$$\dot{k}_z \approx -\partial_z \mathbf{U}_h \cdot \mathbf{k}_h \tag{89}$$

which is a function of z. If the test wave finds itself in a region in which k_z increases, its vertical group velocity $\dot{z}$ decreases, and it tends to stay in the same region. If the region is large enough, k_z will tend to infinity linearly in time, and $\dot{z}$ will be proportional to $1/t^2$; therefore z will tend to a critical layer value z_c. This situation will persist until the time and/or horizontal dependence of the background removes the critical layer. The picture of HP is that such "critical layer events" are a major part of the transport through wave number space. The large excursions of k_z, shown in Figure 14, are interpreted by HP as such events. A diffusion picture, on the other hand, would correspond to the evolution of k_z for each realization taking place in small steps, giving rise to a random walk.

Two roughly defined time scales, the correlation time τ_c and the interaction time τ_I, can be deduced from (86). In a certain sense (not to be discussed here) there exists an "exact" diffusivity, with a value given by the integral along the actual phase space path:

$$D_{ij} = \int_0^\infty d\tau \langle \partial_i U[x,t] \cdot k(t) \partial_j U (x(t-\tau), t-\tau) \cdot k(t-\tau) \rangle \tag{90}$$

The correlation time τ_c is the scale of τ which contribute because the correlation function is large for $\tau \leqslant \tau_c$. If it is true for times $\tau \leqslant \tau_c$ that

$$x(t-\tau) \approx x - \frac{d\sigma}{dk}\tau$$
$$k(t-\tau) \approx k(t) \tag{91}$$

then (86) follows. The interaction time τ_I is the time required for at least one of the equations in (91) to be violated. Thus (86) requires $\tau_c < \tau_I$.

HP assume that the action is only changed when the vertical wave number of the wave packets gets large, at which point it becomes unstable. *Broutman* [1984], on the other hand, suggests that caustics might also lead to strong nonlinearities resulting in instability. His considerations are based on ray tracing for deterministic problems. His estimate for the energy concentration, which is proportional to the nonlinearities, is taken from the ray tracing. He neglects the diffractive spreading at a caustic as well as the random effects. Thus his interesting suggestion really remains untested. Statistical properties of intensities at caustics for other random wave problems have been worked out [*Berry and Upstill,* 1980] and this work ought to be extended to the internal wave problem. Alternatively, caustics and intensities could be calculated by ray tracing. As a ray approaches a caustic, the maximum intensity at the caustic is given by the ray tracing intensity a distance L before or after the caustic, where *Landau and Lifshitz* [1975] and a little algebra)

$$L = 0.2\,\lambda^{1/3} R^{2/3} \tag{92}$$

In this expression λ is the wavelength and $1/R$ is the difference in curvatures of the caustic and the ray.

The Meiss–Watson Transport Theory

Meiss and Watson [1982, henceforth MW] developed a transport theory for internal test waves propagating in a random internal wave background based on the assumption that the correlation time is much smaller than the interaction time. The test wave group velocity can be considered constant over a correlation time. MW therefore make a weak correlation approximation. The weak correlation assumption implies a diffusionlike picture of the transport. The test waves take small steps in phase space, with an uncorrelated forcing at each step. If specialized to transport in vertical wave number space MW's transport equation for the density of waves $\rho(k_z)$ takes the form

$$\partial_t \rho(k_z) = 2\int dK_z\, dk_z'\, G(k_z, k_z' K_z, t)$$
$$\delta(k_z + K_z - k_z')\,[\rho(k_z') - \rho(k_z)] \tag{93}$$

The kernel G does not contain any memory effects because of the weak correlation assumption.

Comparison

A comparison of induced diffusion (in the sense of *McComas and Bretherton* [1977]), the eikonal Monte Carlo calculations of *Henyey and Pomphrey* [1983], and the transport theory of *Meiss and Watson* [1982] was carried out by *Henyey et al.* [1984, henceforth HPM]. HPM chose a model for the background which includes only large vertical wavelengths (a background mode number cutoff at $j = 20$ was imposed). This enforced scale separation was to ensure the validity of the eikonal calculation. The eikonal results are therefore "exact," and can be used to test the validity of the other two theories. The HPM model ignores horizontal space dependence of the background, and chooses all background frequencies equal to f.

In general, there are two differences between the Meiss–Watson theory and induced diffusion. The first of these involves the scale separation approximation

$$Q(\mathbf{k} + \mathbf{K}) \approx Q(\mathbf{k}) + \mathbf{K} \cdot \partial_{\mathbf{k}} Q(\mathbf{k}) \tag{94}$$

where Q is any quantity depending on $\mathbf{k}$. MW do not use this approximation, but retain finite K. Thus, MW obtain the integral transport equation (93) where induced diffusion obtains the differential diffusion equation (40). If scale separation is strictly true, which it is for the HPM model, however, this difference between MW's theory and ID is insignificant. Indeed, if we assume that replacements such as (94) are valid the MW integral transport equation (93) becomes equivalent to the diffusion equation

$$\partial_t \rho = \partial_{k_z} D(k_z, t)\, \partial_{k_z} \rho \tag{95}$$

where $D(k_z, t)$ is a time–dependent vertical diffusivity.

The second difference between the Meiss–Watson theory and induced diffusion is that the diffusion coefficient in (40) is time independent whereas the kernel G in (93) and the diffusion coefficient in (95) are time dependent. ID assumes that the test wave is initially correlated with the background when it appears in the ID kinematic regime while MW assume it is uncorrelated. Thus, the time integration in (86) for the ID diffusivity starts at $t - \tau = -\infty$. (Whether this makes sense depends on the generation process for the test waves.) The time–dependent diffusion coefficient in (95) can be obtained by starting the integral at $t - \tau = 0$. MW show that the time dependence gives rise to initial transports that are slower than ID predicts. Figure 16 shows the initial decay rate of the autocorrelation function of the test wave amplitude and compares it to the ID decay rate.

HPM choose a different means of comparison and are led to the same conclusion. They solve the diffusion equation (95) with the initial condition $\rho(t=0) = \delta(k_z - 58b^{-1})$, corresponding to mode number 50 at a depth of $b = 1.3$ km. The boundary conditions are determined by the observation that resonant kinematics limits the possible k_z values. The resonant condition is that the phase velocity of the background equals the group velocity of the test wave, $\Omega/K_z = d\sigma/dk_z$, with $\Omega = f$ for HPM. Since HPM include only $K_z < 23b^{-1}$, and fix the test wave horizontal wave number $k_h = 40b^{-1}$, the resonant condition restricts k_z to the range $|k_z| < 160b^{-1}$. During the initial transient, resonant kinematics are not applicable, but very little action gets beyond this limit. Thus, the cutoff at $K_z = 23b^{-1}$ only influences the diffusion equation by implying reflecting boundary conditions for the diffusion equation at $|k_z| = 160b^{-1}$.

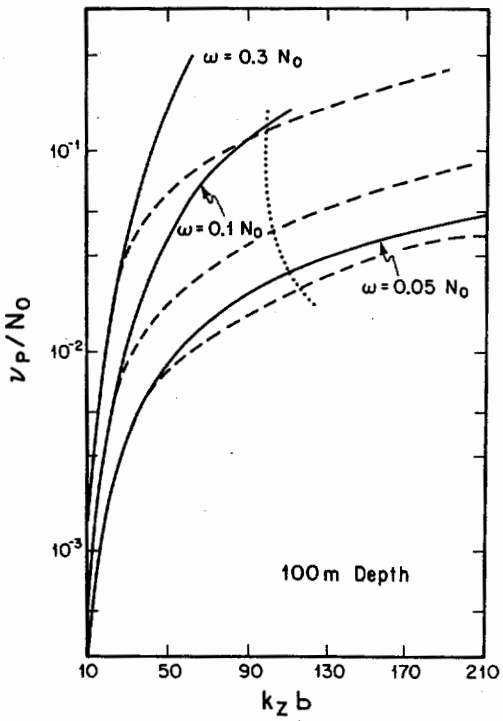

Fig. 16. Decay rate of the autocorrelation function as a function of vertical wave number for several frequencies. The dashed curves represent the initial decay rate according to the Meiss–Watson transport theory. The solid curves represent the decay rate for induced diffusion [from *Meiss and Watson*, 1982].

HPM diagonalize the diffusion operator with such boundary conditions:

$$\partial_{k_z} D(k_z,t)\,\partial_{k_z}\psi_n(k_z,t) = -\lambda_n(t)\,\psi_n(k_z,t) \quad (96)$$

The lowest eigenvalue is $\lambda_0 = 0$ with eigenfunction $\psi_0(k_z,t) = (\sqrt{2}|k_z|_{\max})^{-1}$ which corresponds to the equilibrium state of equipartition of action. The smallest nonzero eigenvalue and eigenfunction determine the final approach of the system to equilibrium. The dominant time behavior was found by HPM to be in $\lambda_1(t)$ rather than in $\psi_1(k_z,t)$. (This was also true of higher eigenvalues and eigenfunctions.) For example, the overlap of $\psi_1(k_z,0)$ with $\psi_1(k_z,\infty)$ was found to be 0.9. Since $\psi_1(k_z,\infty) \approx \psi_1(k_z,0)$ the solution for the intensity of this eigenfunction can be written approximately as

$$\rho_1(t) \approx \rho_1(0)\, e^{-\int \lambda_1(t)dt} \quad (97)$$

A graph of $\lambda_1(t)$ is shown in Figure 17. The effect of the time-dependent diffusion coefficient is to delay the approach to equilibrium. The time delay t_d is found by comparing integrals

$$\int_0^t \lambda_1(t)\,dt = \int_0^{t_d} \lambda_1(\infty)\,dt \quad (98)$$

and yields a delay time of about $t_d = 1/30$ of an inertial period. Apart from this time delay, however, there are no other significant differences between MW and ID.

Since ID and MW are similar for the model of HPM, a comparison of the ID results with the eikonal Monte Carlo results is seen to be a test of the weak interaction and correlation assumptions made by ID and MW, but not made by HP. The same parameter set was used by HPM for the eikonal and ID calculations. Figure 18 shows the comparison of the eikonal results with those of ID for average and rms vertical wave numbers as functions of time. As can be seen, the results are grossly different. Additionally, the eikonal results show higher transport rates and no respect for the resonant kinematic bound of $|k_z| \leqslant 160\,b^{-1}$. Nonresonant effects are clearly important for a significant time period. A more "deterministic" transport is generally much faster than a random diffusion. Thus the faster rates shown by the eikonal results, which are "exact" for the chosen model, support the picture proposed by HP in which the transport is dominated by "critical layer events." It also indicates that the weak interaction and correlation assumptions of ID and MW which led to a diffusion picture are not valid.

The inadequacy of the ID theory (or of MW) should be obtainable from the perturbation expansion that derives it. We have noted in section 3 that the relevant expansion parameter for simple stochastic differential equations is the "Kubo number" $\nu_I \tau_c$, where ν_I is a nonlinear interaction rate, and τ_c a correlation time of the random force. One might think of evaluating the Kubo number for the induced diffusion problem; however, this presents a number of problems. Both ν_I and τ_c are hard to estimate at best, and perhaps not even very meaningful. The decorrelation of the force $[\partial_z \mathbf{U}(\mathbf{x},t)\cdot\mathbf{k}]$ depends on the motion of the wave packet through the random background. The velocity of the background has structure on a wide range of vertical scales, and, as can be seen from the eikonal calculations (see, for example, Figure 14), the group velocity of a packet evolves in a complicated way. Thus, there is no easy way to estimate a single correlation time which characterizes the interaction. The interaction rate ν_I to be used is also ambiguous. The rate at which energy leaves a mode is an upper bound on this rate, but might overestimate it. If the energy goes to another mode with nearly the same frequency and then returns to the original mode before the frequency difference has time to decorrelate the phase, it is just as if no interaction has occurred, so ν_I should be smaller. Finally, the Kubo number is only a meaningful quantity to study in isolation if the coefficients which multiply this expansion parameter in the perturbation series are of order unity. These coefficients involve commutators of diffusion operators,

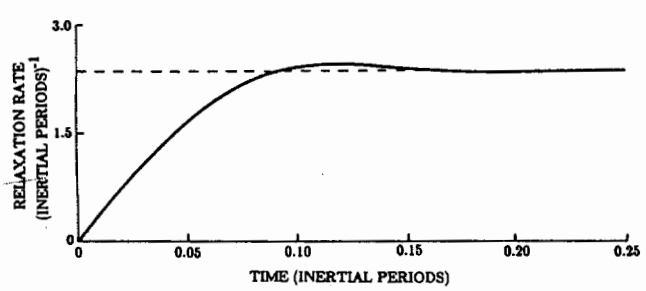

Fig. 17. The Meiss–Watson diffusion rate λ_1 as a function of time (solid curve). After $t \geqslant 0.22$ inertial periods the diffusion rate has reached its asymptotic value of 4.86×10^{-3} (dashed line) [from *Henyey et al.*, 1984].

and it is possible to invent models for which the Kubo number is arbitrarily large, but weak interaction theory is exact because the commutators vanish.

The alternative to estimating the Kubo number itself is to estimate the size of the corrections to ID by going to the next order in perturbation theory, and comparing the new term with the old. HPM carried out this calculation using the Van Kampen formalism [*Van Kampen*, 1981], restricting their calculation to finding the correction to the vertical wave number diffusivity.

The integral for the diffusivity (equation (86)) is carried out along the constant velocity line

$$z(t-\tau) = z(t) - v(t)\tau \qquad (99)$$

However, the wave packet experiences a force along its trajectory which causes it to differ from the straight–line extrapolation. The correction to ID (and MW) arises from the difference between the two paths. HPM estimated the magnitude of the first correction to the diffusivity by a calculation including the diffractive spreading of the trajectories between $t-\tau$ and t. To obtain convergent expressions for the corrections to the diffusivity HPM use a Gaussian cutoff in the background at $j = 20$ rather than a step function. The comparison between the induced diffusion prediction for the diffusivity and its correction is shown in Figure 19. The correction is not small. It is also seen that the background cutoff does not induce a cutoff in the correction. Presumably higher–order corrections are larger still, and nondiffusive terms in the transport equation (those with other than two k_z derivatives) are as large as the corrections to the diffusivity term. It appears that the perturbation expansion is badly divergent, and the lowest order term used by ID and MW badly misrepresents the transport.

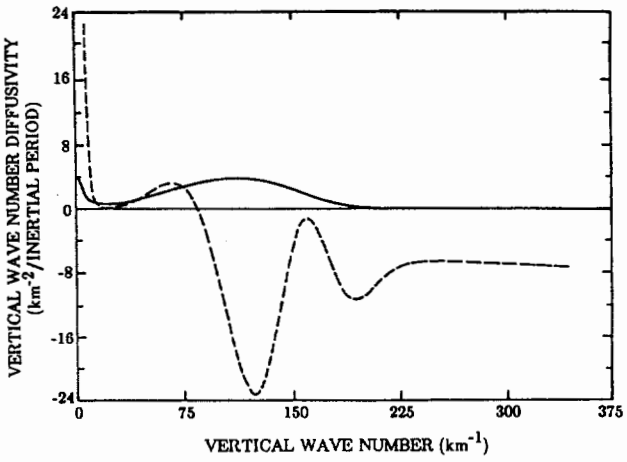

Fig. 19. Comparison of ID diffusivity D_ζ (solid curve) with "second Van Kampen" correction (dashed curve). The correction is not small [from *Henyey et al.*, 1984].

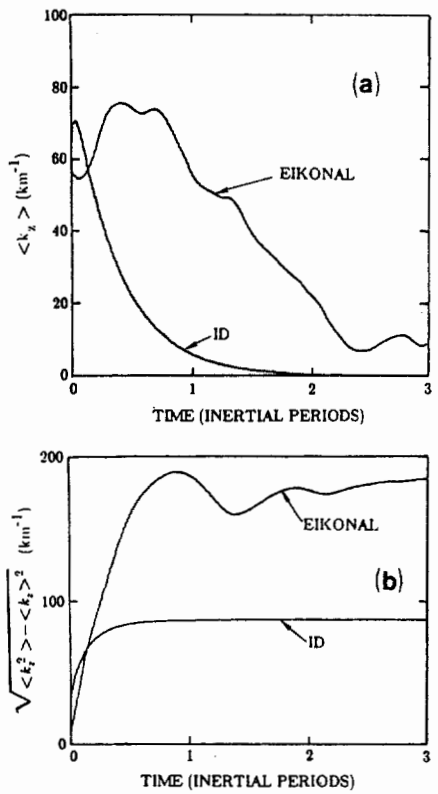

Fig. 18. (*a*) Average and (*b*) root–mean–square vertical wave numbers as a function of time for eikonal and induced diffusion calculation. The average (denoted by angle brackets) is constructed from 50 realizations of the background. The eikonal decay of $<k_z>$ is much slower than that of ID, and it is considerably delayed. The eikonal calculation also predicts a much higher level of the root–mean–square vertical wave numbers than does ID, and takes considerably longer to become established [from *Henyey et al.*, 1984].

Putting in the Garrett–Munk spectrum and a Gaussian cutoff, both of which were used in the comparison of Figure 19, HPM find

$$\frac{D_{\text{correction}}}{D_{\text{ID}}} = \frac{2}{f}\,\frac{N^2 j_* E b k_h^2}{v^3}\left(\frac{dv}{dk_z}\right)^2 \qquad (100)$$

times an integral which numerically evaluates to order one for all k_z. The GM mode number parameter is $j_* = 3$, E is the dimensionless energy density of the background flow, $E \approx 6.3 \times 10^{-5}$, and b is the e–folding scale of $N(z)$, $b = 1.3$ km. According to the ideas from simple stochastic differential equations, one should interpret the quantity on the right–hand side of (100) as the square of a Kubo number. HPM were unable to use such an interpretation to identify ν_I and τ_c. Presumably the wide range of correlation time scales and interaction time scales is responsible for the absence of a simple interpretation.

Under the simplifications (87) and (88), with $N/f = 50$, (100) reduces to

$$\frac{D_{\text{correction}}}{D_{\text{ID}}} = 600\text{ m}\left(\frac{k_h}{2\pi}\right) \qquad (101)$$

HP suggest that the scale separation assumption is not too bad for $2\pi/k_h < 1000$ m. Thus, throughout this region, the correction is not small compared to induced diffusion.

Both the comparison with the eikonal and the estimate of the neglected terms in ID suggest that weakly nonlinear theory does not apply to the transport of small–scale internal waves in the ocean.

6. NUMERICAL SIMULATIONS

Throughout this paper, we have noted the many instances of theoretical ambiguity. For the most part,

such ambiguities arise in areas that appear to be outside of the domain of validity of theoretical approximation. Slow time scales of weak interaction appear, in fact, to be quite rapid. Scale–separated interactions compete with, and may be overwhelmed by, interactions among like scales. Strong interaction theories have not been very well developed in regards to internal wave interaction. Moreover, strong interaction theory rests on conjectures which are not demonstrably justified. In this section, we turn to yet another approach, namely direct numerical simulation.

Numerical simulation will here refer to the integration forward in time of some set of approximate equations for unaveraged flow fields. Such numerical simulations can proceed from equations at various levels of approximation. For example, in section 5 we have considered numerical integration of eikonal equations. However, the eikonal equations represent a relatively "high" level of assumption, i.e., the assumed dominance of scale–separated interactions. Seeking to test the validity of such assumptions, research has resorted to numerical integration of the more "primitive" incompressible Boussinesq equations with uniform rotation and uniform stratification in the mean. This research is reviewed here.

All numerical simulations assume a fluid which is stratified with respect to heat only and admit diffusion both of momentum and of heat. Heat diffusion may be considered to be an effective density diffusion upon taking account of a constant coefficient of thermal expansion. The equations of motion for velocity and density fluctuations about the mean state are then as follows:

$$\partial_t \mathbf{u} + \mathbf{u}\cdot\nabla\mathbf{u} + \mathbf{f}\times\mathbf{u} + \frac{g}{\rho_0}\hat{\mathbf{z}}\rho + \frac{1}{\rho_0}\nabla p - \nu\nabla^2\mathbf{u} = 0 \tag{102a}$$

$$\partial_t \rho + \mathbf{u}\cdot\nabla\rho + Rw - \kappa\nabla^2\rho = 0 \tag{102b}$$

$$\nabla\cdot\mathbf{u} = 0 \tag{102c}$$

Here $R \equiv \partial\tilde{\rho}/\partial z$ is the assumed uniform gradient of mean density so that $N^2 = -gR/\rho_0$. Since a constant N^2 is chosen the fine–structure contamination problem (section 2) does not occur.

Equations (102) are suitable for investigating nonlinear interactions among internal waves whose scales are short compared with the scale of variation of the mean environment. Equations (102) also describe strongly overturning, buoyancy–modified turbulence. Although our goal here is not to investigate strong buoyancy–modified turbulence per se, we recognize that this is a limit of large–amplitude, small–scale internal wave dynamics. The question at hand is how internal wave dynamics gives way to buoyant turbulence dynamics. More specifically, how can direct numerical simulation elucidate the dynamics that are intermediate between internal waves and buoyant turbulence?

Our review is based on five studies [*Orlanski and Cerasoli,* 1980, 1981; *Riley et al.,* 1981; *Weissman et al.,* 1981; *Frederiksen and Bell,* 1983, 1984; *Shen and Holloway,* 1986]. Other numerical investigations have addressed specific mechanisms such as critical layer interactions [*Fritts,* 1979; *Hirt* 1981], Kelvin–Helmholtz instability [*Patnaik et al.,* 1976], or stability of standing waves [*Orlanski and Ross,* 1973].

Numerical experiments are similar in many regards to laboratory experiments and have certain advantages and disadvantages. Among the advantages are (1) complete information on the evolution of the flow fields and (2) controllability of experimental conditions including continuous variation of physical parameters.

The principal disadvantage is one of finite computer resolution. Even on very large, fast machines, it is now impractical or exceedingly costly to integrate forward in time more than about 10^5 variables. This means that a representation in three spatial dimensions of (102) has only been practical on an equivalent grid of 32 x 32 x 32 points, say. There being no great disparity between the largest and smallest scales resolved, it is necessary either to introduce an ad hoc "subgrid scale parameterization" or else to execute at such low Reynolds and Peclet numbers that the velocity and density fluctuation fields are strongly damped. Advances in machine capability are overcoming, in part, these limitations. Simulations of buoyant turbulence at up to 128^3 may be performed in the near future.

A means of avoiding both the computational cost and the strong damping of the three–dimensional simulation is to constrain the flow to two dimensions by imposing the condition that fluctuating velocity and density fields are independent of one horizontal coordinate. There is no physical basis for such a constraint. However, as a two–dimensional problem, resolutions from 64 x 64 to 256 x 256 (or other comparable but nonsquare combinations) are quite practical on many modern machines. The greater range between largest and smallest resolved scales allows sufficient damping of small scale fluctuations while the large, energy–containing scales are relatively weakly damped. Most important, perhaps, the several theoretical approaches discussed in previous sections either are given in two–dimensional form or are readily restated in two–dimensional form. Thus, relatively high resolution, two–dimensional simulations would appear to find a natural role in theory testing.

Before turning to specific simulation results, we should recognize one further limitation. The numerical model requires a specification of boundary conditions. Ideally we might wish to consider a flow with boundaries removed to infinity. Or we might consider top and bottom boundaries, thereby imposing a vertical modal structure, while removing side boundaries to infinity. Intuitively we may imagine that "infinity" only means "far away." Unfortunately, with as few as 32 equivalent grid points across the domain, boundaries are hardly very "far away." Arguments of *Holloway* [1979] suggest that boundaries are "far away" when the scale L of the flow domain is large in the sense that

$$L > |\mathbf{c}_g(\mathbf{k})|/\nu(\mathbf{k}) \tag{103}$$

where $\mathbf{c}_g(\mathbf{k})$ is the group velocity at wave vector $\mathbf{k}$ and $\nu(\mathbf{k})$ is the wave–wave interaction rate at $\mathbf{k}$. To the extent that weak resonant interaction theory is valid, $\nu \approx \nu_p$ (cf. equation (35)). Inequality (103) should be satisfied for all energetic $\mathbf{k}$. An interpretation of (103) is that information, tending to propagate along wave rays,

should be destroyed by nonlinear interactions over a distance shorter than the distance between boundaries. A consequence is that weakly interacting waves, hence small ν or ν_p, are more difficult to simulate whereas strongly interacting waves ($\approx$ turbulence) are easier.

Three–Dimensional Case

In principle, the most direct assault on (102) is a full three–dimensional simulation. However, for reasons just outlined, namely the limited computer resolution and high cost of obtaining such resolution, three–dimensional simulation is not, at present, a practical means for investigating the oceanic GM environment. Nonetheless, three–dimensional simulations have been performed related to the decay of stratified turbulence. We review briefly the results of *Riley, et al.* [1981], hereafter RMW. To our knowledge these are the only such published simulations.

The purpose of RMW was to perform numerical simulations related to laboratory experiments of *Lin and Veenhuizen* [1974], *Dickey and Mellor* [1980] and *Stillinger et al.* [1983]. In the laboratory experiments, turbulence is excited either by horizontally towed bars or grids, or by vertically dropping a grid, or by forcing a fluid through a grid. In the frame of reference fixed to the mean fluid, the situation appears as an initial value problem: at a nominal time $t = 0$, a state of strongly excited, nearly homogeneous, nearly isotropic (presumably) turbulence is instantaneously imposed upon a uniformly stratified fluid. For $t > 0$, no further excitation is imposed. The ensuing decay is examined.

RMW imitate such experiments by creating a random, homogeneous, isotropic velocity field as an initial condition. More specifically, RMW initiate a random phase vector potential field $\mathbf{A}(\mathbf{x})$ such that the velocity field given by $\mathbf{u} = \nabla \times \mathbf{A}$ has prescribed power spectrum

$$E_u(k) \propto k^4 e^{-2(k/k_m)^4} \tag{104}$$

This velocity field is unlike hydrodynamical turbulence since none of the straining, energy–cascading character is permitted due to randomness of phase. Therefore RMW elect to allow the velocity field to evolve for approximately one turbulent time scale (L/u) in a neutrally stratified environment. The resulting velocity field after unit time is then taken as the "initial" velocity field. At the corresponding "initial" time, the density field is taken to be just the unperturbed uniform density gradient. The choice to assume an initially turbulent velocity field with no corresponding density fluctuation field is open to question; RMW justify the choice as roughly describing actual fields just after passage of the grid.

Specifically, the simulations of RMW consist of (102) in the case of no mean rotation ($f = 0$) and unit Prandtl number ($Pr = \nu/\kappa = 1$). The method of integration is pseudospectral: that is, flow variables are spatially Fourier–transformed; differential operators are evaluated algebraically in the transform space; and variables are transformed by fast Fourier transform (FFT) back to configuration (physical) space to evaluate local products of variable fields [cf. *Orszag*, 1971].

Although the method is pseudospectral, the spatial resolution of RMW corresponds to 32 x 32 x 32 grid points. Viscosity and diffusivity must be relatively large in order to prevent accumulation of variances at the highest resolved wave numbers. The result is a very modest microscale Reynolds number of $R_\lambda \approx 27$ at $t = 0$.

For given initial velocity field, three cases with increasing role of stratification are considered. These are given in terms of a turbulent Froude number $Fr = u'/NL$ where u' is the rms turbulent velocity and L is the integral length scale. At $t = 0$ the three cases are given as

Case 1
$$Fr = \infty$$
Case 2
$$Fr = 3.63$$
Case 3
$$Fr = 1.83$$

A main result as described by RMW is that after about one buoyancy period ($\tau_b = 2\pi/N$), cases 2 and 3 undergo apparent transitions from strong, turbulent decay to a more weakly decaying mix of internal waves and horizontal vortical flow. This transition is seen in a number of diagnostics:

1. The first is decay of total energy. The total perturbation energy is defined as a sum of kinetic and potential energies

$$\begin{aligned} \mathrm{TE} &= \mathrm{KE} + \mathrm{PE} \\ \mathrm{KE} &= \frac{1}{2}\,\overline{\mathbf{u}\cdot\mathbf{u}} \\ \mathrm{PE} &= -\frac{1}{2}\,\frac{g}{\rho_0}\,R^{-1}\,\overline{\rho^2} \end{aligned} \tag{105}$$

The overbar denotes average over the flow domain and R is the specified ambient (constant) stratification. Initially all energy is kinetic. With stratification, there is exchange of KE and PE. During an early period, TE decays quite similarly in each case. At later times, the more stratified flows (cases 2 and 3) retain more TE. In part the larger retained energy in stratified flows may be explained as an inhibition of processes which would transfer energy to smaller, dissipation scales. This inhibition may be seen in the next two measures.

2. The second is velocity derivative skewness. The skewness is defined by

$$S_i = \overline{(\partial u_i/\partial x_i)^3}\,/\,\overline{(\partial u_i/\partial x_i)^2}^{3/2} \tag{106}$$

$$i = 1, 2, 3, \text{no summation over } i$$

and has a value $S_i \approx -0.4$ at $t = 0$ due to unstratified turbulent evolution prior to $t = 0$. Transition at about $t = \tau_b$ is characterized by abrupt inhibition of the vertical skewness S_3 with relatively no effect on horizontal skewnesses S_1 and S_2.

3. A further diagnostic, related to velocity derivative skewness, is the transfer of KE and of PE across the spectrum. (N.B: this measure does not take into account exchange of KE and PE through vertical buoyancy flux.) Experiments of RMW show that increasing stratification markedly reduces the transfer rate of KE but that this reduction is largely compensated by increased transfer of PE.

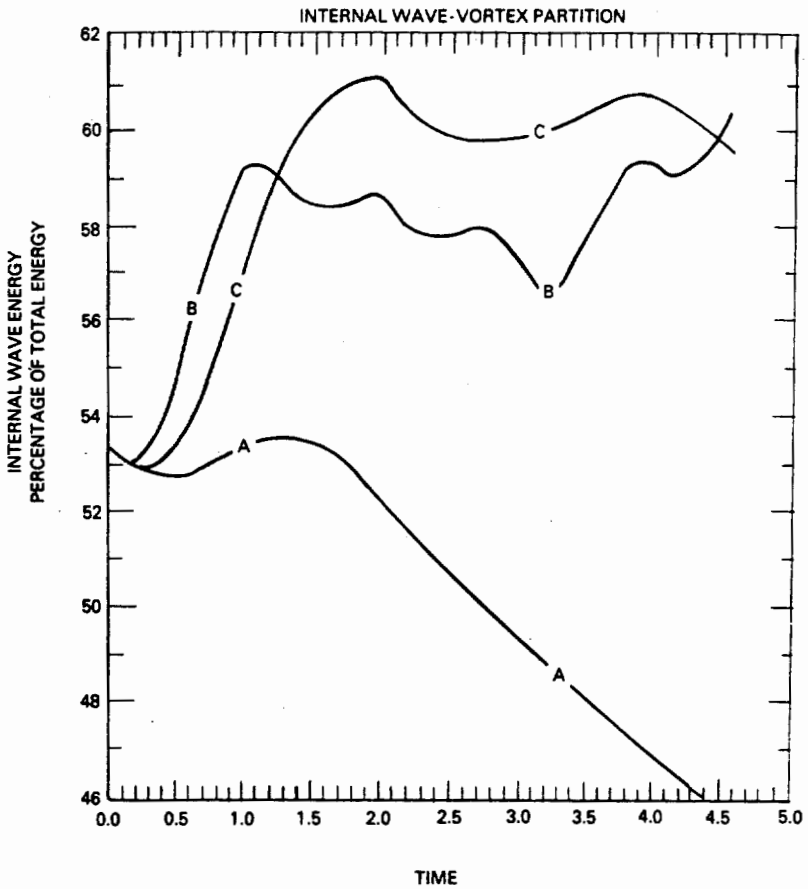

Fig. 20. Percentage of wave energy versus times for three–dimensional simulation of RMW. Curve A represents case 1 ($Fr = \infty$); curve B represents case 3 ($Fr = 1.83$), and curve C represents case 2 ($Fr = 3.63$) [from *Riley et al.*, 1981].

4. Total dissipation rates for KE and for PE were calculated. After an initial adjustment period, RMW observe that the ratio of dissipation rates (KE: PE) tends to about a value of 2.

5. One of the expected effects of stratification is increasing anisotropy. RMW observe this anisotropy in the growth of longitudinal microscale μ_i where

$$\mu_i^2 = \overline{u_i^2} / \overline{(\partial u_i / \partial x_i)^2} \qquad \text{no summation over } i \tag{107}$$

Growth of the μ_i is characteristic of decaying, unstratified turbulence. When stratification is present, horizontal components of μ_i grow much as in the unstratified case; however, growth of the vertical component μ_3 is inhibited.

6. A final diagnostic considered by RMW is designed to separate the motion field into a part due to "waves" and a part due to "vortices." The distinction is based upon consideration of the spatial Fourier expansion coefficients $\mathbf{u}_\mathbf{k}$ of the velocity field $\mathbf{u}(\mathbf{x})$ at any time. By incompressibility, $\mathbf{k} \cdot \mathbf{u}_\mathbf{k} = 0$, $\mathbf{u}_\mathbf{k}$ lies in a plane normal to $\mathbf{k}$. The horizontal component in that plane is denoted $u_{\mathbf{k},V}$. The orthogonal component in that plane is denoted $u_{\mathbf{k},W}$. The subscripts V and W refer to "vortex" and "wave" since for the linearized equation of motion, the $u_{\mathbf{k},W}$ set describes internal wave propagation while the $u_{\mathbf{k},V}$ set describes a field of vertical vorticity. (This distinction is appropriate for a case such as RMW which omits mean rotation; the more general decomposition has been described in section 2 above.)

Figure 20 shows the fraction of wave energy as a function of time for the three cases considered by RMW. Because RMW start their integration with no fluctuation potential energy and an isotropic velocity field, total energy is initially approximately equally divided between "waves" and "vortices." For the stratified cases 2 and 3 in Figure 20 the fraction of wave energy tends toward the equipartition value 2/3 but does not quite reach it. However, RMW do not calculate whether this deviation is due to the conversion of wave energy to vortical energy or due to the more rapid energy loss of wave energy by transfer to dissipation scales.

Two-Dimensional Case

Whereas the cost of computation has limited direct numerical simulation in three dimensions, extensive simulations in two dimensions have been performed. A natural question remains: to what extent, or in what regimes of parameters or of wave numbers, may two–dimensional simulation resemble three–dimensional flow interaction? It may be that subsequent detailed comparisons of two– and three–dimensional simulations will resolve this question. One may speculate that in three

dimensions, wave breakdown and dissipation at small scales will proceed more efficiently than in two dimensions. This view is supported by the known tendency in two–dimensional turbulence to block energy transfer to large wave number [*Fjørtoft,* 1953; *Kraichnan*, 1967; *Batchelor*, 1969] and also from observed effects of three–dimensional perturbations in the destabilization of two–dimensional rolls in mixing layers. On the other hand, for all scales of motion, the cross product of pressure and density gradient provides source/sink terms for vorticity, thereby enabling energy transfer to smaller scales.

While the question of relating two–dimensional simulations to three–dimensional flows remains open, the utility of two–dimensional simulation for testing theoretical hypotheses is clear. All of the physics of weak–wave and strong–wave interaction, and of wave number local and nonlocal interaction, are retained. A variety of mechanisms for forcing and for dissipation can be explored and the ways that wave–wave interaction (weak, strong or "breaking") achieve an equilibrium spectrum with given forcing and dissipation can be examined in detail.

All two–dimensional simulations integrate the Boussinesq equations of motion for flows which are nonrotating and uniformly stratified in the mean and restricted to motion only in a vertical plane. The coupled non–dimensionalized equations for density and for horizontal vorticity then take the form

$$\partial_t \zeta - J(\psi, \zeta) = \partial_x \rho + \nabla \cdot (\nu \nabla \zeta) \qquad (108a)$$

$$\partial_t \rho - J(\psi, \rho) = -\partial_x \psi + \nabla \cdot (\kappa \nabla \rho) \qquad (108b)$$

Here $\zeta = \nabla^2 \psi$ is the vorticity, ψ is the stream function in the sense $u = \partial_z \psi$, $w = -\partial_x \psi$, ρ is the excess of density above a linear mean density gradient, non–dimensionalized such that the linear gradient is of unit slope, and ν and κ are eddy viscosity and diffusivity coefficients. We note that effects of rotation can be included by adding a term $f \partial_z v$ on the right side of (108*a*) and a third equation

$$\partial_t v - J(\psi, v) = -f \partial_z \psi + \nabla \cdot (\nu \nabla v) \qquad (109)$$

where v is the component of velocity normal to the vertical plane and f is the Coriolis parameter scaled by buoyancy frequency.

The most extensive two–dimensional simulations published to date are those reported by *Orlanski and Cerasoli* [1980, 1981], hereafter OC. Later we will discuss also simulations by *Weissman, et al.* [1981], hereafter WMR, *Frederiksen and Bell* [1983, 1984], hereafter FB, and *Shen and Holloway* [1986], hereafter SH. OC specify the eddy diffusivities in the following phenomenological way:

$$\nu = \kappa = \nu_L \qquad \partial_z \rho < 0$$

$$\nu = \kappa = \nu_L + \nu_{NL} \left| \frac{\partial_z \rho}{\nu \ell^2} \right|^{1/3} \qquad \partial_z \rho > 0 \qquad (110)$$

This specification was proposed by *Orlanski and Ross* [1973] and is intended to model the enhanced dissipation when overturning ($\partial_z \rho > 0$) occurs.

Boundary conditions for OC were taken to be rigid, free–slip and adiabatic on the horizontal and vertical sides of a closed box. In some cases the upper lid boundary was modified to simulate forcing by undulating plates corresponding to a laboratory device. In other cases, the flow field was excited by random body forces applied to the vorticity and density fields. Computations were based upon a finite difference scheme employing 51 grid points in the horizontal by 61 in the vertical.

OC attempted to address a question whether "wave–wave interaction" or "wave breaking" limits wave amplitudes. At low amplitudes, as evidenced by the relative absence of overturning regions, OC do not obtain a "universal" spectrum. At higher amplitudes, interactions fill out the spectrum and "breaking" dominates as given by the explicit role of (110), and OC claim that a degree of saturation is obtained. However, the quantitative basis for this claim is not clear.

On a point of theoretical interest, OC remark that the interaction time scale seems to vary as $E^{-1/2}$, where E is total wave energy. Although OC do not give explicitly the basis of their interaction time scale, we might assume that this quantity should approximate ν_p^{-1}, cf. (35). From (35) one sees that $\nu_p^{-1} \propto E^{-1}$, for a given spectral shape. If comparison of the two time scales is appropriate, then the weakness assumptions in (35) are violated at the energy levels investigated by OC. Whether an E^{-1} dependence could be recovered at small E is not examined.

To obtain a clearer picture of wave interactions, OC compare the evolution of an isolated triad of waves with the evolution of the triad when embedded in a many–wave background. The presence of a background is shown to cause departures from the evolution of an isolated triad. This can be seen in Figure 21 which shows "energy triangle diagrams." In these diagrams total energy is decomposed into three parts: the energy in some wave, say wave 1, energy in another wave, say wave 3, and then the remaining energy. In an initially quiescent background, trajectories on the triangle diagrams make long, looping, quasi–periodic passages. A preexisting background of internal waves quickly breaks up the trajectories, and leads to a more chaotic motion over a more limited region.

OC test the response of a developed wave field to perturbations in two sets of experiments. In one set, a narrow energy spike is put into the spectrum at various wave numbers. In the other set, random energy forcing is applied in selected wave number bands. The two sets of experiments produce similar results and so here we describe only the latter, or "band–random," set. Three bands were forced corresponding to low, intermediate and high wave numbers. Forcing was isotropic and applied equally to the density and vorticity fields. The nature of time dependence of forcing is not specified by OC. When forcing is applied in low wave numbers, energy levels are observed to rise and oscillate for a while. Oscillations later cease and energy levels decrease. OC interpret the oscillatory behavior as evidence of wave–wave interaction, with subsequent cessation and decrease of energy as resulting from wave breaking. Forcing over intermediate wave numbers yields only a temporary increase of energy which OC suggest is due to nearness to wave breaking. Forcing in the high–wave number band is lost immediately to dissipation. An interesting aside is that OC note an apparent

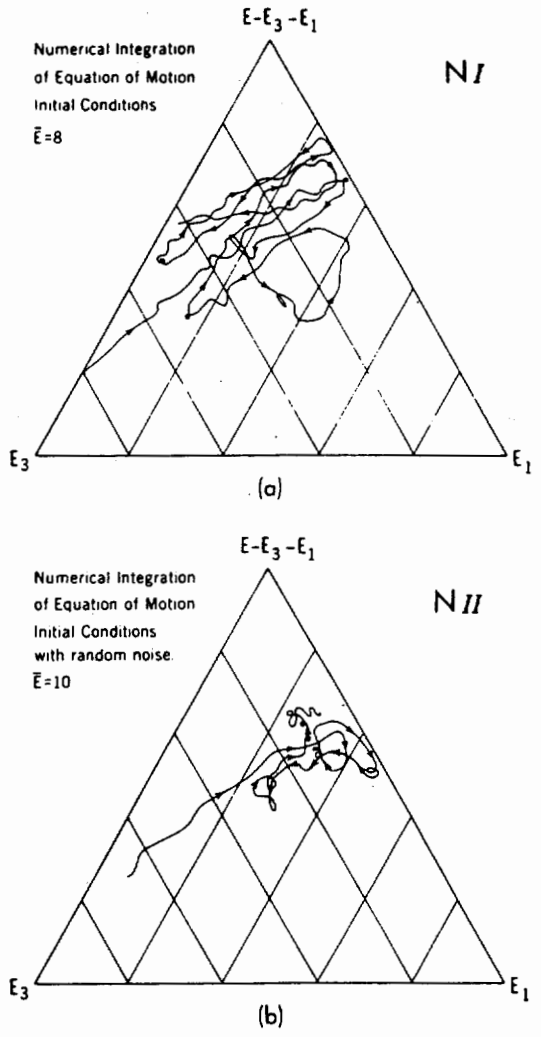

Fig. 21. Energy triangle diagram showing the evolution of a wave triad for two cases. Total energy is decomposed into three parts: the energy E_1 in wave 1, the energy E_3 in wave 3, and the remaining energy $E - E_1 - E_3$. In the first experiment (N_I) the wave triad has an initial energy density of 8 cm^2 s^{-2} and is put into a quiescent background. The second experiment N_{II} starts with the same triad components, but in the presence of a random internal wave background with a mean energy density of 2 cm^2 s^{-2} [from *Orlanski and Cerasoli,* 1980].

steepening of wave number spectra during periods of intense breaking.

To further analyze the energetics, OC separate the net energy change at each wave number into a part due to nonlinear transfer and a part due directly to the dissipation operator (110). For each of the band–forced experiments it is observed that nonlinear transfer tends to dominate over dissipation. However, because of strong time dependence of both transfer and dissipation, there is some difficulty in obtaining reliable averages. An interesting claim occurs to the effect that wave–wave interactions lead to energy transfers that are local in wave number whereas the stronger (breaking) interactions permit nonlocal transfer of energy that need not pass through intermediate wave numbers. Another suggestion of OC is that energy dissipation may be proportional to the excess of energy over some "universal" level.

Three further studies using the two–dimensional (vertical plane) idealization are WMR, FB, and SH. These studies differ from OC in a couple of significant ways. The method is pseudospectral as discussed previously with respect to RMW. Compared with a finite difference scheme in OC, the pseudospectral method provides greater accuracy, e.g., linearized waves propagate on the correct dispersion relation, not suffering numerical dispersion. The equations of motion are (108). However, neither WMR, FB nor SH employ a nonlinear, stability–dependent dissipation such as (110). A further important difference from OC arises in the statement of boundary conditions. Whereas the OC model assumes rigid, adiabatic sidewalls, WMR, FB, and SH employ periodicity conditions in the horizontal. (FB and SH also employ periodicity in the vertical.) For these cases, patterns of vertically sheared, horizontal and nearly horizontal flow can occur. Also, waves of frequencies up to N are readily supported. The WMR report is "preliminary" as its authors remark. Here we review FB and SH.

Simulations performed by FB are designed largely for the purpose of comparison with the theoretical developments by *Carnevale and Frederiksen* [1983, CF] discussed in section 4. Spectral truncation for FB corresponds to physical representation at 64 x 64 grid points. Four kinds of experiments are performed: (1) inviscid evolution, (2) viscous decay, (3) forced–dissipative equilibrium, and (4) breakdown from a standing wave.

Inviscid cases are run from prescribed initial conditions with no forcing and no dissipative mechanism present. The equations of motion (108) with $\nu = \kappa = 0$ then conserve total energy

$$E = \sum_{\mathbf{k}} \frac{1}{2}\left(k^{-2}|\zeta_{\mathbf{k}}|^2 + |\rho_{\mathbf{k}}|^2\right) = \sum_{s=\pm 1}\sum_{\mathbf{k}} E^s_{\mathbf{k}} \tag{111a}$$

and cross–correlation

$$C = \sum_{\mathbf{k}} \zeta_{\mathbf{k}}\rho_{-\mathbf{k}} = -\sum_{s=\pm 1}\sum_{\mathbf{k}} Sk\, E^s_{\mathbf{k}} \tag{111b}$$

where

$$E^s_{\mathbf{k}} = |A^s_{\mathbf{k}}|^2 \qquad A^s_{\mathbf{k}} = \frac{1}{2}\left(k^{-1}\zeta_{\mathbf{k}} - s\rho_{\mathbf{k}}\right) \tag{112}$$

Here $\zeta_{\mathbf{k}}$ are Fourier expansion coefficients for vorticity, $\rho_{\mathbf{k}}$ are coefficients for density, $A^s_{\mathbf{k}}$ are wave amplitude coefficients, and $E^s_{\mathbf{k}}$ are wave mode energies. The index $s = \pm 1$ describes nominal left/right–going waves. Given only the conserved quadratic quantities E and C, a statistical equilibrium or maximum entropy state

$$E^s_k = \left(a - sbk\right)^{-1} \tag{113}$$

should be approached on ensemble average from almost all initial conditions. Constants a and b in (113) depend upon initial conditions through the initial, and conserved, values of E and C.

A particular item of interest for FB is the linear vertical wave momentum which FB define as

$$P_z = \sum_{s=\pm 1}\sum_{\mathbf{k}} k_z E^s_{\mathbf{k}} / \sigma^s_{\mathbf{k}} \tag{114}$$

where $\sigma^s_{\mathbf{k}} = s\, k_x\, k^{-1}$. For a continuous system in $\mathbf{k}$ space,

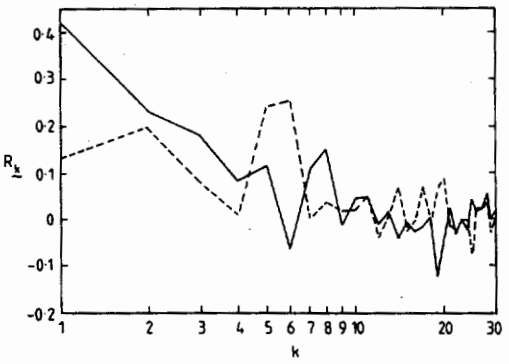

Fig. 22. Cross–spectrum R_k as a function of wave number k for two different runs of FB's two–dimensional simulation. The spectra are averaged in time for about 8.4 s [from *Fredericksen and Bell*, 1983].

CF identified P_z as a conserved property under resonant interactions that is not conserved under slightly off–resonant interactions. It is in this sense that CF suggest that resonant interaction theory is a "singular" limit for a vanishingly small amplitude. If P_z were a conserved property, then (113) would be modified to

$$E_{\mathbf{k}}^{s} = \left(a - sbk - sckk_z / k_x\right)^{-1} \tag{115}$$

where c is a constant dependent upon initial P_z. Numerical experiments by FB confirm evolution toward (113) rather than (115) while values of P_z are observed to wander over time.

A focal diagnostic quantity in FB is overall entropy which is given by cf. *Carnevale et al.* [1981]

$$S = \frac{1}{2} \sum_{s=\pm 1} \sum_{\mathbf{k}} \ln E_{\mathbf{k}}^{s} \tag{116}$$

CF's theory demonstrates that S on ensemble average increases monotonically toward a maximum value when (113) is attained. Experiments by FB in which realization values of $E_{\mathbf{k}}^{s}$ are used in (116) indeed show realization entropy increasing, with fluctuations, in a way that is consistent with CF. A further property of CF's theory is that, for a given energy level, higher–stratification N should suppress the rate of increase of S without affecting the asymptotic maximum of S. FB demonstrate also this property.

FB make several observations based upon their viscous decay experiments. Especially, they remark that kinetic and potential energies remain approximately in equipartition as would be the case for wavelike fields in the absence of rotation. This equipartition, with the corresponding implication that

$$R_{\mathbf{k}} = \text{Real} < A_{\mathbf{k}}^{s} \, A^{-s}{}_{\mathbf{k}} > \approx 0 \tag{117}$$

is important to the theory of CF for which (117) is assumed. Condition (117) states that left– and right–going waves are nearly uncorrelated and corresponds to a nearly vanishing vertical buoyancy flux.

How well (117) is satisfied is difficult to say given the statistical variability among realizations and the temporal quasi–oscillatory fluctuations in any realization. Moreover, the degree to which (117) is satisfied must depend upon the relative strength of nonlinearities. No simple measure of nonlinearity is given by FB. As a suitable measure we may take the "characteristic inverse Richardson number" [*Munk*, 1981]

$$Ri^{-1} \equiv \frac{\overline{(\partial u/\partial z)^2}}{N^2} \tag{118}$$

where $\overline{(\partial u/\partial z)^2}$ is the variance of vertical shear averaged over the flow domain. Roughly we might estimate Ri^{-1} for FB as follows:

The high–energy case for FB is reported as total energy $E = 10^{-2}\,\text{m}^2\text{s}^{-2}$ and buoyancy frequency $N = 0.757\,\text{s}^{-2}$. Supposing E to be roughly equipartitioned between KE and PE, and assuming that velocity variance is more in the horizontal than the vertical component, we take an upper bound on horizontal velocity variance $\overline{u^2}$ as $10^{-2}\text{m}^2\ \text{s}^{-2}$. An estimate of $\overline{(\partial u/\partial z)^2}$ requires assigning a representative vertical wave number. For the "reddish" spectra of FB, truncated at wave number 30, it may be reasonable to guess that a wave number k_1 such that $(\partial u/\partial z)^2 = k_1^2 u^2$ is not larger than $k_1 = 4$. Thus it would appear that FB explore values of Ri^{-1} up to a value of 0.3 perhaps. This number will be important in the comparison of FB with SH, the latter to be described shortly.

The third category of experiments by FB are forced–dissipative cases which are run out to a condition of approximate statistical stationarity. Forcing is of white noise random type, applied isotropically over wave numbers such that $k^2 <= 36$ and such that kinetic and potential energies are supplied equally. The amplitude of forcing was adjusted to achieve cases with different degrees of nonlinearity. The strongest cases may have obtained Ri^{-1} values up to about 0.3 as estimated previously.

Forced–dissipative experiments confirm earlier FB results from viscous decay experiments. Especially, the flows seem to remain close to an equipartition of kinetic and potential energy with the corresponding implication that the vertical buoyancy flux nearly vanishes. There may be some room for doubt on this point. Figure 22, from FB, shows the cross–spectrum $R_{\mathbf{k}}$ which likewise would vanish with the buoyancy flux. It would appear that $R_{\mathbf{k}} != 0$ tends to occur in low wave numbers. However, FB point out that there may be a good deal of realization variability especially at low wave numbers. FB suggest that, averaged over a suitably large ensemble, smaller R_k might result. Moreover, $R_{\mathbf{k}} != 0$ seem to occur in low wave numbers which are subject to forcing, with uncertain consequences.

A further observation from forced–dissipative experiments is that the ratio of horizontal to vertical kinetic energy tends to increase over time. This occurs despite the isotropic nature of the forcing and is thus a manifestation of nonlinear interaction tendencies.

The fourth type of experiment by FB examines the breakdown of energy from an initially standing wave of mode $k_x = 2$, $k_z = 1$. Interesting observations are that entropy as given by (116) and energy of the higher wave number modes both tends to increase in an oscillatory way with a period equal to half the period of the standing wave. FB observe that energy growth at higher wave number tends to occur during the phase of the standing wave when its potential energy is near a maximum. A

mechanism for such phase–dependent, preferential energy transfer is not apparent although FB remark that similar oscillatory energy growth at half the standing wave period is also characteristic of the generalized Mathieu equation model for internal wave instability [*Mied,* 1976; *Drazin,* 1977; *Klostermeyer*, 1982].

We now turn to *Shen and Holloway* [1986] who also employ spectral transform techniques to investigate the circumstances that determine the amplitudes of equilibrium spectra. Spectral fluxes and conversions of energy are studied. Also, the average and fluctuations of frequency of individual waves are examined.

Experiments of SH are performed at a resolution corresponding to 64 x 64 points, with some higher–resolution tests at 128 x 128 points. Initial conditions consist of random phase assignment with spectral energy levels given by

$$E(\omega,k_z) = 4E_0\frac{\beta_0}{\pi}\frac{\lambda_0}{\pi}\left(\lambda_0^2+\omega^2\right)^{-1}\left(\beta_0^2+k_z^2\right)^{-1} \qquad (119a)$$

or

$$E(k_x,k_z) = 4E_0\frac{\beta_0}{\pi}\frac{\lambda_0}{\pi}\frac{k_z^2}{k^3}\left(k^2\lambda_0^2+k_x^2\right)^{-1}\left(\beta_0^2+k_z^2\right)^{-1} \qquad (119b)$$

The spectral shapes are intended to imitate the GM model under constraints of the vertical plane idealization and nonrotation. Singularities occur on the k_x and k_z axes which are arbitrarily resolved by choosing $E(0,k_z) = E(1,k_z)$ and $E(k_x,0) = E(k_x,1)$. The values β_0 and λ_0 are scaling constants while E_0 specifies the average total energy density.

Forcing and dissipation are then applied and integrations are carried forward in time until a statistically stationary regime is established. Given uncertainty in the actual energetic forcing of internal waves, SH somewhat arbitrarily choose to force only the horizontal currents in the three gravest modes $k_x = 0$, $k_z = 1,2,3$. For comparison, another case is executed with isotropic forcing of both density and velocity fields at low wave numbers such that $k^2 <= 9$. By limiting forcing to gravest modes, most of wave space is free to exhibit effects of energy cascades. Two types of forcing are explored. A phase coherent, nonlinear force $F_k = A^2\Psi_k/k^2|\Psi_k|^2$ is applied where Ψ_k is the stream function coefficient in the forced mode. Also a random force governed by $\dot{F}_k + \lambda F_k = A^2R$, where R is the realization of a complex Gaussian process, is applied. The choice of the two forcings was intended as a sensitivity test and results were observed to be fairly independent of the nature of the forcing. Dissipation in SH is given by a linear differential operator ∇^4, sometimes called a "hyperdiffusion," applied to the vorticity and density fields. As compared with a more customary ∇^2 diffusion (cf. FB), the ∇^4 operator removes variance at higher wave numbers, again leaving more of wave space free to exhibit effects of nonlinear interaction.

By adjustment of forcing and dissipation, SH set up four very different cases to study. Characterizing the degree of nonlinearity by Ri^{-1} (cf. (118)), the four cases are

Case 1:

$$Ri^{-1} \approx 0.01$$

Case 2:

$$Ri^{-1} \approx 0.1$$

Case 3:

$$Ri^{-1} \approx 1$$

Case 4:

$$Ri^{-1} \approx 7$$

Snapshots of typical fields in these four cases are shown in Figure 23. The relation of the different cases to oceanic conditions depends upon a question of resolution. A typical value of Ri^{-1} in the ocean depends upon the observed scales of motion which contribute to $(\partial u/\partial z)^2$. If only large scales are observed, say of the order of tens of meters to 100 m, results such as cases 2 or 1 may be obtained. With resolution down to a meter, a situation like case 3 may be obtained. At still finer resolution, and in a turbulent "patch," a picture such as case 4 might be seen although the two–dimensional idealization would then be quite suspect.

A popular conjecture [cf. *Munk,* 1981], is that internal wave amplitudes may be limited by wave overturning as Ri^{-1} approaches unity. Figure 23 shows that, indeed, overturning becomes manifest near $Ri^{-1} \approx 1$. Moreover, the extent of forcing and dissipation required to maintain stationarity increases only slightly between cases 1 and 2, whereas very much stronger forcing is required to maintain case 3 with even stronger forcing in case 4. The total dissipation rates for the four cases from SH, as well as some additional cases, are graphed against Ri^{-1} in Figure 24. At least qualitatively, the simulations appear to support a "saturation by breaking" hypothesis. Quantitative interpretation of Figure 24 is hazardous, however, on account of the two–dimensional idealization.

A point denoted case 5 in Figure 24 is noteworthy insofar as this case is run at the higher 128 x 128 resolution and seems to suggest increased dissipation with increased resolution for given Ri^{-1}. In case 5, Ri^{-1} ranges over values from about 1.5 to 1.6 which are expected to yield frequent overturning. Such overturning and the time–evolving, complicated morphology of flow features in case 5 are shown in Figure 25.

Wave number spectra in k_x, k_z and in total k of kinetic energy and of available potential energy (density variance) are shown in Figure 26 for the four cases of SH. At smaller Ri^{-1} (cases 1 and 2), KE and PE stay in approximate equipartition except at low wave numbers where direct forcing of horizontal kinetic energy is applied. These results are consistent with experiments by FB which appear to be also in the Ri^{-1} range of cases 1 and 2. At larger Ri^{-1}, in cases 3 and 4, equipartition breaks down and KE and PE spectra become dissimilar. Slopes of both KE and PE spectra in small Ri^{-1} cases fall off roughly as k^{-3} in either k_x or k_z. At larger Ri^{-1}, slopes of KE spectra steepen nearer to $k_z^{-3.5}$ while slopes of PE spectra shallow to less than k_z^{-2} in case 4. The behavior at large Ri^{-1} reflects a tendency toward two–dimensional turbulence: near conservation of vorticity inhibits KE cascade to large wave numbers, steepening the KE spectra, while density increasingly acts as a passive scalar with a shallower variance spectrum. Another consequence, which is also an

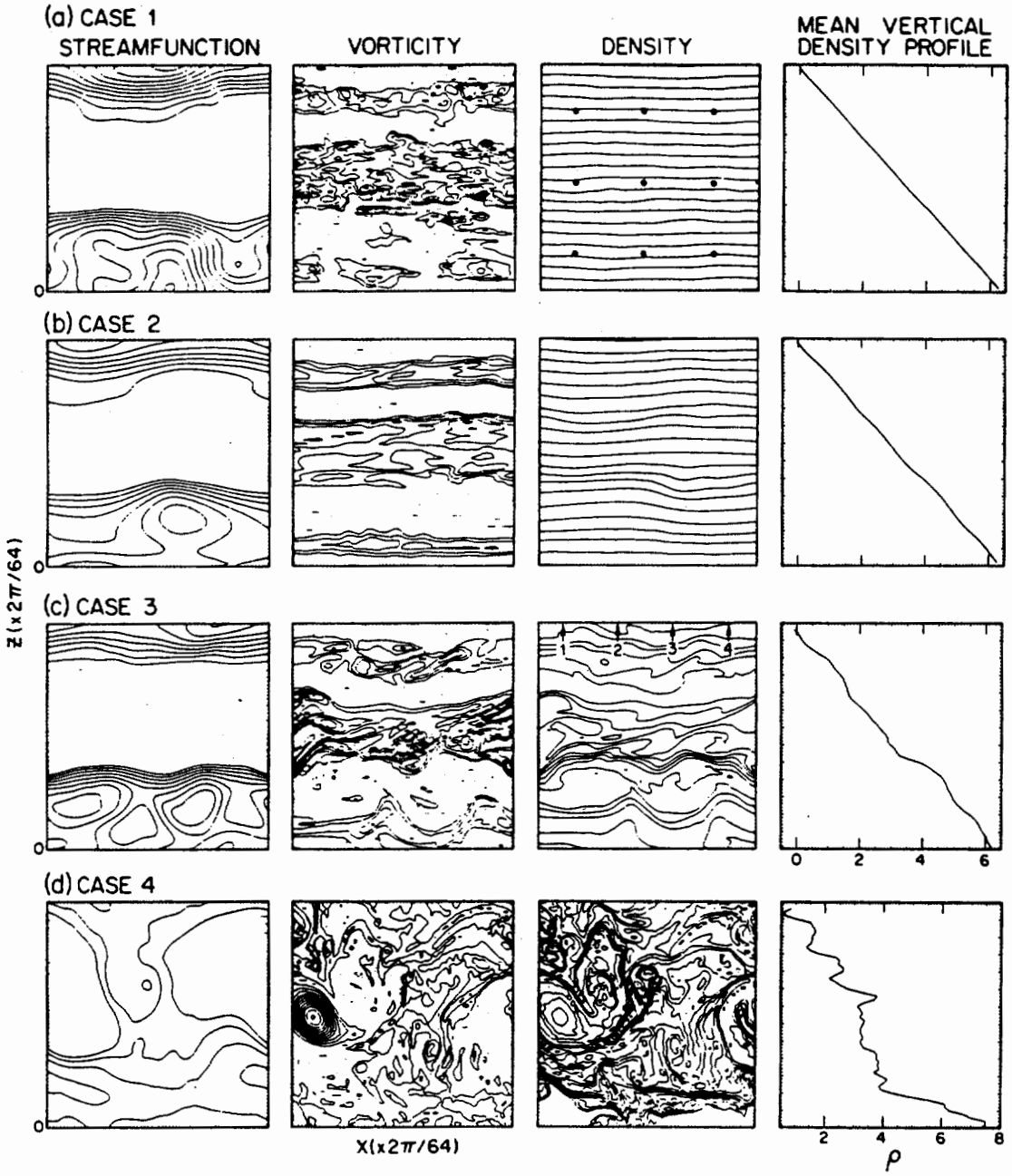

Fig. 23. Instantaneous fields of stream function, vorticity, density, and vertical profiles of horizontally averaged density, for the four cases of SH [from *Shen and Holloway,* 1986].

apparent artifact of two dimensions, is that the rate of dissipation of PE tends to exceed the rate for KE by a factor of about 2 at larger Ri^{-1}.

SH further studied the conversion of kinetic to potential energy and the energy transfer across the spectrum. Results for case 3 are shown in Figure 27. All quantities have been time–averaged over several buoyancy periods. The energy redistribution is here decomposed into three parts:

1. KE transfer is the rate at which KE increases or decreases at any wave vector **k** due to nonlinear transfer of KE to or from other regions of the spectrum. Summed over the spectrum, the transfer vanishes; this is a pure redistribution with no overall gain or loss of KE.

2. PE transfer is the rate of PE increase or decrease at any **k** due to transfer and is a pure redistribution with no overall gain or loss of PE.

3. Finally there is KE–PE conversion. In a stratified fluid under gravity, KE and PE may be exchanged by means of vertical mass flux $\overline{\rho w}$. Upward flux $\overline{\rho w} > 0$ is a sink for KE and corresponding source for PE.

As seen in Figure 27, KE transfer exhibits a pattern of KE loss at intermediate scales with compensating gains at large and small scales. This pattern is characteristic for two–dimensional flows in which KE transfer alone conserves both overall KE and overall vorticity variance. Although vorticity at each fluid element may change on account of gravitational torques, KE transfer is nonetheless constrained [*Fjørtoft*, 1953; *Kraichnan*, 1967].

PE transfer is somewhat simpler since no secondary

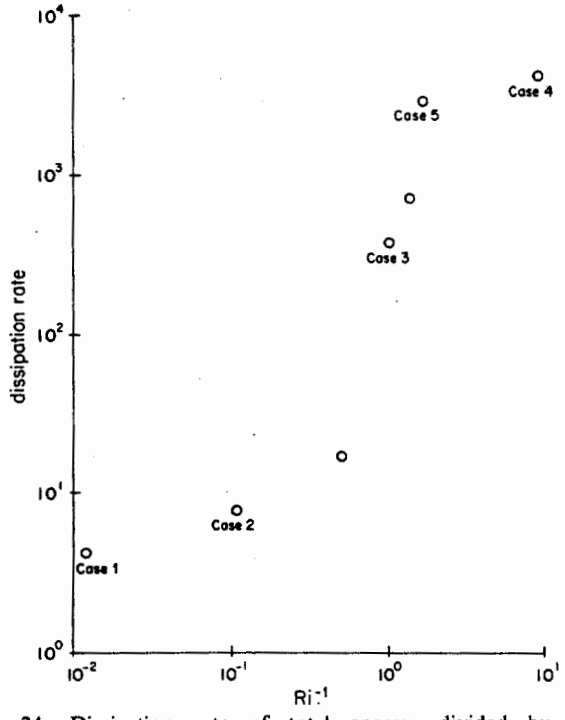

Fig. 24. Dissipation rate of total energy, divided by the coefficient of the dissipation operator graphed against Ri^{-1}. The viewer is strongly cautioned from quantitative interpretation of this figure on account of the two–dimensional idealization underlying the computation (from *Holloway*, 1984].

conservation constraints occur as in the case of KE. PE is removed at low wave numbers and supplied to higher wave numbers by the physical process of shearing and deforming larger–scale density features into smaller–scale features.

When we come to KE - PE conversion, the results may seem surprising. One expects that the vertical buoyancy flux is a consequence of manifest overturning: thus, on the scale of manifest overturning, one may expect upward mass flux or KE → PE. Instead, from Figure 27 we see that the very longest resolved scales are sustaining upward mass flux whereas over most of the rest of wave space (including any scale of manifest overturning) there is downward flux or reconversion PE → KE. Results here shown for case 3 are near $Ri^{-1} \approx 1$. However, even at very much smaller Ri^{-1}, SH find qualitatively similar patterns of KE − PE conversion although at much reduced, time–averaged values. It would seem that nonzero $\overline{\rho w}$ can be sustained by nonlinear interaction even in the complete absence of manifest overturning.

We return to the behavior noted by FB in the decay of a large–scale standing wave. Transfer of energy to smaller scales was seen to occur preferentially when the standing wave was in its potential energy phase; hence the transfer was quasi–periodic with a period of about half the standing wave period. Such behavior may simply be a consequence of two–dimensionality. Kinetic energy cannot be transferred directly from large to small scales whereas potential energy can be so transferred, as seen also in Figure 27. Importantly, systematic draining of potential rather than kinetic energy from large scales is consistent with, and under some circumstances must demand, KE to PE conversion via $\overline{\rho w} > 0$ at large scales even for rather small Ri^{-1}. An overall energy balance sketched in Figure 28 may be very particular to the two–dimensional idealization.

Finally, numerical simulations may be used directly to test the assumptions underlying resonant interaction theory. For example, resonant interaction assumes that the motion field consists of waves propagating at their natural frequencies. Stronger interactions are presumed to "smear" individual waves over a range of frequencies and, possibly, to induce mean frequency shifts. Defining instantaneous "frequency" as the rate of change of complex phase, SH calculate the standard deviation σ_ω. They find that σ_ω varies proportionally to $k\ Ri^{-1/2}$, suggestive of a "random Doppler shifting" [*Holloway*, 1979].

7. CONCLUSIONS

Nonlinear interactions among internal gravity waves provide an important link between the large generation and the small dissipation scales. Their proper understanding and modeling is hence paramount for a variety of important scientific and practical problems.

Here we summarize the main points of the review, suggest directions for immediate future work, and try to put the results in some broader perspective.

Summary

The main points of the review are as follows:

1. Studies of the nonlinear interactions have excluded the interaction with the vortical (i.e., potential vorticity carrying) mode of motion. This is true for all studies but that of *Riley et al.* [1981], which is a pioneering study in this respect. Lagrangian studies exclude the vortical mode when making an expansion about an equilibrium state and assuming solutions proportional to $\exp\{-i\omega t\}$. Numerical models exclude the vortical mode when confining themselves to motions in a nonrotating vertical plane. In the ocean, it is unclear how much of the observed fluctuations are due to the vortical mode of motion. This is especially true for the small scales that contain most of the shear.

2. The resonant interaction calculations have provided most of the conventional wisdom about the role of nonlinear interactions. A large and impressive amount of work (about 20 man–years) has been spent to evaluate the transfer integral (32) for various model spectra. These calculations resulted in the following scenario. The primary effect of resonant interactions is to make the spectrum vertically symmetric at high–wave numbers (by the elastic scattering mechanism), and smooth at high–wave numbers and high frequencies (by the fast induced diffusion mechanism), and to create an inertial peak (by the parametric subharmonic instability mechanism). The Garrett and Munk model spectra are symmetric and smooth and have an inertial peak. The secondary effect is to adjust the spectrum to deliver a constant downscale flux under the ID and PSI mechanism. For the GM76 spectrum the downscale flux is of the order of 10^{-3} W m^{-2}. This rate is roughly compatible with other estimates of the energy flux through the internal wave spectrum.

3. The range of validity of the resonant interaction approximation is not known. The resonant approximation

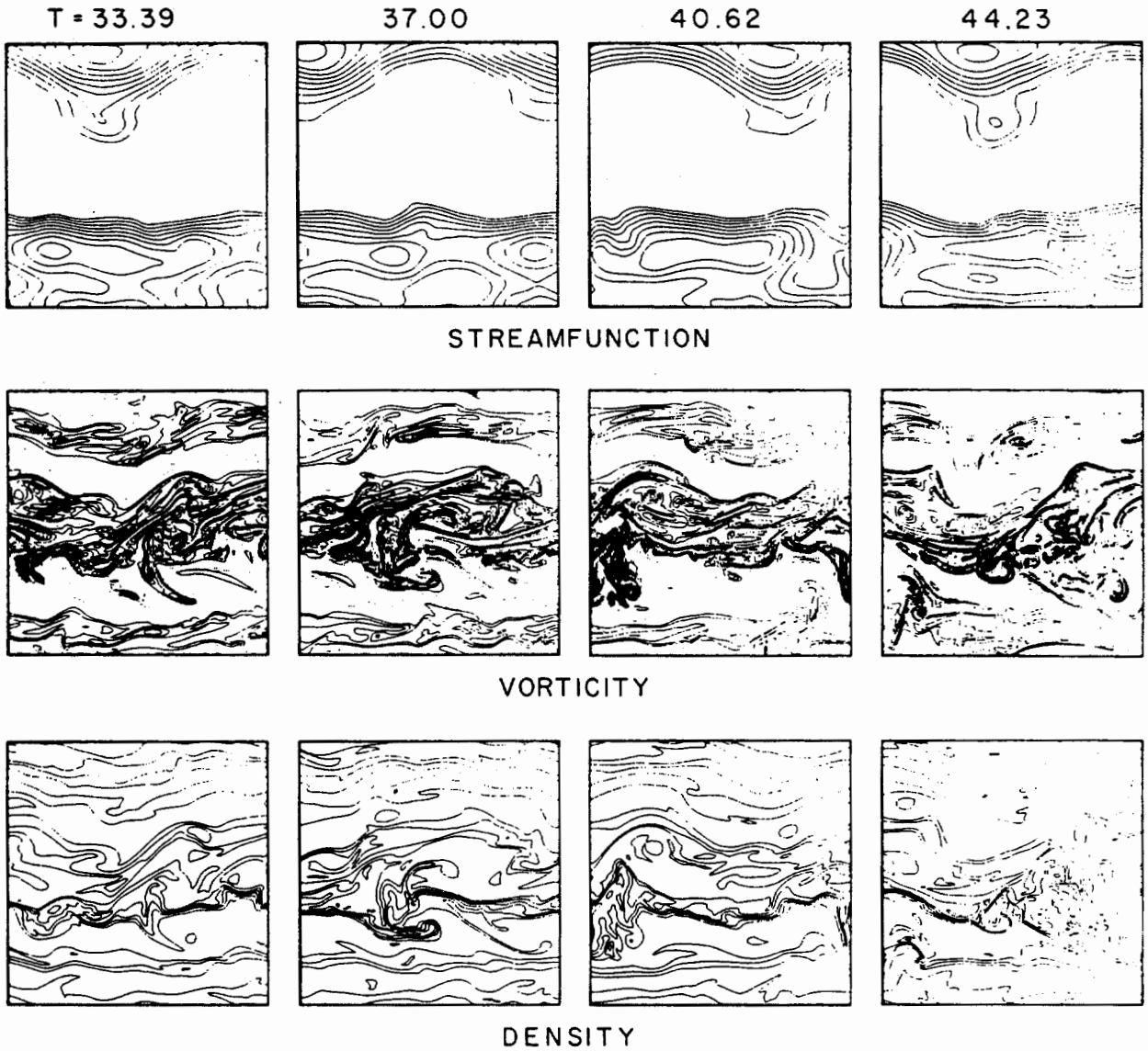

Fig. 25. Fields of stream function, vorticity, and density at successive times. Time is scaled by the mean buoyancy frequency. Positive stream function is contoured in solid lines; negative stream function dashed. Sense of flow is here defined such as to keep more positive stream function to the left [from *Holloway*, 1984].

can be regarded as the first order of a perturbation expansion. There is, however, no simple expansion parameter. The derivation requires a number of assumptions. Their appropriateness for the oceanic internal wave field is either difficult or impossible to check.

A simplified criterion often cited states that the resonant interaction approximation is not valid if the interaction time is smaller than the wave period. This is not necessarily an adequate criterion. The ratio of interaction time to wave period measures the broadening of the resonance surfaces (i.e., how well waves are described by the linear dispersion relation). The resonant interaction approximation is valid if this broadening is inconsequential, i.e., if the nonlinear interactions are "coherent" within this broadened volume of phase space. A simplified quantitative formulation of this latter criterion has not been given yet for the oceanic internal wave field and might not even exist.

There does not exist a deductively well-established theory for finite amplitude or strong interactions among internal waves. If such a theory were available and contained the resonant approximation as a limit, the range of validity of the resonant approximation could systematically be examined. Analysis of the direct interaction approximation in two dimensions suggests that the resonant interaction approximation might perhaps be a "singular" limit of finite amplitude theory, since resonant interactions conserve the linear vertical wave momentum that, in general, is not conserved.

4. The validity of the resonant approximation must be seriously doubted in the induced diffusion region. The resonant calculations suggest that high-frequency, high-wave number internal waves interact primarily with large-scale near-inertial currents. The waves are weakly and randomly refracted by the near-inertial shear and perform a random walk in vertical wave number space which

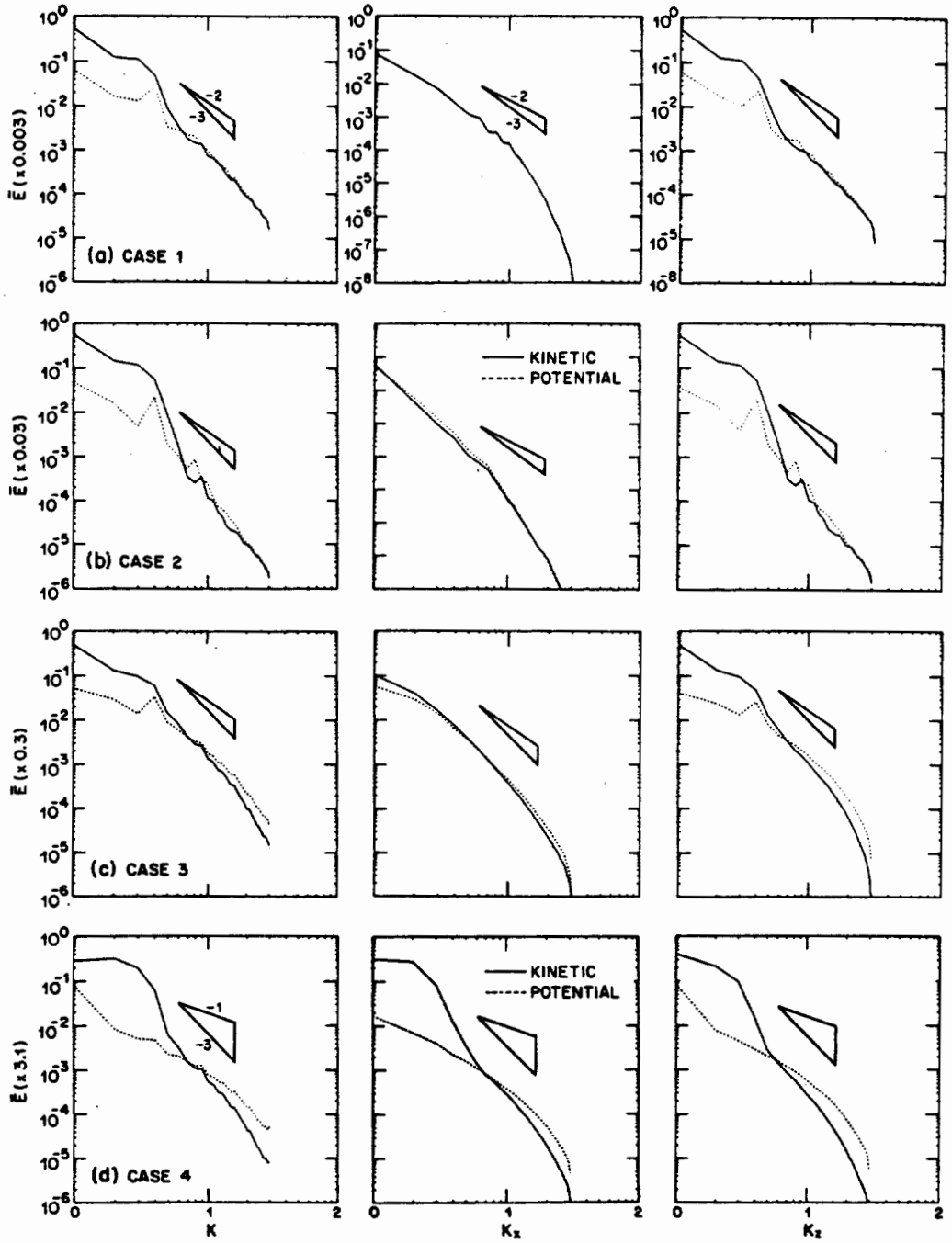

Fig. 26. Wave number spectra in total k, k_x, and k_z of kinetic and potential energy for the four cases of SH [from *Shen and Holloway*, 1986].

can be described as a diffusion of wave action. The more general eikonal calculations, which assume a scale separation between the waves and the refractive background but no weak interaction, show a completely different picture: The high–frequency, high–wave number waves undergo large and systematic excursions in vertical wave number space and encounter critical levels. Nonlinearities in the refraction equation are essential for these large excursions. Furthermore, corrections to the weak interaction, induced diffusion case can be calculated for a Garrett and Munk spectrum and turn out to be large. Resonant interaction theory hence does not seem to be applicable to high–frequency, high–wave number internal waves.

5. Strong interaction theories and direct numerical modeling are not yet in a stage to be directly applicable to oceanic internal wave fields. Strong interaction theories are technically and computationally so complex that it is extremely difficult to apply them to interactions within a realistic oceanic internal wave field. Their main merit so far has been the unveiling of general theoretical concepts. Similarly, direct numerical modeling is severely limited by finite computer resolution. So far only three low–resolution, two–dimensional models have been integrated to statistical equilibrium. For one three–dimensional model the initial tendencies have been explored. These models have been used for gaining prin-

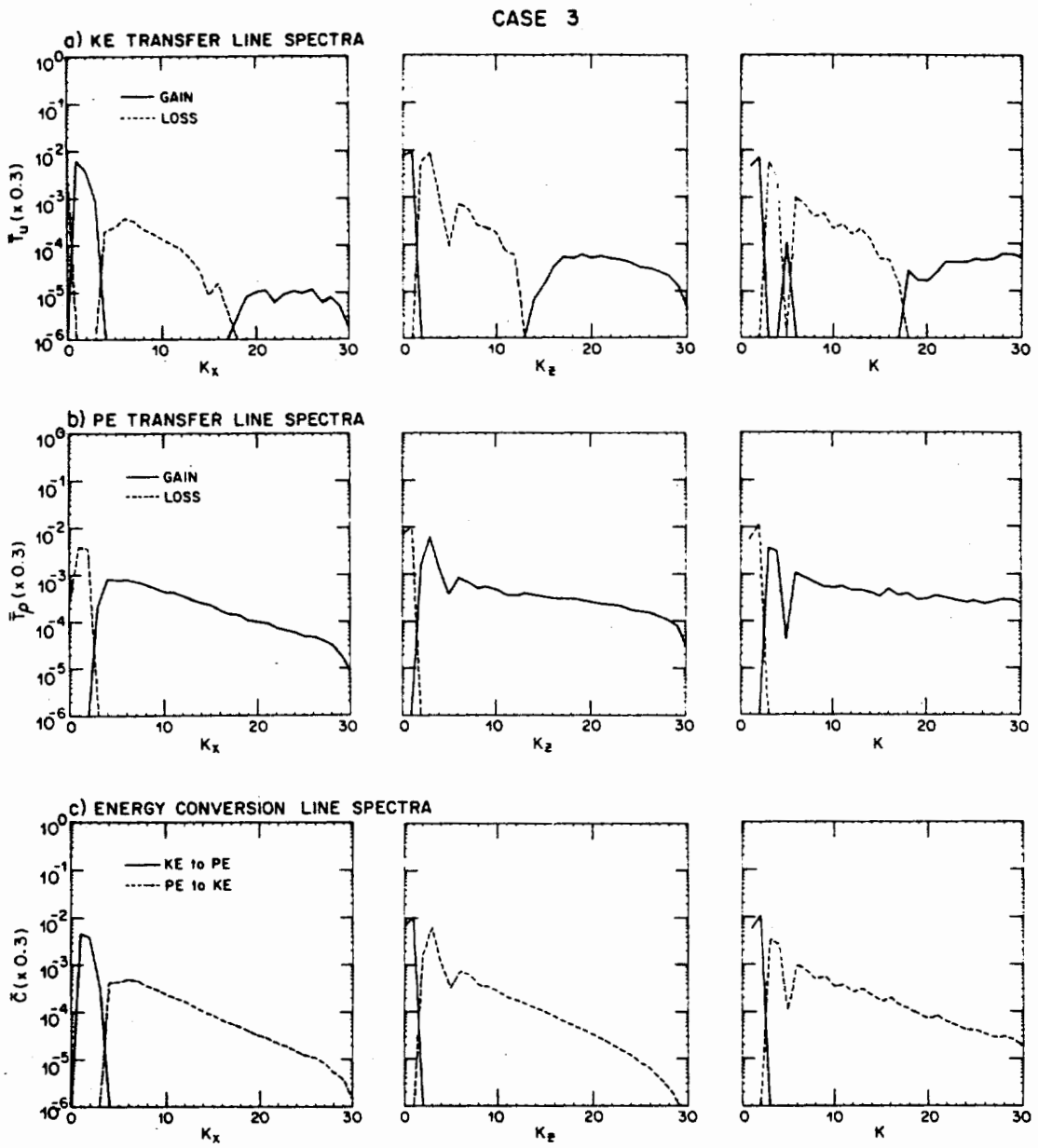

Fig. 27. Time–averaged transfer rate of kinetic energy and of potential energy and conversion rate from kinetic to potential energy as a function of k_x, k_z, and total k [from *Shen and Holloway,* 1986].

cipal insights and for theory testing but not for direct comparison with the ocean.

Future Work

A substantiation of the nonlinear interaction results and further insight into their role are expected to come from research in the following areas:

Rationalization of the results of the nonlinear interaction calculations within the complete energy balance of internal waves. The nonlinear interaction calculations suggest that internal wave energy is generated at low wave numbers and high frequencies and dissipated at high–wave numbers and inertial frequencies. Does this conform with our limited knowledge of the energy sources and sinks of internal waves? Are there apparent inconsistencies?

Validation of the resonant and eikonal approximations. Both the resonant and eikonal approximations are based on assumptions. The resonant approximation assumes that the nonlinear interactions are weak and hence confined to resonant interactions. The eikonal approximation assumes that the nonlinear interactions are dominated by scale–separated interactions and that the large–scale background flow is not affected by the interaction. We need to understand if and where these approximations are adequate.

Modeling the transport of small–scale internal waves by eikonal techniques. Integration of the eikonal equations provides an efficient and versatile approach to study the interaction between small–scale and large–scale internal waves. Unlike the resonant interaction approach, which has been extensively studied over the past 10 years, the eikonal approach has just recently been applied to the internal wave problem and still holds promise of new

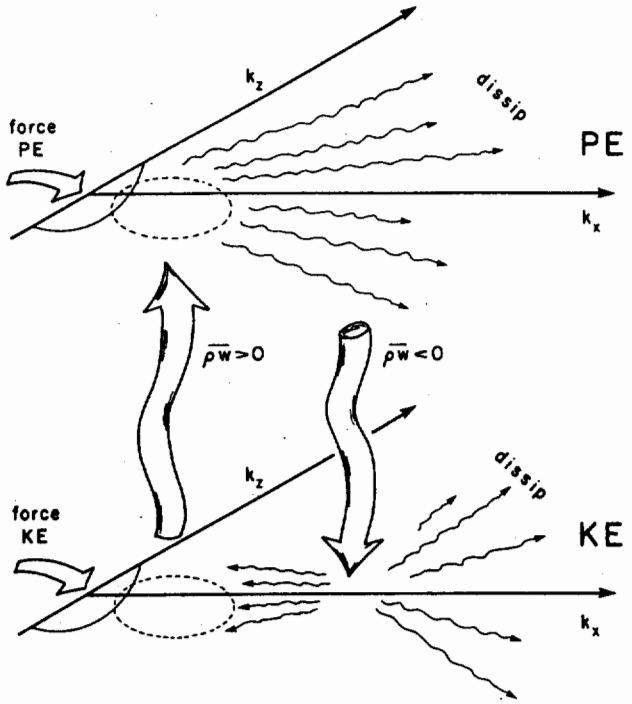

Fig. 28. Sketch depicting the energy balance on two planes, one representing kinetic energy, the other representing potential energy. External forcing of KE and, sometimes, of PE applies at low wave numbers. KE is converted to PE at low wave numbers by $\overline{\rho w} > 0$. Then PE is scattered to higher wave numbers where some is reconverted to KE by $\overline{\rho w} < 0$. KE is then distributed to both low and high wave numbers [from *Holloway*, 1984].

insights. The principal limitations of the eikonal approach are its built–in assumptions. Additionally, the integration of the eikonal equations does not constitute a transport theory. One still has to average over an ensemble of waves or background flows in order to determine the transports through the spectrum. At present, this ensemble average is determined by Monte Carlo simulations.

Direct numerical modeling of internal wave interactions. Direct numerical modeling is another promising approach to study internal wave interactions. Direct numerical modeling has a number of appealing advantages. It is not restricted to weak or scale–separated interactions. It can easily include the interaction with the vortical mode, and it also yields space–time results (as opposed to spectral results) that are directly comparable to oceanic measurements. The main limitation is the computer resolution. Even with optimistic estimates of the increase in computer power we are more than a few years away from a full three–dimensional simulation at oceanic Reynolds and Peclet numbers.

Perspective

The nonlinear interaction studies reviewed in this paper bear on some broader oceanographic issues.

Universality of observed internal wave field. Observed internal wave spectra from many different locations and times show a remarkable agreement with the "universal" GM spectrum, although significant deviations with definite patterns have been seen in recent years. The resonant interaction calculations suggest that the GM spectrum is close to a steady state with respect to nonlinear interactions over a wide range of wave numbers and frequencies and that deviations rapidly relax. The spectrum also supports a downscale energy flux from large to small scales. If this is true, nonlinear interactions are a prime candidate for explaining the universality of the spectrum. The exact mechanism by which the universal spectrum is maintained is, however, not clear. *Munk* [1981] suggests a saturation mechanism due to wave breaking by shear instability. He assumes that the energy flux through the spectrum is a sensitive function of the Richardson number or rms shear. The shear depends on the energy E of the wave field and the high–wave number cutoff β_c. A slight increase in energy leads to a large increase in energy flux. A large energy input into the wave field can therefore be transferred to dissipation scales by only a slight change in energy level, assuming β_c to be constant. Another explanation [*Garrett and Munk* 1979; *McComas and Müller*, 1981*b*] is based on the apparent long dissipation time scale, of the order of 50 to 100 days in the main thermocline. In 100 days the large–scale, energy–containing waves travel of the order of 1000 km. This long dissipation time and large propagation distance can account for a relatively constant energy level, as energy inputs at different times and locations are smoothed out or spread out over these scales.

Overall energy and enstrophy cascade. Oceanographers generally presume that there exists an overall energy and enstrophy cascade from the large planetary scales where velocity, density, and potential vorticity variances are generated to the microscales where these variances are dissipated. The resonant interaction calculations predict an energy flux from large– to small–scale internal waves. This result supports the concept of an overall energy cascade and makes the internal wave field an important link in that cascade. It is, however, unclear how enstrophy (the variance of potential vorticity) is cascaded to the dissipation scales and what the role of the internal wave field would be in such an enstrophy cascade. Recall that internal waves do not carry potential vorticity.

Internal wave–induced mixing. It is often assumed that the energy cascade through the internal wave spectrum provides the major energy source for small–scale turbulence and that a certain fraction of this energy is used for mixing. If this is true, the vertical (cross–isopycnal) mixing coefficient can be estimated and parameterized in terms of the energy flux Q_E across the internal wave spectrum, without knowing the details of the overturning, breaking and subsequent mixing events. *McComas and Müller's*, [1981*b*] estimate of the energy flux leads to a mixing coefficient $K_v \sim 10^{-5}\mathrm{m}^2\mathrm{s}^{-1}$, as a function of the energy E and bandwidth β_* of the internal wave field. Insofar as their energy flux is determined by the low–wave number, energy–containing region of the spectrum, where the resonant approximation seems to be valid, their estimate of K_v might turn out to be fairly robust to corrections of the interaction rates at high–wave numbers. Indeed, we seem to have achieved a zeroth–order understanding [*Garrett*, 1984] where the dynamic estimates of K_v from the energy flux Q_E agree in order of magnitude with kinematic estimates based on the statistics of the frequency and thickness of mixing events

and direct estimates from microstructure measurements. However, important issues such as the depth dependence of K_v and the importance of the various terms in the turbulent kinetic energy budget still need to be resolved.

A zeroth–order understanding has only been reached for mixing in the ocean interior. There is the possibility that a large fraction of the cross–isopycnal mixing is done in the boundary layers of the ocean. Internal waves might also provide the energy source for such mixing in boundary layers. Internal waves being reflected off a sloping bottom show a huge energy flux imbalance that can be tapped for mixing [*Eriksen*, 1985]. How much of that imbalance is actually used for mixing depends on nonlinear relaxation effects and has not been estimated yet.

Effect on large–scale motions. For large–scale and meso scale motions, internal waves are subgrid motions. Divergences or convergences of the internal wave momentum and mass flux appear in the equations for the larger–scale motions and effect their evolution. There is a clear need to understand these effects and parameterize them, perhaps by internal wave–induced diffusion coefficients. Observational estimates are scarce; the theoretical estimates of *Müller* [1976] are inaccurate since he did not account for the special wave number structure of the oceanic internal wave field. We are clearly far away from even a zeroth–order understanding of these effects. As outlined in this review, further understanding of the nonlinear interactions among internal gravity waves might contribute to the solution of some of these broader oceanographic problems.

NOTATION

a	wave amplitude.
A	action density.
$A(\mathbf{k})$	action density spectrum.
b	depth scale of Brunt Väisälä frequency.
D_{ij}	diffusion tensor.
E	energy density.
$E(\mathbf{k})$	energy density spectrum.
f	Coriolis frequency.
j	mode number.
j_*	mode number bandwidth.
$\mathbf{k} = (k_x, k_y, k_z)$	wave number vector.
$\mathbf{k}_h = (k_x, k_y)$	horizontal wave number vector.
K_V	vertical mixing coefficient.
N	Brunt Väisälä frequency.
p	pressure.
$\mathbf{P}$	wave momentum.
Q_A	action flux.
Q_E	energy flux.
Ri	Richardson number.
S	shear.
$S(\mathbf{k})$	shear content spectrum.
$s = \pm 1$	index.
t	time.
$T^{\pm}$	transfer function.
$\mathbf{u} = (u, v, w)$	current velocity.
$\mathbf{x} = (x, y, z)$	position vector.
α	wave amplitude.
β_c	vertical cutoff wave number.
β_*	vertical wave number bandwidth.
Γ	coupling coefficient.
ϵ	dissipation rate.
ζ	vorticity.
χ	diffusivity coefficient.
μ	relaxation rate.
ν	viscosity coefficient.
ν_p	relaxation rate.
ν_B	Boltzmann rate.
ξ	vertical displacement.
π	potential vorticity.
ρ	density.
ρ_0	constant reference density.
$\tilde{\rho}$	background density.
σ	intrinsic frequency.
τ_{diss}	dissipation time scale.
τ_c	correlation time.
ψ	stream function.
ω	frequency.
Ω	frequency.

Acknowledgments. We would like to thank Chris Garrett, Jorgen Frederiksen and a referee for helpful and clarifying comments. This work was supported by the Office of Naval Research. The Center for Studies of Nonlinear Dynamics is affiliated with the University of California, San Diego.

REFERENCES

Batchelor, G. K., Computation of the energy spectrum in homogeneous two–dimensional turbulence, *Phys. Fluids, 12*, suppl. II, 233–239, 1969.

Benney, D. J., and P. G. Saffman, Nonlinear interactions of random waves in a dispersive medium, *Proc. R. Soc. London, Ser. A, 289*, 301–320, 1966.

Berry, M. V., and C. Upstill, Catastrophe optics: Morphologies of caustics and their diffraction patterns, *Prog. Opt., XVIII*, 257, 1980.

Bretherton, F. P., Resonant interactions between waves: The case of the discrete oscillations, *J. Fluid Mech., 20*, 457–479, 1964.

Bretherton, F. P., and C. J. R. Garrett, Wavetrains in inhomogeneous moving media, *Proc. R. Soc., London, Ser. A, 302*, 529–554, 1968.

Briscoe, M. G., Preliminary results from the trimoored internal wave experiments (IWEX), *J. Geophys. Res., 80*, 3877–3884, 1975.

Briscoe, M. G., Observations on the energy balance of internal waves during Jasin, *Phil. Trans. R. Soc. London, Ser. A, 301*, 427–444, 1983.

Briscoe, M. G., and R. A. Weller, Preliminary results from the long–term upper–ocean study (LOTUS), *Dyn. Atmos. Oceans, 8*, 243–265, 1984.

Broutman, D., The focusing of short internal waves by an internal wave, *Geophys. Astrophys. Fluid Dyn., 30*, 199–225, 1984.

Brown, E. D., and W. B. Owens, Observations of the horizontal interactions between the internal wave field and the mesoscale flow, *J. Phys. Oceanogr., 11*, 1474–1480, 1981.

Cairns, J. L., and G. O. Williams, Internal wave observations from a midwater float, 2, *J. Geophys. Res., 81*, 1943–1950, 1976.

Carnevale, G. F., and J. S. Frederiksen, A statistical dynamical theory of strongly nonlinear internal gravity waves, *Geophys. Astrophys. Fluid Dyn., 23*, 175–207, 1983.

Carnevale, G. F., and P. C. Martin, Field theoretical techniques in statistical fluid dynamics: With application to nonlinear wave dynamics, *Geophys. Astrophys. Fluid Dyn., 20*, 131–163, 1982.

Carnevale, G. F., U. Frisch and R. Salmon, H–theorems in statistical fluid dynamics, *J. Phys., A, Math. Gen., 14*, 1701–1718, 1981.

D'Asaro, E. A., Absorption of internal waves by the benthic boundary layer, *J. Phys. Oceanogr., 12*, 323–336, 1982.

D'Asaro, E. A., Wind forced internal waves in the North Pacific and Sargasso Sea, *J. Phys. Oceanogr., 14*, 781–794, 1984.

D'Asaro, E. A., and P. Müller, New directions in internal wave and microstructure research, *Eos, Trans. AGU, 65*, 378–380, 1984.

Davis, R. E., and A. Acrivos, Solitary internal waves in deep water, *J. Fluid Mech., 29*, 593–608, 1967.

Desaubies, Y. J. F., Analytical representation of internal wave spectra, *J. Phys. Oceanogr., 6*, 970–981, 1976.

Desaubies, Y. J. F., and M. G. Gregg, Reversible and irreversible finestructure, *J. Phys. Oceanogr., 11*, 541–566, 1981.

DeWitt, R. J., and J. Wright, Self–consistent effective–medium theory of random internal waves. *J. Fluid Mech., 115*, 283–302, 1982.

DeWitt, R. J., and J. Wright, Self–consistent effective–medium parameters for oceanic internal waves, *J. Fluid Mech., 115*, 283–302, 1982.

Dickey, T. D., and G. L. Mellor, Decaying turbulence in neutral and stratified fluids, *J. Fluid Mech., 99*, 13–31, 1980.

Drazin, P. G., On the instability of an internal gravity wave, *Proc. R. Soc. London, Ser. A, 356*, 411–432, 1977.

Eriksen, C. C., Measurements and models of finestructure, internal gravity waves, and wave breaking in the deep ocean, *J. Geophys. Res., 83*, 2989–3009, 1978.

Eriksen, C. C., Observations of internal wave reflection off sloping bottoms, *J. Geophys. Res., 87*, 525–538, 1982.

Eriksen, C. C., Implications of ocean bottom reflection for internal wave spectra and mixing, *J. Phys. Oceanogr., 15*, 1145–1156, 1985.

Fjørtoft R., On the changes in the spectral distribution of kinetic energy for two–dimensional nondivergent flow, *Tellus, 5*, 225–230, 1953.

Flatté, S. M., R. Dashen, W. H. Munk, K. Watson, and F. Zachariasen, *Sound Transmission Through a Fluctuating Ocean*, Cambridge University Press, New York, 1979.

Fofonoff, N. P., Spectral characteristics of internal waves in the ocean, *Deep Sea Res., 216* (suppl.), 58–71, 1969.

Frankignoul, C., Observed anisotropy of spectral characteristics of internal waves induced by low–frequency currents, *J. Phys. Oceanogr., 4*, 625–634, 1974.

Frederiksen, J. S., and R. C. Bell, Statistical dynamics of internal gravity waves–turbulence, *Geophys. Astrophys. Fluid Dyn., 26*, 257–301, 1983.

Frederiksen, J. S., and R. C. Bell, Energy and entropy evolution of interacting internal gravity waves and turbulence, *Geophys. Astrophys. Fluid Dyn., 128*, 171–203, 1984.

Fritts, D. C., The excitation of radiating waves and Kelvin–Helmholtz instabilities by the gravity wave–critical level interaction, *J. Atmos. Sci., 36*, 12–23, 1979.

Fu, L., Observations and models of inertial waves in the deep ocean, *Rev. Geophys., 19*, 141–170, 1981.

Gargett, A. E., Vertical eddy diffusivity in the ocean interior, *J. Mar. Res., 42*, 359–393, 1984.

Gargett, A. E., and G. Holloway, Dissipation and diffusion by internal wave breaking, *J. Mar. Res. 42*, 15–27, 1984.

Gargett, A. E., and T. R. Osborn, Small–scale shear measurements during the Fine and Microstructure Experiment (FAME), *J. Geophys. Res., 86*, 1929–1944, 1981.

Gargett, A. E., T. J. Hendricks, T. B. Sanford, T. R. Osborne, and A.J. Williams III, A composite spectrum of vertical shear in the upper ocean, *J. Phys. Oceanogr., 11*, 1258–1271, 1981.

Garrett, C. J. R., Mixing in the ocean interior, *Dyn. Atmos. Oceans, 3*, 239–265, 1979.

Garrett, C. J. R., Turning points in universal speculation on internal waves, in *A Celebration of Geophysics and Oceanography 1982*, Ref. Ser.,84–5, 38–46, edited by C. Garrett and C. Wunsch, Scripps Institution of Oceanography, La Jolla, Calif., 1984.

Garrett, C. J. R., and W. H. Munk, Internal wave spectra in the presence of finestructure, *J. Phys. Oceanogr., 1*, 196–202, 1971.

Garrett, C. J. R., and W. H. Munk, Space–time scales of internal waves, *Geophys. Fluid Dyn., 2*, 225–264, 1972*a*.

Garrett, C. J. R., and W. H. Munk, Oceanic mixing by breaking internal waves, *Deep Sea Res., 19*, 823–832, 1972*b*.

Garrett, C. J. R., and W. H. Munk, Space–time scales of internal waves: A progress report, *J. Geophys. Res., 80*, 291–297, 1975.

Garrett, C. J. R., and W. H. Munk, Internal waves in the ocean, *Annu. Rev. Fluid Mech., 11*, 339–369, 1979.

Gregg, M. C., A comparison of finestructure spectra from the main thermocline, *J. Phys. Oceanogr., 7*, 33–40, 1977.

Gregg, M. C., and M. G. Briscoe, Internal waves, finestructure, microstructure, and mixing in the ocean, *Rev. Geophys., 17*, 1524–1548, 1979.

Hasselmann, K., Feynman diagrams and interaction rules of wave–wave scattering processes, *Rev. Geophys., 4*, 1–32, 1966.

Hasselmann, K., Nonlinear interactions treated by the methods of theoretical physics (with application to the generation of waves by wind), *Proc. R. Soc., London, Ser. A 299*, 77–100, 1967.

Hasselmann, K., W. Munk, and G. MacDonald, Bispectrum of ocean waves, in Proceedings of the Symposium on Time Series Analysis, edited by M. Rosenblatt, pp. 125–139, John Wiley, New York, 1963.

Henyey, F. S., Hamiltonian description of stratified fluid dynamics, *Phys. Fluids, 26*, 40–47, 1983.

Henyey, F. S., and N. Pomphrey, Eikonal description of internal wave interactions: A non–diffusive picture of "induced diffusion," *Dyn. Atmos. Oceans, 7*, 189–208, 1983.

Henyey, F. S., N. Pomphrey and J. D. Meiss, Comparison of short–wavelength internal wave transport theories, LJI–R–84–248, La Jolla Institute, 1984.

Hirt, C. W., A numerical study of critical layer absorption, in *Nonlinear Properties of Internal Waves*, edited by B. J. West, pp. 141–157, American Institute of Physics, New York, 1981.

Holloway, G., On the spectral evolution of strongly interacting waves, *Geophys. Astrophys. Fluid Dyn., 11*, 271–287, 1979.

Holloway, G., Oceanic internal waves are not weak waves, *J. Phys. Oceanogr., 10*, 906–914, 1980.

Holloway, G., Theoretical approaches to interactions among internal waves, turbulence and finestructure, in *Nonlinear Properties of Internal Waves*, edited by B. J. West, pp. 79–112, American Institute of Physics, New York, 1981.

Holloway, G., On interaction time scales of oceanic internal waves, *J. Phys. Oceanogr., 12*, 293–296, 1982.

Holloway, G., A conjecture relating oceanic internal waves and small–scale processes, Atmos. Ocean, 21, 107–122, 1983.

Holloway, G., Probing the internal wave strong interaction regime by numerical experimentation, in *Internal Gravity Waves and Small–Scale Turbulence, Proceedings, 'Aha Huliko'a Hawaiian Winter Workshop*, edited by P. Müller and R. Pujalet, pp. 221–248, Hawaii Institute of Geophysics, Honolulu, 1984.

Holloway, G., and M. C. Hendershott, Stochastic closure for nonlinear Rossby waves, *J. Fluid Mech., 82*, 747–765, 1977.

Johnson, C. L., C. S. Cox and B. Gallagher, The separation of wave–induced and intrusive oceanic finestructure, *J. Phys. Oceanogr., 8*, 846–860, 1978.

Kadanoff, L. P., and G. Baym, *Quantum Statistical Mechanics*, W. A. Benjamin, New York, 1962.

Kadomtsev, B. B., *Plasma Turbulence, Academic, Orlando, Fla., 1965.*

Klostermeyer, J., On parametric instabilities of finite–amplitude internal gravity waves, *J. Fluid Mech., 119*, 367–377, 1982.

Kolmogorov, A. N., The local structure of turbulence in an incompressible viscous fluid for very large Reynolds numbers, *C. R. Acad. Sci., URSS, 30*, 301–305, 1941.

Kraichnan, R. H., The structure of isotropic turbulence at very high Reynolds numbers, *J. Fluid Mech., 5*, 497–543, 1959.

Kraichnan, R. H., Lagrangian–history closure approximation for turbulence, *Phys. Fluids, 8*, 575–598, 1965.

Kraichnan, R. H., Inertial ranges in two–dimensional turbulence, *Phys. Fluids, 10*, 1417–1423, 1967.

Kubo, R., Generalized cumulant expansion method, *J. Phys. Soc. Jpn., 17*, 1100–1120, 1962.

Kunze, E., and T. B. Sanford, Observations of near inertial waves in a front, *J. Phys. Oceanogr., 14*, 566–581, 1984.

Landau, L. D., and E. M. Lifshitz, Classical Theory of Fields, pp. 148–150, Pergamon, New York, 1975.

Leith, C. E., Atmospheric predictability and two–dimensional turbulence, *J. Atmos. Sci., 28*, 145–161, 1971.

Levine, M. D., Internal waves in the ocean: A review, *Rev. Geophys., 21*, 1206–1216, 1983.

Lin, J., and Y. Pao, Wakes in stratified fluids, *Annu. Rev. Fluid. Mech., 11*, 317–338, 1979.

Lin, J. T., and S. D. Veenhuizen, Measurements of the decay of

grid generated turbulence in a stably stratified fluid, *Bull. Am. Phys. Soc., 19*, 1142–1143, 1974.

Lueck, R., W. R. Crawford, and T. R. Osborn, Turbulent dissipation over the continental slope off Vancouver Island, *J. Phys. Oceanogr., 13*, 1809–1818, 1983.

Lumley, J. L., The spectrum of nearly inertial turbulence in a stably stratified fluid, *J. Atmos. Sci. 21*, 99–102, 1964.

Martin, P. C., E. D. Siggia, and H. A. Rose, Statistical dynamics of classical systems, *Phys. Rev. A, 8*, 423–437, 1973.

Martin, S., W. F. Simmons, and C. Wunsch, The excitation of resonant triads by single internal waves, *J. Fluid Mech., 53*, 17–44, 1972.

McComas, C. H., Equilibrium mechanisms within the oceanic internal wave field, *J. Phys. Oceanogr., 7*, 836–845, 1977.

McComas, C. H., and F. P. Bretherton, Resonant interaction of oceanic internal waves, *J. Geophys. Res., 83*, 1397–1412, 1977.

McComas, C. H., and M. G. Briscoe, Bispectra of internal waves, *J. Fluid Mech., 97*, 205–213, 1980.

McComas, C. H., and P. Müller, Time scales of resonant interactions among oceanic internal waves, *J. Phys. Oceanogr., 11*, 139–147, 1981*a*.

McComas, C. H., and P. Müller, The dynamic balance of internal waves, *J. Phys. Oceanogr., 11*, 970–986, 1981*b*.

McEwan, A. D., and R. M. Robinson, Parametric instability of internal gravity waves, *J. Fluid Mech.*, 67, 667–687, 1975.

McEwan, A. D., D. W. Mander, and R. K. Smith, Forced resonant second order interactions between damped internal waves, *J. Fluid Mech., 55*, 589–608, 1972.

Meiss, J. D., and K. M. Watson, Internal–wave interactions in the induced–diffusion approximation, *J. Fluid Mech., 117*, 315–341, 1982.

Mied, R. P., The occurrence of parametric instabilities in finite amplitude internal gravity waves, *J. Fluid Mech., 78*, 763–784, 1976.

Miropol'skiy, Y. Z., and K. D. Sabinin, Soviet American symposium on internal waves in the ocean, *Oceanology, 17*, 234–236, 1977.

Monin, A. S., Turbulence spectrum in a thermally stratified atmosphere (in Russian), *Izv. Akad. Nauk. SSSR, Ser. Geofiz. 3*, 397–407, 1962.

Müller, P., On the diffusion of momentum and mass by internal gravity waves, *J. Fluid Mech., 77*, 789–823, 1976.

Müller, P., Spectral features of the energy transfer between internal waves and a larger scale shear flow, *Dyn. Atmos. Oceans, 2*, 49–72, 1977.

Müller, P., Small–scale vortical motions, in *Internal Gravity Waves and Small–Scale Turbulence, Proceedings, 'Aha Huliko'a Hawaiian Winter Workshop,* edited by P. Müller and R. Pujalet, pp. 249–261, Institute of Geophysics, Honolulu, 1984.

Müller, P., and D. Olbers, On the dynamics of internal waves, *J. Geophys. Res., 80*, 3848–3860, 1975.

Müller, P., and R. Pujalet (eds.), *Internal Gravity Waves and Small–Scale Turbulence, Proceedings, 'Aha Huliko'a Hawaiian Winter Workshop,* Hawaii Institute of Geophysics, Honolulu, 1984.

Müller, P., and G. Siedler, Consistency relations for internal waves, *Deep Sea Res., 23*, 613–628, 1976.

Müller, P., D. J. Olbers, and J. Willebrand, The IWEX spectrum, *J. Geophys. Res., 83*, 479–500, 1978.

Munk, W. H., Internal wave spectra at the buoyant and inertial frequencies, *J. Phys. Oceanogr., 10*, 1718–1728, 1980.

Munk, W. H., A survey of internal waves and small–scale processes, in *Evolution of Physical Oceanography*, edited by B. A. Warren and C. Wunsch, pp. 264–291, MIT Press, Cambridge, Mass., 1981.

Mysak, L. A., and M. S. Howe, A kinetic theory for internal waves in a randomly stratified ocean, *Dyn. Atmos. Oceans, 1*, 3–31, 1976.

Olbers, D. J., Nonlinear energy transfer and the energy balance of the internal wave field in the deep ocean, *J. Fluid Mech., 74*, 375–399, 1976.

Olbers, D. J., The propagation of internal waves in a geostrophic current, *J. Phys. Oceanogr., 11*, 1224–1233, 1981.

Olbers, D. J., Models of the oceanic internal wave field, *Rev. Geophys., 21*, 1567–1606, 1983.

Orlanski, I., and C. P. Cerasoli, Resonant and non–resonant wave–wave interactions for internal gravity waves, in *Marine Turbulence,* edited by J. C. J. Nihoul, pp. 65–100, Elsevier, New York, 1980.

Orlanski, I., and C. P. Cerasoli, Energy transfer among internal gravity modes: Weak and strong interactions, *J. Geophys. Res., 86*, 4103–4124, 1981.

Orlanski, I., and B. B. Ross, Numerical simulation of the generation and breaking of internal gravity waves, *J. Geophys. Res., 78*, 8808–8826, 1973.

Orszag, S.A., Numerical simulation of incompressible flows within simple boundaries, I, Galerkin (spectral) representations, *Stud. Appl. Math., 50*, 293–327, 1971.

Osborn, T. R., and C. S. Cox, Oceanic fine structure, *Geophys. Astrophys. Fluid Dyn., 3*, 321–345, 1972.

Patnaik, P. C., F. S. Sherman, and G. M. Corcos, A numerical simulation of Kelvin-Helmholtz waves of finite amplitude, *J. Fluid Mech., 73*, 215-240 (1976).

Phillips, O. M., On the dynamics of unsteady gravity waves of finite amplitude, I, *J. Fluid Mech., 9*, 193–217, 1960.

Phillips, O. M., On the dynamics of unsteady gravity waves of finite amplitude, II, *J. Fluid Mech., 11*, 145–155, 1961.

Phillips, O. M., On the Bolgiano and Lumley–Shur theories of the buoyancy subrange, in *Atmospheric Turbulence and Radio Wave Propagation,*" edited by A. M. Yaglom and V. I. Tatarsky, Navka, Moscow, 1965.

Phillips, O. M., The Dynamics of the Upper Ocean, Cambridge University Press, New York, 1966.

Phillips, O. M., On spectra measured in an undulating layered medium, *J. Phys. Oceanogr., 1*, 1–6, 1971.

Phillips, O. M., Wave interactions–The evolution of an idea, *J. Fluid Mech., 106*, 215–227, 1981.

Phythian, R., The functional formalism of classical statistical dynamics, *J. Phys. A Math. Gen., 10*, 777–789, 1977.

Pinkel, R., Doppler sonar observations of internal waves: Wave–field structure, *J. Phys. Oceanogr., 13*, 804–815, 1983.

Pinkel, R., A wave number–frequency spectrum of upper ocean shear, *J. Phys. Oceanogr., 15*, 1453–1469, 1985.

Pomphrey, N., Review of some calculations of energy transport in a Garrett–Munk ocean, in *Nonlinear Properties of Internal Waves,* edited by B. J. West, 113–128, American Institute of Physics, New York, 1981.

Pomphrey, N., J. D. Meiss and K. M. Watson, Description of nonlinear internal wave interactions using Langevin methods, *J. Geophys. Res., 85*, 1085–1094, 1980.

Prigogine, I., *Nonequilibrium Statistical Mechanics,* Interscience, New York, 1962.

Richardson, L. F., The supply of energy from and to atmospheric eddies, *Proc. R. Soc. London, Ser. A, 97*, 354–373, 1920.

Riley, J. J., R. W. Metcalfe, and M. A. Weissman, Direct numerical simulations of homogeneous turbulence in density–stratified fluids, in *Nonlinear properties of internal waves*, vol 76, edited by B. J. West, pp. 79–112, American Institute of Physics, New York, 1981.

Roth, M. W., M. G. Briscoe and C. H. McComas III, Internal waves in the upper ocean, *J. Phys. Oceanogr., 11*, 1234–1247, 1981.

Ruddick, B., Critical layers and the Garrett–Munk spectrum, *J. Mar. Res., 38*, 135–145, 1980.

Ruddick, B. R., and T. M. Joyce, Observations of interactions between the internal wavefield and low–frequency flows in the North Atlantic, *J. Phys. Oceanogr., 9*, 498–517, 1979.

Shen, C., and G. Holloway, A numerical study of the frequency and the energetics of nonlinear internal gravity waves, *J. Geophys. Res., 91*, 953–973, 1986.

Stillinger, D. C., K. N. Helland, and C. W. Van Atta, Experiments on the transition of homogeneous turbulence to internal waves in a stratified fluid, *J. Fluid Mech., 131*, 91–122, 1983.

Thorpe, S. A., Turbulence in stably stratified fluid: A review of laboratory experiments, *Boundary Layer Meteorol., 5*, 95–119, 1973.

Thorpe, S. A., The excitation, dissipation, and interaction of internal waves in the deep ocean, *J. Geophys. Res., 80*, 328–338, 1975.

Van Kampen, N. G., *Stochastic Processes in Physics and Chemistry,* North–Holland, Amsterdam, 1981.

Weinstock, J., On the theory of temperature spectra in a stably stratified fluid, *J. Phys. Oceanogr. 15*, 475–477, 1985.

Weissman, M. A., R. W. Metcalfe, and J. J. Riley, Nonlinear internal wave interactions, in *Nonlinear Properties of Internal Waves*, vol. 76, edited by B. J. West, pp. 253–266, American Institute of Physics, New York, 1981.

Woods, J. D., Wave induced shear instability in the summer thermocline, *J. Fluid Mech., 32*, 791–800, 1968.

Wunsch, C., Geographical variability of the internal wave field: A search for sources and sinks, *J. Phys. Oceanogr., 6*, 471–485, 1976.

Wunsch, C., and S. Webb, The climatology of deep ocean internal waves, *J. Phys. Oceanogr., 9*, 235–243, 1979.

Young, W. R., P. B. Rhines, and C. J. R. Garrett, Shear–flow dispersion, internal waves, and horizontal mixing in the ocean, *J. Phys. Oceanogr., 12*, 515–527, 1982.

F. Henyey, Center for Studies of Nonlinear Dynamics, La Jolla Institute, 3252 Holiday Court, Suite 208, La Jolla, CA 92037.

G. Holloway, Institute of Ocean Sciences, Patricia Bay, P. O. Box 6000, Sydney, British Columbia, V8L 4B2, Canada.

P. Müller, Department of Oceanography and Hawaii Institute of Geophysics, University of Hawaii, Honolulu, HI, 96822.

N. Pomphrey, Plasma Physics Laboratory, Princeton University, Princeton, NJ 08544.

(Received March 15, 1985;
accepted February 22, 1986.)